Mouse Models of Muscular Dystrophy and Type 2 Diabetes

BY

NATHAN W. ROBERTS
B.S., Marquette University, 2009

THESIS

Submitted as partial fulfillment of the requirements
For the degree of Master of Science in Physiology and Biophysics
In the Graduate College of the
University of Illinois at Chicago, 2015

Chicago, Illinois

Defense Committee:

Jesus Garcia-Martinez, Chair
Ahlke Heydemann, Advisor
Beata Wolska, Medicine

Acknowledgements

I would like to thank my thesis committee, Ahlke Heydemann, Jesus Garcia-Martinez, and Beata Wolska for their support during my time in the program. I would like to thank the past and present members of the Heydemann laboratory for their assistance and support with these projects. A big thank you to the McNally group at Northwestern for providing the laboratory with breeding pairs of the DBA2/J gamma sarcoglycan knockout mice. I would like to thank Dr. Robert Gaffin of the UIC CCVR Core for the echocardiography he performed for the lab and for teaching me how to perform echocardiography on mice.

NWR

CONTRIBUTION OF AUTHORS

Chapter I is an introduction and background explanation of why mouse models are used and the diseases examined in the following chapters. Chapter II is a published manuscript (Nathan W. Roberts, Jenan Holley-Cuthrell, Magdalis Gonzalez-Vega, Aaron J. Mull, and Ahlke Heydemann, "Biochemical and Functional Comparisons of mdx and Sgcg−/− Muscular Dystrophy Mouse Models," BioMed Research International, vol. 2015, Article ID 131436, 11 pages, 2015. doi:10.1155/2015/131436) of which I am the first author, primary author responsible for design and conducting of the experiment and I was responsible for data analysis. Jenan Holley-Cuthrell, Magdalis Gonzalez-Vega, and Aaron J. Mull all assisted in mouse harvest and tissue processing. Ahlke Heydemann , my mentor, oversaw the work and wrote the manuscript. Chapter III is a published manuscript (Increased AMP-activated protein kinase in skeletal muscles of Murphy Roth Large mice and its potential role in altered metabolism. Tirsit K. Berhanu , Jenan Holley-Cuthrell , Nathan W. Roberts , Aaron J. Mull , Ahlke Heydemann . Physiological Reports Published 20 March 2014 Vol. 2 no. e00252 DOI: 10.1002/phy2.252) in which I was the fourth author. I assisted in the harvest of the animals as well as reviewing the manuscript. Chapter IV represents as of yet unpublished data pertaining to the impact of a high fat diet on the MRL heart. I anticipate that this data, along with further work, will be published in the future. In Chapter V I summarize the data presented in this work and the impact it could have on research into the diseases covered; as well as a brief discussion on possible future directions for the work.

TABLE OF CONTENTS

LIST OF TABLES

LIST OF FIGURES

LIST OF FIGURES (continued)

LIST OF ABBREVIATIONS

A’	Velocity of mitral annulus (septal side) tissue during atrial contraction
AMPK	5' AMP-activated protein kinase
B6	C57Bl/6 mouse strain
CD	Chow Diet
CD36/Fat	CD36 molecule
CPT1b	Carnitine palmitoyltransferase 1B
CS	Citrate synthase
D2	DBA2/J mouse strain
DM	Diabetes mellitus
DMD	Duchenne muscular dystrophy
DNA	Deoxyribonucleic acid
ECAR	Extracellular acidification rate
E	Velocity of blood flow across mitral valve in early diastole
E’	Velocity of mitral annulus (septal side) tissue during early diastole
E’/A’	Ratio of E’ to A’
E / E’	Ratio of E to E’
EDV	End diastolic volume of the left ventricle
ETC	Electron transport chain
EF	Ejection fraction
ESV	End systolic volume of the left ventricle
FOXO1	Forkhead box protein O1
FS	Fractional shortening
G6P	Glucose-6-phosphate
GAPDH	Glyceraldehyde 3-phosphate dehydrogenase
Glut1	Glucose transporter 1
Glut4	Glucose transporter 4

LIST OF ABBREVIATIONS (continued)

H&E	Hematoxylin and eosin stain
HFD	High Fat Diet
HKII	Hexokinase II
IVRT	Isovolumetric relaxation time
IVSd	Left ventricle septal thickness during diastole
LBK	Serine/threonine kinase 11
LVAWd	Left ventricle anterior wall thickness during diastole
LVAWs	Left ventricle anterior wall during systole
LVPWd	Left ventricle posterior wall thickness during diastole
LV mass	Left ventricle mass derived from echocardiography
mRNA	Messenger RNA
MD	Muscular dystrophy
MRL	Murphy Roths Large mouse strain
mtDNA	Mitochondrial DNA
n	Sample size
OCR	Oxygen consumption rate
pAMPK	Phosphorylated 5' AMP-activated protein kinase
PAAT	Pulmonary artery acceleration time
PGC1-alpha	Peroxisome proliferator-activated receptor gamma coactivator 1-alpha
PLN	Phospholamban
RNA	Ribonucleic acid
SGCG	Gamma sarco glycan
SV	Stroke volume
tRNA	Transfer ribonucleic acid
T1D	Type 1 Diabetes
T2D	Type 2 Diabetes

VDAC	Voltage-dependent anion channels
Wt	Wild type

SUMMARY

Mouse models for two diseases were assessed in this work. Muscular dystrophy and Type 2 Diabetes are the diseases of interest. Two muscular dystrophy mouse strains were compared to identify the more severely affected strain; the DBA2/J-Sgcg knock out and the mdx mouse model are the two strains assessed. The mdx mouse mode has been used for many years but does not develop a severe muscular dystrophy phenotype. The DBA2/J-Sgcg knock out is a more recent mouse model and has been shown to be highly fibrotic . The MRL mouse was fed a high fat diet to assess their cardiac capacity to resist the high fat diet and associated obesity. Data existed already showing that the high fat diet does not result in systemic hyperglycemia.

The D2-Sgcg knock out mice were shown to have more severe fibrosis and greater muscle membrane permeability than the mdx mouse. This validates use of the D2-Sgcg knock out mouse in studies pertaining to prevention of fibrogenesis and maintaining the stability of the muscle membrane. As the peaks in both fibrosis and muscular membrane permeability occurred early in life, the D2-Sgcg knock out mouse represents a more rapid disease model than the mdx mouse.

The MRL heart was found to resist the high fat diet and obesity at the physiological level. C57Bl/6 control mice fed the high fat diet showed thicker left ventricle walls after twelve weeks on the diet whereas the MRL mice fed the high fat diet did not show any changes in left ventricle wall thickness compared to their chow diet counterparts. At the molecular level the story is less clear. pAMPK was found to be lower in the MRL heart regardless of diet. This does not agree with current literature which shows that elevated pAMPK can protect the heart. Thus there are undoubtedly other, as of yet, unidentified alterations within the MRL heart that help it resist the high fat diet and obesity. Changes

seen at the mRNA and protein levels indicate that the MRL heart is being affected in some capacity by the diet and obesity but the extent to which is presently unknown.

I: Introduction

A. Background

In medical research using human subjects is both unethical and inefficient. Ethically speaking the use of human subjects for the vast amount of medical research is unattainable. Medical research requires precise conditions and events. As such to use human subjects we would have to place them in identical housing, feed them identical food, allow them access to identical activities. It would nullify their rights as human beings and effectively be a form of internment. Use of human subjects for basic medical research is additionally inefficient because of the genetic diversity that humanity encompasses. Families would be best but age is also a concern as the subjects would have to be kept in identical environments from birth again circling back to ethical concerns. Additionally due to historical and cultural concerns the human body is considered sacrosanct by many cultures thus making the required harvest of samples complicated. Animals in turn have been used for centuries to uncover the mysteries of life to get around this cultural concern. Advances in science within the past two centuries have turned what were explorative and inquisitive studies, simple research, into a highly defined and structured system. The advent of genetic manipulation brought two species to the front, drosophila (fruit flies), and the mouse.

Fruit flies are a fast growing, fast reproducing system that is easy to genetically manipulate (Venken and Bellen 2014). Gene analogs, which are genes that are nearly identical to human gene, in fruit flies allows investigation into gene regulation and basic research within fruit flies that can be extrapolated to humans. There is of course the problem that fruit flies are very different from humans, this is where lower mammals come into play. Mice and rats both reproduce quickly. Mice have the upper hand as they have been used and worked with far more; in turn leading to the creation of simple methods to create genetically modified mice. Importantly as well, laboratory mice are heavily inbred

and are effectively clones of each other. Together these are the core reasons as to why mice are used for medical research. They represent an affordable, fast reproducing, easily manipulatable mammal model to work with. There are still differences between mice and humans, dogs and higher mammals help to bridge this gap but there will always be a need to test new drugs on willing patients at the end stages of drug development. For the basic end of medical research however, animal models work well.

While both species can be manipulated, the mouse is more applicable to medical research. Mice represent a better model than drosophila as they are closer physiologically to humans than drosophila. Considerable effort has been put into development of systematic approaches to modify the mouse genome. Continued work to improve the efficacy of these techniques, which combined with the in-bred mouse lines used in animal work, allows for the generation of modified pure breeding strains (Hall, Limaye et al. 2009). As eluded too, mice have a generational cycle of roughly 2 months. This allows for rapid growth of a colony in addition to the previously mentioned time frame for pure breeding modified strains.

Another aspect of the mouse that makes them viable research subjects is that in most cases human diseases can be closely replicated in the mouse (Bedell, Largaespada et al. 1997). While it is not possible to perfectly replicate conditions from humans into mice, there is enough similarity that the mouse can serve as a good model for many monogenic diseases. Two fields of research that make use of mouse strains and genetically modified mice are muscular dystrophy and diabetes mellitus, both contribute to an early death in humans and most mouse models of the diseases.

The Muscular Dystrophies (MD) are a set of debilitating, lethal myopathies. Individuals with severe forms of MD typically do not survive their second decade (Strehle and Straub 2015). Lose of

mobility appears early on in severe forms of MD and can appear later in life with mild or moderate forms of MD (Guiraud, Aartsma-Rus et al. 2015). Research over the past few decades has prolonged the time before the patients become wheelchair bound and an increase in the life span of patients (Strehle and Straub 2015). This work has not been without side effects however. Corticosteroids are commonly prescribed to maintain mobility early in life but the side effects result in patients discontinuing use (Strehle and Straub 2015). Assisted ventilation has improved mortality; however it requires daily use during sleep (Strehle and Straub 2015).

Due to an increasing life span there has been an increase in the cardiac component of MD mortality (Strehle and Straub 2015). The mutations which cause MD impact the ability of the skeletal muscle cells and cardiomyocytes to properly transfer and manage the stresses involved in muscle contraction (van Westering, Betts et al. 2015). Disruption of these processes leads to tearing of the muscle membrane which alters the intracellular ion concentrations through loss of ion regulation, in turn disrupting proper cell contraction. This cascade of events eventually causes cell death. As the cells die they are replaced by myofibroblasts and fibrotic scar tissue (Guiraud, Aartsma-Rus et al. 2015). Accumulation of fibrosis in the heart ultimately compromises the heart's ability to contract properly by disrupting the propagation of contraction signals. Curing the genetic causes of the disease is ideal. However as MD is always lethal palliative treatments are necessary as an immediate stop-gap until gene therapy has progressed sufficiently to be both safe and effective.

Diabetes Mellitus (DM) comes in two forms. The first is Type 1 Diabetes (T1D), also called juvenile diabetes, it accounts for ~5% of the total population of diabetic patients (ADA). T1D occurs when the body fails to produce insulin (van Belle, Coppieters et al. 2011). This blunts the body's response to ingested sugars. Lose of glucose for energy production forces organs to shift to using fats,

lipids, for their energy. Byproducts of fat consumption accumulate in the blood faster than the body can clear it, resulting in ketoacidosis (van Belle, Coppieters et al. 2011). This condition can lead to a diabetic coma. Prolonged elevated blood glucose will damage all cells and tissues of the body, leading to many serious sequelae.

Type 2 Diabetes (T2D) accounts for the remaining ~95% of diabetes cases in the United States (ADA). T2D is characterized by systemic resistance to insulin (Kharroubi and Darwish 2015). Obesity, sedentary lifestyles, and poor diets all increase the risk of developing T2D (Kharroubi and Darwish 2015). Like T1D, T2D results in elevated blood glucose. Unlike T1D however, it does not develop ketoacidosis in most cases. As ~95% of diabetic patients in the United States have T2D and the epidemic has just begun, we focused our efforts on that form of DM.

Sixty five percent of all diabetes related mortalities are due to cardiovascular complications (CDC). Obese individuals are at greater risk for developing T2D and its cardiovascular complications, one of which is diabetic cardiomyopathy (DC) (Grundy, Benjamin et al. 1999). Elevated circulating and intracellular lipids place metabolic strain on cardiomyocytes as the heart upregulates lipid uptake as a result of insulin resistance but does not upregulate lipid oxidation. Lipid droplets accumulate in the heart as a result of this imbalance and lipotoxicity can occur (Grundy, Benjamin et al. 1999). Over time cellular and tissue damage accumulate, leading to the development of DC.

Metformin, a drug given to pre-T2diabetic and T2D patients to reduce blood glucose levels, is presently understood to work through elevating pAMPK levels (Viollet, Guigas et al. 2012). Elevated pAMPK stimulates skeletal muscle glucose uptake and suppresses liver gluconeogenesis, lowering blood glucose of the individual (Viollet, Guigas et al. 2012). This helps maintain the health of the patient.

Research on mouse models of MD has shown that only a partial restoration of functional dystrophin is required to restore function to near healthy conditions (Godfrey, Muses et al. 2015). This brings hope for researchers and patients as it removes the requirement of near normal restoration and instead allows for drugs that partially restore dystrophin function. Exon skipping and read-through pharmaceuticals benefit from this and show promise that they may be useful to specific populations of patients with MD (Wein, Alfano et al. 2015).

The mdx mouse strain and the strains derived from it are presently the predominately used mouse strains to study muscular dystrophy. First identified in 1977 the mdx mouse is the result of a *de novo* mutation of the dystrophin gene within the C57Bl/10Scsn mouse strain (JAX.org). The mutation caused the formation of a stop codon within the dystrophin gene resulting in loss of the protein. This mimics the genetic mutation known to cause Duchenne Muscular Dystrophy (DMD) in humans. However unlike human patients, mdx mice do not pass away as a result of the disease early in life. Thus the model presents an excellent example of a stop-codon induced loss of dystrophin but not necessarily a good model to test compounds on.

Gamma sarcoglycan is one of four sarcoglycans that form a tetramer in the cell membrane of muscle cells, the sarcolemma. Loss of gamma sarcoglycan in humans results in Limb-Girdle Type 2C muscular dystrophy (LGMD) (Bonnemann and Finkel 2002). This form of muscular dystrophy is less severe than DMD. Whereas DMD affects nearly all muscle, the slow twitch muscles tolerate the condition better for still unknown reasons, LGMD predominately affects muscles closer to the torso of the patient (Bonnemann and Finkel 2002).

Diabetes and Muscular Dystrophy animal models were assessed as separate projects. The diabetes project grew from the (Berhanu, Holley-Cuthrell et al. 2014)(Chapter 3) and (Mull, Berhanu et al. 2014) papers which showed that the MRL mouse has elevated pAMPK in its skeletal muscle and that the mouse resists hyperglycemia following twelve weeks of the high fat diet. A hypothesis then formed stating that the MRL heart would be protected from the high fat diet and obesity by elevated pAMPK levels. This hypothesis was examined in Chapter 4 of this document. Presently the mdx mouse is the mouse model of choice for muscular dystrophy research. However the time required for the mice to sufficiently develop the condition is prolonged for the needs of research. The DBA2/J gamma sarcoglycan knock out mouse has been used more recently by the McNally lab formerly of University of Chicago. They were gracious enough to supply the laboratory with breeding pairs to propagate the mutant strain at UIC. These animals were compared against the mdx mouse in Chapter 3 of this document.

B. **References**

Bedell, M. A., D. A. Largaespada, et al. (1997). "Mouse models of human disease. Part II: recent progress and future directions." Genes & development **11**(1): 11-43.

Berhanu, T. K., J. Holley-Cuthrell, et al. (2014). "Increased AMP-activated protein kinase in skeletal muscles of Murphy Roth Large mice and its potential role in altered metabolism." Physiological reports **2**(3): e00252.

Bonnemann, C. G. and R. S. Finkel (2002). "Sarcolemmal proteins and the spectrum of limb-girdle muscular dystrophies." Seminars in pediatric neurology **9**(2): 81-99.

Godfrey, C., S. Muses, et al. (2015). "How much dystrophin is enough: the physiological consequences of different levels of dystrophin in the mdx mouse." Human molecular genetics **24**(15): 4225-4237.

Grundy, S. M., I. J. Benjamin, et al. (1999). "Diabetes and cardiovascular disease: a statement for healthcare professionals from the American Heart Association." Circulation **100**(10): 1134-1146.

Guiraud, S., A. Aartsma-Rus, et al. (2015). "The Pathogenesis and Therapy of Muscular Dystrophies." Annual review of genomics and human genetics.

Hall, B., A. Limaye, et al. (2009). "Overview: generation of gene knockout mice." Current protocols in cell biology / editorial board, Juan S. Bonifacino ... [et al.] **Chapter 19**: Unit 19 12 19 12 11-17.

Kharroubi, A. T. and H. M. Darwish (2015). "Diabetes mellitus: The epidemic of the century." World journal of diabetes **6**(6): 850-867.

Mull, A. J., T. K. Berhanu, et al. (2014). "The Murphy Roths Large (MRL) mouse strain is naturally resistant to high fat diet-induced hyperglycemia." Metabolism: clinical and experimental **63**(12): 1577-1586.

Strehle, E. M. and V. Straub (2015). "Recent advances in the management of Duchenne muscular dystrophy." Archives of disease in childhood.

van Belle, T. L., K. T. Coppieters, et al. (2011). "Type 1 diabetes: etiology, immunology, and therapeutic strategies." Physiological reviews **91**(1): 79-118.

van Westering, T. L., C. A. Betts, et al. (2015). "Current understanding of molecular pathology and treatment of cardiomyopathy in duchenne muscular dystrophy." Molecules **20**(5): 8823-8855.

Venken, K. J. and H. J. Bellen (2014). "Chemical mutagens, transposons, and transgenes to interrogate gene function in Drosophila melanogaster." Methods **68**(1): 15-28.

Viollet, B., B. Guigas, et al. (2012). "Cellular and molecular mechanisms of metformin: an overview." Clinical science **122**(6): 253-270.

Wein, N., L. Alfano, et al. (2015). "Genetics and Emerging Treatments for Duchenne and Becker Muscular Dystrophy." Pediatric clinics of North America **62**(3): 723-742.

II: Muscular Dystrophy comparison of the DBA2/J-sgcg mouse versus the mdx mouse

The following has been replicated directly from the 2015 publication under the Creative Commons from the article: Nathan W. Roberts, Jenan Holley-Cuthrell, Magdalis Gonzalez-Vega, Aaron J. Mull, and Ahlke Heydemann, "Biochemical and Functional Comparisons of mdx and Sgcg−/− Muscular Dystrophy Mouse Models," BioMed Research International, vol. 2015, Article ID 131436, 11 pages, 2015. doi:10.1155/2015/131436

A. **Abstract**

Numerous mouse models have been indispensable for translational research progress. From etiology, diagnosis, prognosis, to potential treatments, the mouse models have provided an essential platform to investigate each of these facets of human diseases. Muscular dystrophy (MD) is the most common human genetic disease occurring in approximately 1 in 2500 births. It is therefore critically important to identify adequate models for this disease. The mdx mouse, which is dystrophin-deficient, has long been used to model this disease. However, this mouse strain displays a rather mild disease course compared to human patients. The mdx mice have been bred to additional genetically engineered mice to worsen the disease. Alternatively, other genes which cause human MD have been genetically disrupted in mice. We are now comparing disease progression from one of these, the ɣ-sarcoglycan null mouse on the DBA2/J background Sgcg-/-, to the mdx mouse line. The Sgcg-/- mice have a more severe phenotype than the mdx mice. Muscle function was assessed by plethysmography and echocardiography. Histologically the Sgcg-/- mice displayed increased fibrosis and variable fiber size. By quantitative Evan's blue dye uptake and hydroxyproline content two key disease determinants, membrane permeability and fibrosis respectively, were also proven worse in the Sgcg-/- mice.

B. Introduction

A satisfactory mouse model is required to fight the devastating effects of Muscular Dystrophy (MD). The mouse model must mimic the human disease in etiology, pathology and potential therapy responses to be optimally useful. In the experiments presented in this manuscript we directly compared the progressive pathology of two MD mouse models side-by-side to identify the most severe and therefore the most human-similar and useful model. We produced comparative time-courses of disease progression of the mdx and ɣ-sarcoglycan null mice (official nomenclature, Dmdmdx and Sgcg-/-D2) using; quantitative membrane permeability and fibrosis assessments, plethysmography, and echocardiography.

Muscular dystrophy in humans is caused by mutations in a number of genes. The genes can be divided into 4 loosely aligned functional classes 1) dystrophin glycoprotein complex (DGC), which includes dystrophin and the sarcoglycans, (Figure 1A) 2) extracellular matrix genes, 3) nuclear membrane genes, and 4) signaling molecules. By far the most frequent mutations are found in the DGC component dystrophin, these mutations cause Duchenne (DMD) or Becker muscular dystrophies in humans and mdx in mice. Mutations in the ɣ- sarcoglycan gene of the DGC cause limb girdle muscular dystrophy type 2C (LGMD-2C) in humans and are designated Sgcg-/- in mice.

The pathology and treatments of human DMD and LGMD-2C are severe and similar (Noguchi, McNally et al. 1995). After the initial disruption of the DGC, disease progression follows a very similar course (Figure 1B). 1) Membrane permeability followed by mislocalized calcium, nitric oxide and other signaling moieties. 2) Repeated rounds of degeneration and regeneration. 3) Inflammation. 4) Necrosis. 5) Replacement with myofibroblasts and scar tissue leading to functional decline. These events do not occur in strict sequence and in a single muscle all of these events are occurring at the same time. The

mdx and Sgcg-/- mice also display the same disease progression, but, as we will demonstrate at different severity levels.

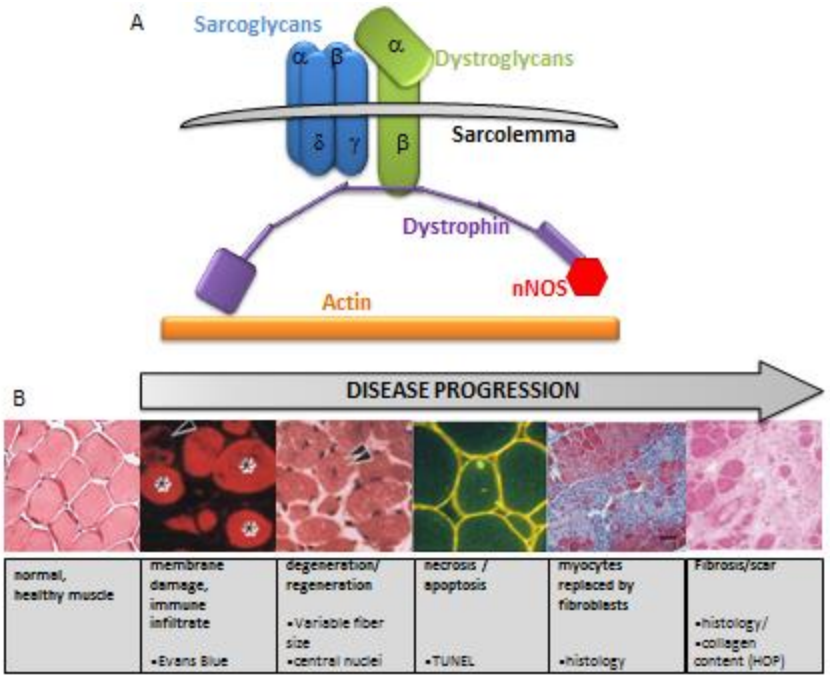

Figure 1-The Dystrophin Glycoprotein Complex and Muscular Dystrophy Pathology in mice. A. Muscular Dystrophy can occur from mutations in the genes that form the Dystrophin Glycoprotein Complex. B. Representative images demonstrating disease progression of muscular dystrophy in a mouse model.

As DMD is the most common form of human muscular dystrophy, the dystrophin deficient mdx mouse is the most commonly used animal model to represent this disease. The mdx mutation was spontaneously identified in a colony of C57Bl/10 mice (Bulfield, Siller et al. 1984). It was later identified to be in the dystrophin gene (Ryder-Cook, Sicinski et al. 1988), which was also identified to be causative for DMD (Hoffman, Brown et al. 1987). The originally mutated mouse was identifiable because the dystrophin gene is on the X-chromosome and the original male could be assessed in the hemizygous state.

However, the mdx mouse model is not an adequate representation of the human disease. The only muscle that is consistently affected is the diaphragm, which shows membrane permeability and fibrotic replacement (Stedman, Sweeney et al. 1991). In addition, the mdx mice have a peak of pathology at 4 weeks old and otherwise the mice have very little pathology (reviewed in (Banks and Chamberlain 2008)).

Additional genetic engineering and breeding have been conducted to worsen the disease. A double knockout was generated with both dystrophin and its homolog uthrophin deleted. These mice are severely affected and only half live beyond 8 weeks old (Grady, Teng et al. 1997). Recently another combination, knocking out both dystrophin and telomerase also caused a very severe phenotype (Sacco, Mourkioti et al. 2010). Neither of these mice represents the etiology of humans suffering from this disease. And the models are more severe than the human disease and therefore are not fully suitable for research.

The mouse model we are assessing is the genetically engineered ɣ-sarcoglycan (Sgcg-/-) null mutation (Hack, Ly et al. 1998) on the DBA/2J (D2) background (Heydemann, Huber et al. 2005). In the

original publication, it was identified that the Sgcg-/- mice on the mixed C57Bl/6J - 129 background have a more severe cardiomyopathy than the mdx mice (Hack, Ly et al. 1998). It was then demonstrated that the Sgcg-/- mutation is more severe when bred onto the D2 background (Heydemann, Huber et al. 2005). The D2 mice carry a naturally occurring in-frame deletion within their Latent TGFβ Binding Protein 4 (LTBP4) gene; the deletion segregates at a high level with severe disease (Heydemann, Ceco et al. 2009). The deletion causes a further increase in the already MD-elevated levels of active TGFβ, which caused the excessive fibrosis observed in the Sgcg-/-D2 mice over three other comparison strains (Heydemann, Ceco et al. 2009). The D2 mouse strain also carries the Dyscalc, naturally occurring polymorphism. This locus is linked to increased cardiac fibrosis in these mice even in the wild type mice (Ivandic, Qiao et al. 1996). The causative gene is still under dispute; Abcc6 (Meng, Vera et al. 2007) or Emp3 (Aherrahrou, Doehring et al. 2007). Further breeding with the mdx mutation, demonstrated that the mdx mutation presents more severely when bred onto the (D2) background (Fukada, Morikawa et al. 2010).

The ultimate usefulness of animal models is in the testing of potential patient therapies. Currently MD patients receive corticosteroids to diminish the skeletal deformities associated with MD and to keep the patients mobile as long as possible. Corticosteroids have not been proven useful in the animal models (Guerron, Rawat et al. 2010), they have limited usefulness in humans as well. They are associated with significant side-effects (Bianchi, Mazzanti et al. 2003; Tidball and Wehling-Henricks 2004) and are not tolerated well for the long periods required for this chronic disease (Bianchi, Mazzanti et al. 2003; Tidball and Wehling-Henricks 2004). Recently, it is also advised to prophylactically prescribe angiotensin receptor blockers or angiotensin converting enzyme inhibitors (reviewed in (Matsumura 2014)). Angiotensin receptor blockers have shown efficacy in both the mdx mouse model (Spurney, Sali et al. 2011) and in humans (Viollet, Thrush et al. 2012). Furthermore, two of the most promising future

therapies for a subset of MD patients are exon-skipping and read-through technologies (Bertoni, Lau et al. 2003; Welch, Barton et al. 2007). Both of these therapies, now on the brink of phase 2 and 3 trials, have proven efficacious in restoring dystrophin expression in the mdx mouse model (Echigoya and Yokota 2014). These two therapies are examples from many more promising therapies justifying the further production and use of MD mouse models.

C. **Materials and Methods**

Animals- Mice were housed following UIC, national and international animal welfare protocols. A 12 hour light/dark cycle is kept year round within the animal facility, food and water are ad libitum. The mice are watched by the veterinary staff of the Biological Research Laboratory at UIC. Animals were housed 5 to a cage after weaning. DBA2/J (D2) mice with the Sgcg +/- were graciously provided by Dr. Elizabeth McNally. The mice have since been bred using Het (Sgcg +/-) x Het breeding pairs and randomized selection of breeds to reduce user induced genetic drift. Het x Het and Het x KO (Sgcg -/-) breeding pairs were established to provide the necessary animals for this study. Mdx mice were acquired from Jackson Laboratories (Bar Harbor Maine); they were housed in the animal facility to ensure identical environments.

Histology- Following harvest the tissues designated for paraffin imbedding were placed into 1.5ml tubes filled with 1 ml of neutral buffered formalin. The fixed tissues were taken to the UIC RRC Histology Core for paraffin imbedding, slicing, Masons Trichrome, Pico Sirius Red, and H&E staining. The resulting slides were imaged on an Aperio ScanScope CS (Leica Biosystems, Nussloch Germany) whole slide imager. Image Scope (Leica Biosystems) was used to visualize the slide images for analysis. ImageJ was used to quantify fiber size variability.

Evans Blue Dye (EBD) –Two days before harvest each mouse is injected with EBD (Sigma Aldrich) at 5ul per gram of animal weight. EBD at 10 mg/ml in PBS was aliquoted and stored at -20C. Following sacrifice, tissue samples were minced and weighed in pre-labelled 1.5 ml tubes. The tissues were frozen in liquid nitrogen and stored at -80C until processing. Tissues to be assayed were removed from the -80 freezer and 1ml of Formamide (Sigma Aldrich) was added to each sample. The samples were then mixed by vortexing and incubating at 55^{o}C for two hours. Following incubation the samples are mixed again by vortexing and spun down at 3k rpm for 1 minute. 200 ul of each sample and standards in triplicate (0 ug, 0.625 ug, 1.25 ug, 2.5 ug, 5 ug, 10 ug, 20 ug of EBD) were transferred to a corresponding well in a 96 well plate, then assessed on a Bio-Tek Synergy HT plate reader at 620 nm. The standards are used to create a linear fit equation, which is then used to calculate the ug EBD concentration of each sample. The ug EBD concentration of each sample is then divided by the initial tissue weight giving a measure of ug EBD / mg tissue weight for each sample. All samples are normalized to the kidney average to mitigate possible injection errors and equalize the dose between mice.

Hydroxyproline Assay (HOP)- The HOP protocol used follows a modified protocol from Flesch et. al. (Flesch, Schiffer et al. 1997). Tissue samples were minced and weighed in pre-labelled 1.5ml tubes. 1 ml of 6M hydrochloric acid (Sigma Aldrich, St. Louis, MO) was added to each tube. The tubes were heated at 105^{o}C for 3 hours. After the heating period the samples were removed from the heat and left to cool to room temperature. 10 ul of each sample was added to a clean, labelled, 1.5ml tube with 150 ul of isopropanol. After being mixed, 75 ul of Solution A (1 part Chloromine T (70 mg chloromine T (Sigma Aldrich) + 1 ml H2O) to 4 parts Acetate Citrate Buffer (57 g of Sodium Acetate (Sigma Aldrich), anhydrous, 435 ml of 1M NaOH, 33.4 g of Citric Acid (Sigma Aldrich), 385ml of Isopropanol, water to 1 liter). The samples are inverted twenty times and left to sit at room temperature for 10 minutes. Immediately following that, 1 ml of Solution B (3 parts Ehrlich's Reagent (3g of p-

dimethylaminobenzaldehyde (Sigma Aldrich), 10ml of EtOH, 675 ul of sulfuric acid (Thermo Fischer Scientific, Waltham MA) (mixed in drop by drop) to 13 parts isopropanol) was added. The samples are again inverted twenty times to mix and then immediately placed into a 58^{o}C water bath. Following a 30 minute incubation the samples are removed from the water bath, quickly mixed, and then buried in ice to quench the reaction. Cooled samples are then spun at 5k for 1 minute, 200 ul of each sample is moved to a corresponding well in a 96 well plate. Along with standards in triplicate (0, 50, 100, 500, 100, 500, 1000, 2000 mM Hydroxyproline (Sigma Aldrich)) the samples are assessed by a Bio-Tek Synergy HT (Bio-Tek, Winooski VT) plate reader at 558 nm. The standards are used to create a linear fit equation, which is then used to calculate the mM hydroxyproline concentration of each sample. The mM hydroxyproline concentration is then divided by the initial tissue weight, giving a final mM hydroxyproline / tissue weight (mg) concentration for each sample.

Plethysmography – Three days before harvest respiratory function was assessed for each mouse. The Buxco Small Animal Plethysmography (Buxco/DSI, St. Paul MN) set-up, using FinePointe (Buxco/DSI) was used. In brief, the machine is calibrated before each day's assessments. Mice are loaded into chambers individually, given an adjustment period, and then assessed for 15 minutes each. Each animal is assessed in at least two chambers sequentially. Breath frequency (f) was used to cull extraneous data sets from any instances in which the animal may have held its breath or breathed very rapidly. This was done by finding the average f for each mouse per total session. Standard deviation was calculated by Microsoft Excel and any data sets falling outside of 1 standard deviation were removed from that individual mouse's data set. The new average for each mouse was then calculated. Enhanced pause (Penh) is a mathematical comparison between early and late expirations a higher value represents increased pathology due to slower – more fibrotic - late expiration. It is calculated by

FinePointe as Penh = (PEF/PIF) x (Te/Rt -1), where PEF = peak expiratory height, PIF = peak inspiratory height, Te = Expiratory time, Rt = Time to expire 65% of the volume.

Echocardiography – Cardiac function was assessed by Dr. Robert Gaffin of the UIC Center for Cardiovascular Research Physiology Core Labs using a Vevo 2100, with the manufacture's supplied software.

Statistics - Statistical analysis was performed using Student T-tests on Microsoft Excel.

D. Results

Multiple murine muscular dystrophy mouse lines have been utilized by researchers to investigate the etiology, pathology and possible treatments for various forms of this devastating disease. In addition, various comparisons have also been conducted ((Heydemann, Huber et al. 2005; Fukada, Morikawa et al. 2010; Gibertini, Zanotti et al. 2014) as examples) to identify the proper model for each experiment. We now present data comparing two mutations which model the most common form of MD; that of muscular dystrophy generated by mutations within the dystrophin-glycoprotein proteins. We have time course comparisons of biochemical, histological and functional characterizations for the mdx and Sgcg-/-D2 mouse strains.

Animal Weights

Animal weights are an initial test of MD disease severity. It is well known that mild MD is associated with an increase in animal mass. Alternatively, a more severe MD is associated with decreased animal mass, likely as a result of muscle atrophy (Connolly, Keeling et al. 2001; Heydemann, Huber et al. 2005). Others have reported that the mdx mice gain weight with respect to their littermate

controls (Connolly, Keeling et al. 2001); indicating a mild disease course, and presumably due to hypertrophy. We now show that the Sgcg-/-D2 mice trend to lower weights than their WT controls at 4 and 12 weeks (Figure 2). We also show these animal weights to aid in the comparative analysis of the functional assessments below.

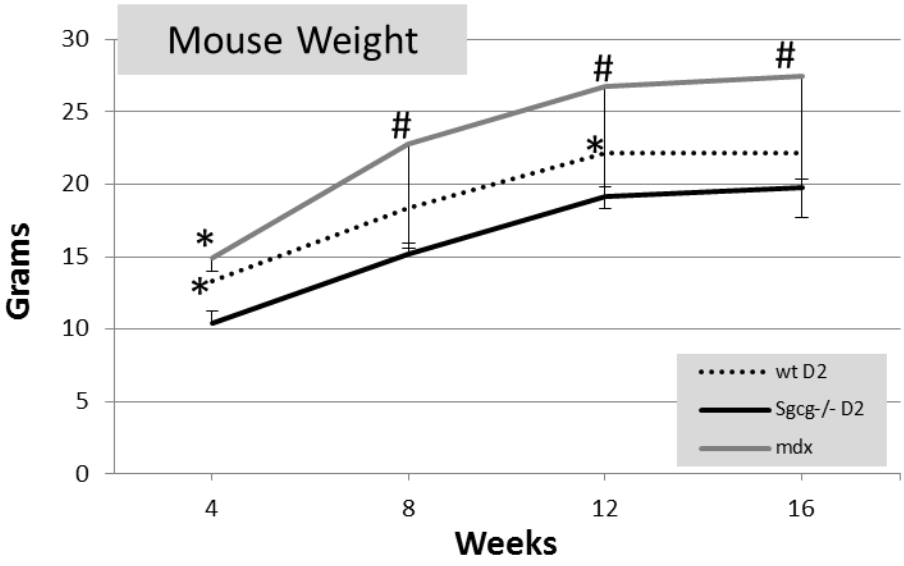

Figure 2- Consistent with severe pathology the Sgcg-/- D2 mice weighed less that their wild type D2 controls throughout the 16 weeks. Wild type D2 mice weighed significantly more than the Sgcg -/- D2 mice at 4 and 12 weeks. *$p<0.05$ significance by Student's T-Test, versus Sgcg -/- D2 animals. n=4-20.

Histologic Assessments

The Sgcg-/-D2 quadriceps muscles have increased fibrosis, increased variation in fiber size and increased central nuclei compared to age matched mdx mice (all 12 week-old, Figure 3). In quadriceps the Picrosirius Red staining indicates increased red, fibrotic areas in the Sgcg-/- D2 tissues (Figure 3). Similarly, the representative Hematoxylin and Eosin (H&E) images demonstrate larger blue/purple, fibrotic regions in the Sgcg-/-D2 mice in quadriceps. Quadriceps muscles from two mdx and two Sgcg-/-D2 mice were quantified for fiber size variability (FSV) with ImageJ software. As only two quadriceps were compared, statistics were not performed, but the values with standard error are indicated in the insets (Figure 3). The Sgcg-/-D2 mice had a wider variation in fiber size (Sgcg -/- D2 3453+/-2023 mm and mdx 2470+/-1830) indicating more ongoing regeneration and a more severe phenotype.

As expected the diaphragms from both mouse groups contained predominant interstitial fibrosis (central panels, Figure 3) and were several cell layers thicker than wild type (wild type images in (Hack, Ly et al. 1998; Heydemann, Huber et al. 2005)). The Sgcg -/- D2 diaphragms contained the most fibrotic areas by Picrosirius Red staining and the largest accumulation of blue/purple regions in the H&E stained sections.

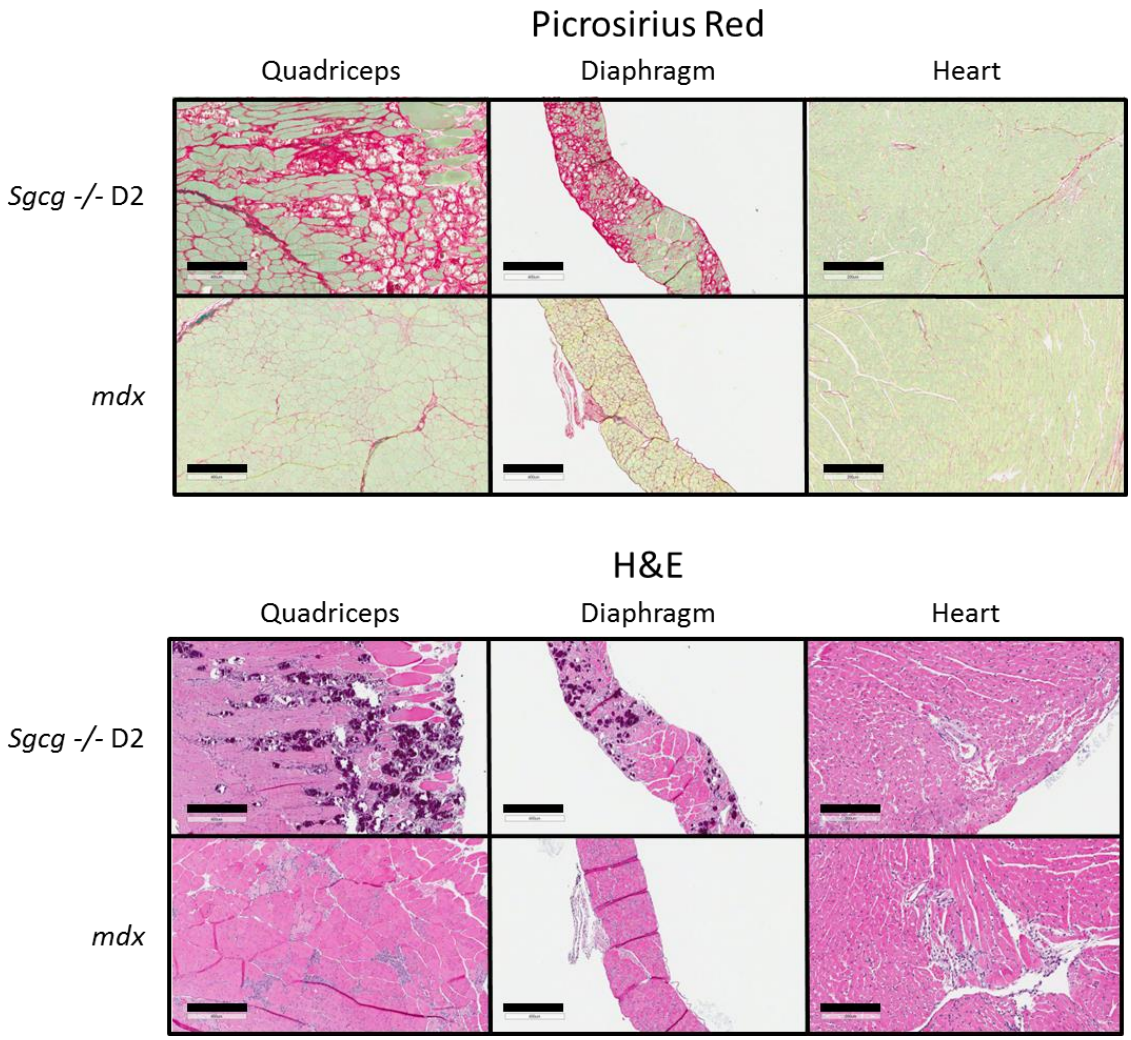

Figure 3- The Sgcg -/- D2 mice displayed the most severe pathology in histochemical assessments. By Picorsirius Red staining the quadriceps and diaphragm of the Sgcg-/- D2 displayed far more red regions which correspond to fibrotic scarring than the mdx tissues. The Hematoxylin and eosin pictures demonstrated the same fibrosis. The fibrosis in the cardiac left ventricles appeared quite similar between the two genotypes. Both mouse models demonstrated interstitial and perivascular fibrosis. Quadriceps and Diaphragm legend bars represent 400um, Heart legend bars represent 200um.

The cardiac ventricles appeared similarly affected by the muscular dystrophy pathology. Both images demonstrate interstitial and perivascular fibrosis. In addition the mdx heart contains some myofibroblast replacement of myofibers in the central portion of the H&E image.

Membrane Permeability

We assessed membrane permeability by quantitatively measuring the amount of Evans blue dye (EBD) that entered the damaged muscle fibers (Heydemann, Huber et al. 2005). EBD binds albumin and only enters damaged muscle fibers (Matsuda, Nishikawa et al. 1995). The Sgcg-/-D2 skeletal muscle had significantly higher membrane permeability at 12 weeks across all four tissues assessed. Additionally the Sgcg -/- D2 mice had greater membrane permeability at 8 weeks in the Gastrocnemius/Soleus and at 8 and 16 weeks in the Gluteus/Hamstrings. Interestingly at 16 weeks an improvement in membrane permeability was identified in all Sgcg -/- D2 skeletal muscles assessed (Figure 4). The mdx disease was most severe at the 4 week time point which was also followed by an improvement (Figure 4). This result is consistent with published reports that the mdx limb based skeletal muscles are severely affected at 4 weeks old and then improve (DiMario, Uzman et al. 1991; Connolly, Keeling et al. 2001). This indicates that the Sgcg-/- D2 mice succumb more severely to early disease pathology than the mdx mice and that both recover slightly due to as yet unknown reasons.

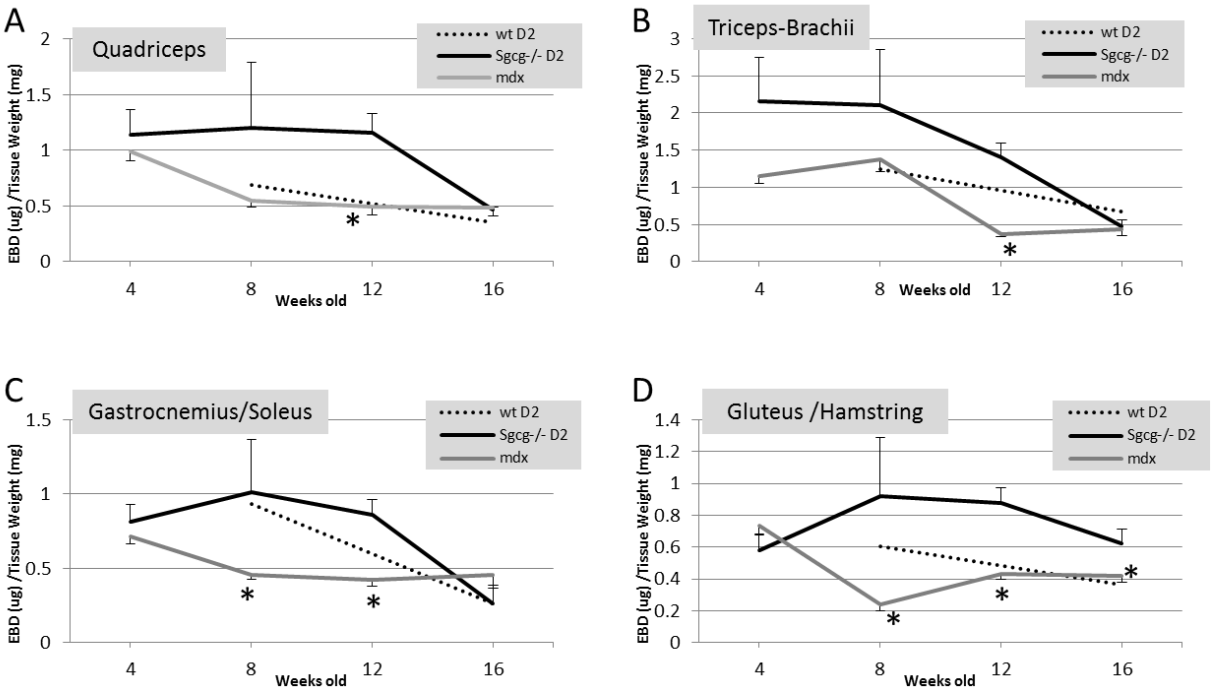

Figure 4- The Sgcg -/- D2 muscles demonstrated significantly increased membrane permeability at 12 weeks old. A. Sgcg -/- D2 mice showed statistically higher EBD in their Quadriceps at 12 weeks compared to the mdx mice. B. Sgcg -/- D2 mice showed statistically higher EBD in their Triceps-Brachii at 12 weeks compared to the mdx mice. C. Sgcg -/- D2 showed statistically higher EBD in their Gastrocnemius and Soleus at 8 and 12 weeks compared to the mdx mice. D. Sgcg -/- D2 Gluteus and Hamstrings showed higher EBD than the mdx mice at 8, 12, and 16 weeks. *$p<0.05$ significance, versus Sgcg -/- D2 animals. Sgcg +/+ D2 at 4, 12 weeks n=0, all others n=3-15.

Collagen Content

To assess fibrosis we performed a quantitative hydroxyproline assay on the harvested muscles (Heydemann, Huber et al. 2005). Hydroxyproline is a modified amino acid, which is only present in collagen, and therefore is a quantitative marker for intramuscular fibrosis. The Sgcg-/- D2 muscles contained the largest amount of hydroxyproline in all limb-based muscles tested at almost all ages (Figure 5). This increase was significant in quadriceps at 12 and 16 weeks, in triceps-brachii at all times tested, in gastrocmemius/soleus at 12 weeks and gluteus/hamstring at 12 weeks. The only point when the mdx tissue contained more hydroxyproline was at 4 weeks in the gluteus/hamstring. Once again, the phenotype of the Sgcg-/-D2 mice progressively worsened until 12 weeks of age and then improved, while the mdx mouse phenotype improved after 4 weeks of age.

The fibrosis content of the diaphragm was considered separately. The diaphragm develops differently than the limb-based skeletal muscles (Merrell and Kardon 2013), is innervated differently (Merrell and Kardon 2013), contains fewer Pax7 positive cells (Bosnakovski, Xu et al. 2008), and is more severely affected in the mdx mice ((Stedman, Sweeney et al. 1991), Figure 5), Sgcg-/-D2 mice ((Heydemann, Huber et al. 2005), Figure 5). The time-course pattern of diaphragm fibrosis is different than the other muscles (Figure 5). Comparing the mdx and Sgcg-/-D2 diaphragm fibrosis revealed no significant differences.

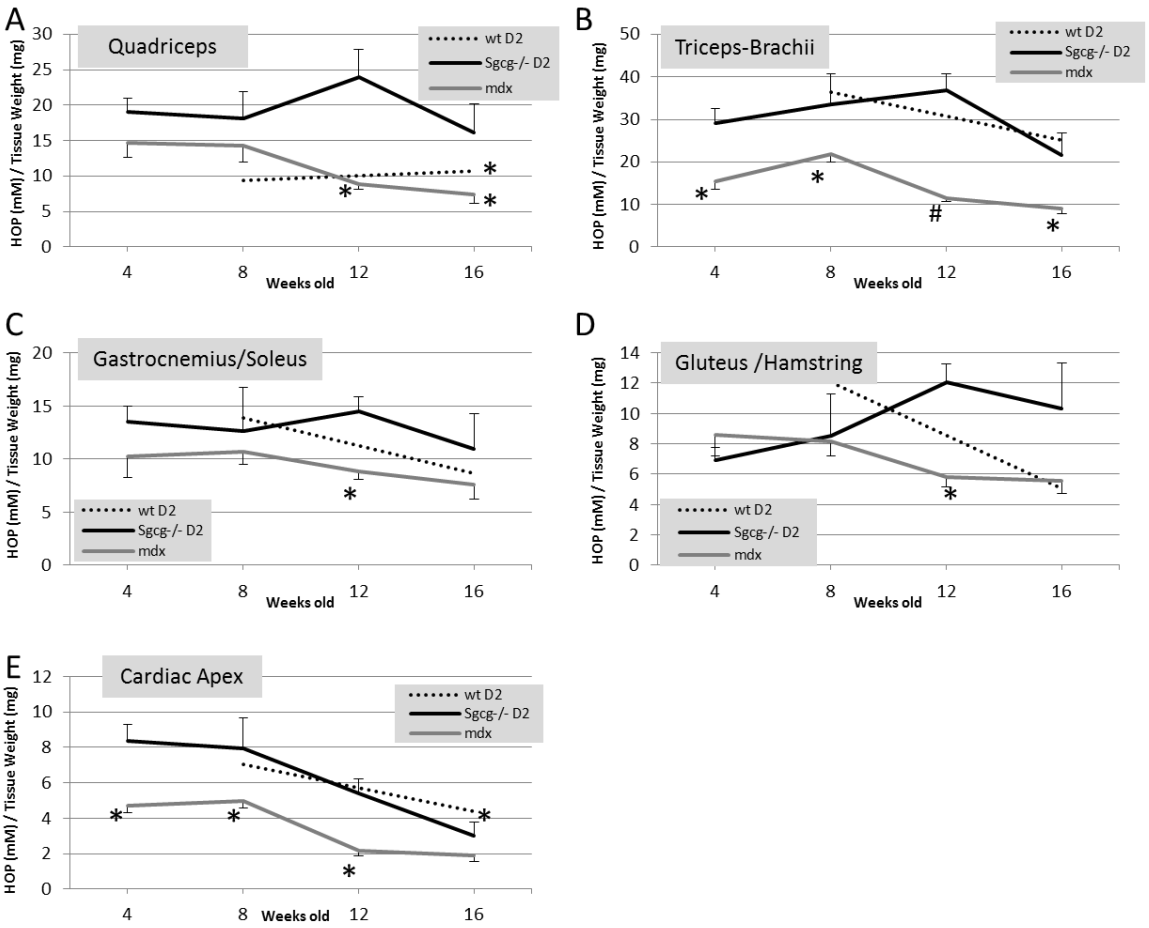

Figure 5-The Sgcg-/- D2 muscles were consistently more fibrotic than the age matched mdx mice by hydroxyproline assay. Sgcg -/- D2 mice showed significantly higher levels of Quadriceps fibrosis at 12 and 16 weeks versus the mdx mice and significantly more fibrosis than their Sgcg +/+ D2 controls at 16 weeks. Sgcg -/- D2 mice had significantly higher fibrosis content in their Triceps-Brachii at all time points compared to the mdx mice. At 12 weeks Sgcg -/- D2 mice have higher fibrosis content than the mdx mice in their Gastrocnemius/Soleus muscles. A similar pattern was seen in the Gluteus/Hamstring muscle group, the Sgcg -/- mice had significantly higher fibrosis content at 12 weeks than the mdx mice. Sgcg -/- mice showed greater collagen content at 4, 8 and 12 weeks compared to the mdx mice. Additionally the Sgcg +/+ mice had higher collagen content than the Sgcg -/- mice at 16 weeks. *p<0.05, #p<0.001 significance, versus Sgcg -/- D2 animals. Sgcg +/+ D2 at 4 and 12 weeks n=0, Sgcg +/+ D2 at 8 weeks n=2, all others n=3-16.

The cardiac ventricle fibrosis also displayed a different pattern than the limb based skeletal muscles (Figure 5F). Mdx mice had less cardiac fibrosis than the Sgcg -/- animals at all ages and this reached significance at 4, 8, and 12 weeks. Interestingly, by 16 weeks of age the HOP values showed no significant differences. Furthermore, hearts from both animal groups demonstrated reduced fibrosis after 8 weeks of age.

Plethysmography

We also analyzed the two different MD mouse models for respiratory function. Plethysmography is an often used and reliable assessment technique of diaphragm function (Huang, Cheng et al. 2011; Nelson, Hunter et al. 2011). The diaphragm is normally very thin and very pliable. In muscular dystrophy the diaphragm becomes thick and rigid due to scar tissue (Heydemann, Huber et al. 2005). Once rigid, the lungs require extended time for inspiration and expiration and a longer pause is apparent on the breath wave (Huang, Cheng et al. 2011; Nelson, Hunter et al. 2011). These three metrics (times of inspiration, expiration and pause) all measure the elasticity of the diaphragm – and to a lesser extent the strength of the intercostal muscles.

No difference was found in the Penh value between any of the D2 groups examined. The Sgcg -/- D2 animals had significantly longer time inspiration (Ti) and time expiration (Te) than the mdx mice at 8, 12, and 16 and 12 and 16 weeks respectively. Additionally the Sgcg -/- D2 animals had significantly slower peak flows for inspiration and expiration (Figure 6D and F). Consistent with the longer inspiration and expiration parameters the Sgcg-/- D2 mice had significantly reduced breath frequency (Figure 6B). The remainder of the plethysmography data can be accessed online in Supplemental Figure 1; when evaluating some of these parameters please be aware that the mdx mice are significantly larger than the D2 mice (Figure 8) and that this will affect many of the volume calculations.

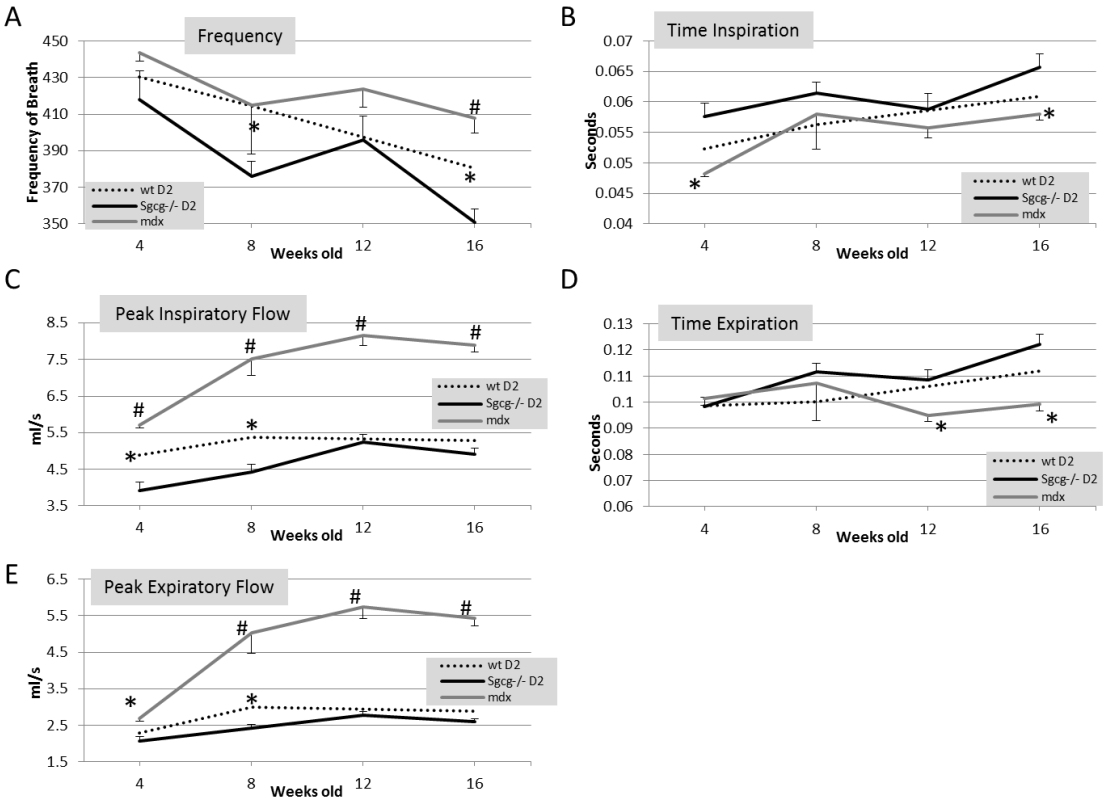

Figure 6-The Sgcg -/- D2 mice consistently had a more severe respiratory phenotype by plethysmography then the mdx animals. A. At 8 and 16 weeks the Sgcg -/- D2 mice breathed significantly slower than the Sgcg +/+ D2 mice. At 16 weeks the Sgcg -/- D2 mice also breathed significantly slower than the mdx mice. B. Sgcg -/- D2 mice inhaled (Ti) slower than the mdx mice at 4 and 16 weeks. C. Sgcg -/- D2 mice had a lower peak inspiratory flow (PIFb) than the mdx mice at all time points, and lower than the Sgcg +/+ D2 mice at 4 and 8 weeks. D. Sgcg -/- D2 mice exhaled slower than the mdx mice at 12 and 16 weeks. E. Sgcg -/- D2 mice had a lower peak expiratory flow (PEFb) than the mdx mice at all time ponts, and lower flow than the Sgcg +/+ D2 at 8 weeks. *p<0.05, #p<0.001 significance, versus Sgcg -/- D2 animals. Sgcg +/+ D2 at 12 weeks n=0, all others n=4-10

Our data is consistent with previous plethysmography data. The following parameters were shown for 12 week old mdx mice; frequency, PIF and PEF to be similar to the numbers presented in the current manuscript (Huang, Cheng et al. 2011). These parameters were all statistically different then the wild type B10 mice used as controls in that experiment. The mdx animals had pathologically lower frequency of breaths, and decreased peak flows.

Echocardiography

To further assess the functional effects of MD on these two mouse strains an echocardiography time-course was conducted. Despite demonstrating increased ventricular fibrosis (Figure 5E), the Sgcg-/- D2 animal's cardiac function was preserved at wild type levels (Figure 7). The mdx animals had significantly higher isovolumetric relaxation time (IVRT), and smaller fractional shortening and ejection fraction. The first demonstrating diastolic dysfunction and the latter two demonstrating systolic dysfunction in the mdx animals. Pulmonary artery acceleration time (PAAT) is a surrogate measure of pulmonary hypertension. A decrease in PAAT indicates increased pulmonary hypertension. PAAT was lower in the Sgcg-/- D2 animals than the mdx and significantly lower at 8 weeks of age, indicating the Sgcg-/- D2 animals were more severely affected than the mdx mice. Please see supplemental figure 2 for complete echocardiography data, and again caution comparing values which are mouse size dependent.

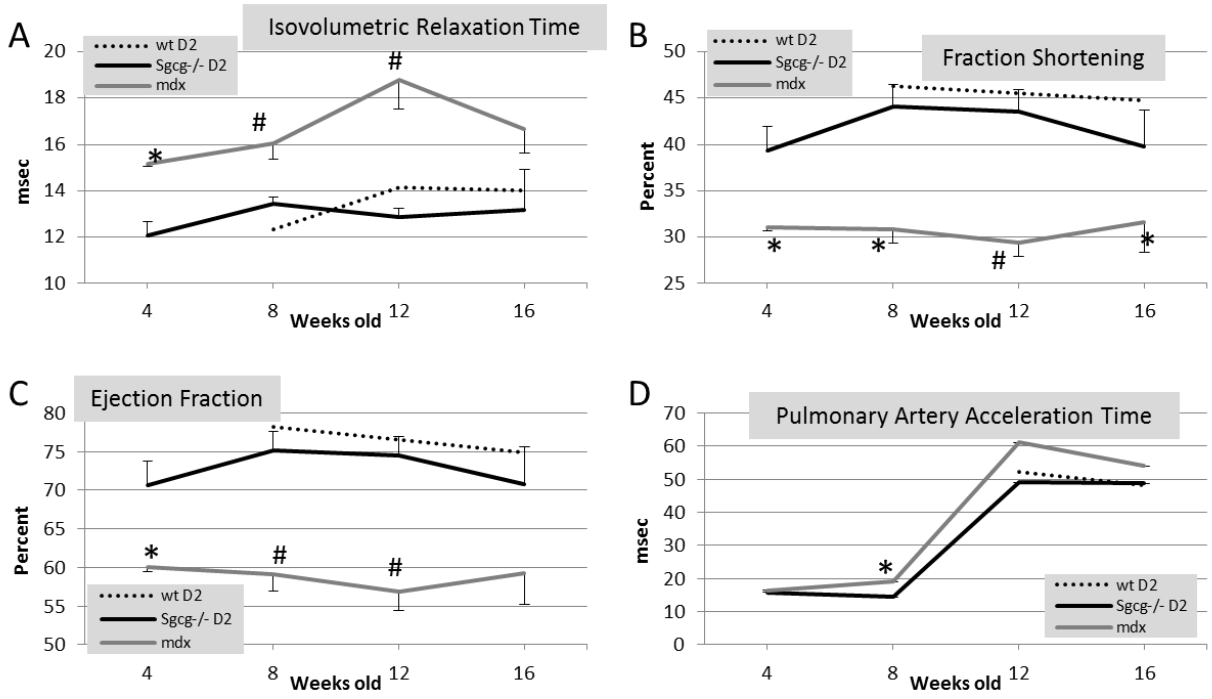

Figure 7-The mdx mice demonstrated a more severe cardiac functional pathology. A. Sgcg -/- D2 mice had a shorter isovolumetric relaxation time (IVRT) than the mdx mice at all time points. B. The Sgcg -/- mice have a higher fractional shortening (FS%). C. Sgcg -/- have a greater ejection fraction (EF%) than the mdx mice at 4, 8, and 12 weeks. D. Pulmonary artery acceleration time (PA AT) was lower in the Sgcg -/- mice at 8 weeks compared to the mdx mice. *$p<0.05$, #$p<0.001$ significance, versus Sgcg -/- D2 animals. Sgcg +/+ D2 at 4 weeks n=0, all others n=4-23.

Despite increased fibrosis in the Sgcg-/- D2 hearts (Figure 5E) and previous publications (Hack, Ly et al. 1998), the mdx mice demonstrated significantly more severe cardiac pathology by echocardiography. Currently we do not have a full explanation for this, although it is obvious that fibrosis is only one of many pathologic occurrences in a muscular dystrophic heart. Conduction system defects have been identified in the mdx mouse heart (Branco, Wolf et al. 2007). In addition calcium is mislocalized in dystrophy (Dunn and Radda 1991) and therefore excitation and contraction will be detrimentally affected.

E. **Conclusion**

Animal models are an essential part of investigating disease etiology, progression and preclinical trials. As muscular dystrophy is the most prevalent human genetic disease these mouse models are essential and a clear understanding of their pathology is required, including comparisons between those models already available. Multiple mouse model comparisons have previously been conducted. Pertinent to the current manuscript, is a comparison between the same mdx mutation breed onto and compared between the C57BL/10 and the D2 mouse strains (Fukada, Morikawa et al. 2010). The mutation was identified to be more severe on the D2 background by muscle weights, fewer myofibers, increased fibrosis and decreased strength. These authors identified that the D2 mouse strain has decreased satellite cell self-renewal and reasoned that this was the pertinent phenotypic causing difference (Fukada, Morikawa et al. 2010). An additional pair of manuscripts phenotypically described the Sgcg-/- mutation in four commonly used strains (Heydemann, Huber et al. 2005). The D2 mice were found to have the most severe disease and using GWAS this was found to be largely due to a deletion within the Latent TGFβ Binding Protein 4 (Heydemann, Ceco et al. 2009). We now wished to directly compare the severe Sgcg-/-D2 mouse to the highly used mdx mouse histologically, biochemically and functionally.

The Sgcg-/- mice were found to have increased membrane permeability and fibrosis in the limb based skeletal muscles analyzed. Many of the D2 muscles demonstrated statistically increased pathology for these two characteristics at most time points analyzed after the initial 4 week time point. The histology confirmed a more severe disease in the Sgcg-/- D2 mice at the 12 week time point used for the histology. Most importantly the Sgcg-/- D2 mice demonstrated cardiac functional impairment by echocardiography compared to the mdx mice at all ages.

Many of the phenotypic differences are trending to significance. One limitation of these experiments is the limited number of animals used, due to the time-course nature of the data. Muscular dystrophy in mice – and humans – is notoriously variable even within the same animal (mice (Heydemann, Huber et al. 2005), and humans (Humbertclaude, Hamroun et al. 2012; Flanigan, Ceco et al. 2013)). Therefore additional mice are likely to push some of the comparisons to significance. Despite this caveat the trends are upheld for many tissues and across many time points indicating the conclusions drawn are sound.

Both the mdx and Sgcg-/-D2 mouse phenotypes get better after an initial bout of pathology. Although this has been discussed in the mdx mice for many years we have not found an explanation for the reduction. In the current experiments the mdx mouse pathology is most severe at the 4 week time point, while the Sgcg-/- mice are most severely affected at 12 weeks. Possible mechanisms behind this recovery could be; satellite cell recovery, immune response is dampened, sufficient remodeling of scar tissue or, likely a combination of these and other mechanisms. Other important questions remain. It would be of great interest to know why the different mouse strains have their peak pathologies at different ages. And it would be ideal to understand if this recovery mechanism can be harnessed for human patients.

Even though we argue that the Sgcg-/-D2 mouse is a better model of human muscular dystrophy we must remember that it is still a model. There are many considerations when using mouse models to represent human disease (reviewed in (Partridge 2013)). There are the obvious differences; bipedal versus quadripedal, free living with multiple stresses versus caged generally without physical activity, and size. The less obvious differences must also be considered. Slight differences in; gene expression patterns, in signaling pathways, and in immune responses exist. As an example, important inter-species differences in the Notch signaling pathway have been identified (Church, Trieu et al. 2014).

F. Acknowledgements

We thank Robert Gaffin of the University of Illinois Center for Cardiovascular Research for the expert electrocardiography. We also thank the University of Illinois, Research Resources Core, Research Histology and Tissue Imaging Core.

G. Funding

This research was funded by a grant from the National Institutes of Health (RO1; RHL102322A). The funder had no role in study design, data collection and analysis, decision to publish, or preparation of the manuscript.

H. Disclosure Statement

The authors have no conflicts, financial or otherwise to declare.

I. Copyright Information

J. **Bibliography**

Aherrahrou, Z., L. C. Doehring, et al. (2007). "Ultrafine mapping of Dyscalc1 to an 80-kb chromosomal segment on chromosome 7 in mice susceptible for dystrophic calcification." Physiol Genomics 28(2): 203-212.

Banks, G. B. and J. S. Chamberlain (2008). "The value of mammalian models for duchenne muscular dystrophy in developing therapeutic strategies." Curr Top Dev Biol 84: 431-453.

Bertoni, C., C. Lau, et al. (2003). "Restoration of dystrophin expression in mdx muscle cells by chimeraplast-mediated exon skipping." Hum Mol Genet 12(10): 1087-1099.

Bianchi, M. L., A. Mazzanti, et al. (2003). "Bone mineral density and bone metabolism in Duchenne muscular dystrophy." Osteoporos Int 14(9): 761-767.

Bosnakovski, D., Z. Xu, et al. (2008). "Prospective isolation of skeletal muscle stem cells with a Pax7 reporter." Stem Cells 26(12): 3194-3204.

Branco, D. M., C. M. Wolf, et al. (2007). "Cardiac electrophysiological characteristics of the mdx (5cv) mouse model of Duchenne muscular dystrophy." J Interv Card Electrophysiol 20(1-2): 1-7.

Bulfield, G., W. G. Siller, et al. (1984). "X chromosome-linked muscular dystrophy (mdx) in the mouse." Proc Natl Acad Sci U S A 81(4): 1189-1192.

Church, J. E., J. Trieu, et al. (2014). "Alterations in Notch signalling in skeletal muscles from mdx and dko dystrophic mice and patients with Duchenne muscular dystrophy." Exp Physiol 99(4): 675-687.

Connolly, A. M., R. M. Keeling, et al. (2001). "Three mouse models of muscular dystrophy: the natural history of strength and fatigue in dystrophin-, dystrophin/utrophin-, and laminin alpha2-deficient mice." Neuromuscul Disord 11(8): 703-712.

DiMario, J. X., A. Uzman, et al. (1991). "Fiber regeneration is not persistent in dystrophic (MDX) mouse skeletal muscle." Dev Biol 148(1): 314-321.

Dunn, J. F. and G. K. Radda (1991). "Total ion content of skeletal and cardiac muscle in the mdx mouse dystrophy: Ca2+ is elevated at all ages." J Neurol Sci 103(2): 226-231.

Echigoya, Y. and T. Yokota (2014). "Skipping multiple exons of dystrophin transcripts using cocktail antisense oligonucleotides." Nucleic Acid Ther 24(1): 57-68.

Flanigan, K. M., E. Ceco, et al. (2013). "LTBP4 genotype predicts age of ambulatory loss in Duchenne muscular dystrophy." Ann Neurol 73(4): 481-488.

Flesch, M., F. Schiffer, et al. (1997). "Contractile systolic and diastolic dysfunction in renin-induced hypertensive cardiomyopathy." Hypertension 30(3 Pt 1): 383-391.

Fukada, S., D. Morikawa, et al. (2010). "Genetic background affects properties of satellite cells and mdx phenotypes." Am J Pathol 176(5): 2414-2424.

Gibertini, S., S. Zanotti, et al. (2014). "Fibrosis and inflammation are greater in muscles of beta-sarcoglycan-null mouse than mdx mouse." Cell Tissue Res 356(2): 427-443.

Grady, R. M., H. Teng, et al. (1997). "Skeletal and cardiac myopathies in mice lacking utrophin and dystrophin: a model for Duchenne muscular dystrophy." Cell 90(4): 729-738.

Guerron, A. D., R. Rawat, et al. (2010). "Functional and molecular effects of arginine butyrate and prednisone on muscle and heart in the mdx mouse model of Duchenne Muscular Dystrophy." PLoS One 5(6): e11220.

Hack, A. A., C. T. Ly, et al. (1998). "Gamma-sarcoglycan deficiency leads to muscle membrane defects and apoptosis independent of dystrophin." J Cell Biol 142(5): 1279-1287.

Heydemann, A., E. Ceco, et al. (2009). "Latent TGF-beta-binding protein 4 modifies muscular dystrophy in mice." J Clin Invest 119(12): 3703-3712.

Heydemann, A., J. M. Huber, et al. (2005). "Genetic background influences muscular dystrophy." Neuromuscul Disord 15(9-10): 601-609.

Hoffman, E. P., R. H. Brown, Jr., et al. (1987). "Dystrophin: the protein product of the Duchenne muscular dystrophy locus." Cell 51(6): 919-928.

Huang, P., G. Cheng, et al. (2011). "Impaired respiratory function in mdx and mdx/utrn(+/-) mice." Muscle Nerve 43(2): 263-267.

Humbertclaude, V., D. Hamroun, et al. (2012). "Motor and respiratory heterogeneity in Duchenne patients: implication for clinical trials." Eur J Paediatr Neurol 16(2): 149-160.

Ivandic, B. T., J. H. Qiao, et al. (1996). "A locus on chromosome 7 determines myocardial cell necrosis and calcification (dystrophic cardiac calcinosis) in mice." Proc Natl Acad Sci U S A 93(11): 5483-5488.

Matsuda, R., A. Nishikawa, et al. (1995). "Visualization of dystrophic muscle fibers in mdx mouse by vital staining with Evans blue: evidence of apoptosis in dystrophin-deficient muscle." J Biochem 118(5): 959-964.

Matsumura, T. (2014). "Beta-Blockers in Children with Duchenne Cardiomyopathy." Rev Recent Clin Trials.

Meng, H., I. Vera, et al. (2007). "Identification of Abcc6 as the major causal gene for dystrophic cardiac calcification in mice through integrative genomics." Proc Natl Acad Sci U S A 104(11): 4530-4535.

Merrell, A. J. and G. Kardon (2013). "Development of the diaphragm -- a skeletal muscle essential for mammalian respiration." FEBS J 280(17): 4026-4035.

Nelson, C. A., R. B. Hunter, et al. (2011). "Inhibiting TGF-beta activity improves respiratory function in mdx mice." Am J Pathol 178(6): 2611-2621.

Noguchi, S., E. M. McNally, et al. (1995). "Mutations in the dystrophin-associated protein gamma-sarcoglycan in chromosome 13 muscular dystrophy." Science 270(5237): 819-822.

Partridge, T. A. (2013). "The mdx mouse model as a surrogate for Duchenne muscular dystrophy." FEBS J 280(17): 4177-4186.

Ryder-Cook, A. S., P. Sicinski, et al. (1988). "Localization of the mdx mutation within the mouse dystrophin gene." EMBO J 7(10): 3017-3021.

Sacco, A., F. Mourkioti, et al. (2010). "Short telomeres and stem cell exhaustion model Duchenne muscular dystrophy in mdx/mTR mice." Cell 143(7): 1059-1071.

Spurney, C. F., A. Sali, et al. (2011). "Losartan decreases cardiac muscle fibrosis and improves cardiac function in dystrophin-deficient mdx mice." J Cardiovasc Pharmacol Ther 16(1): 87-95.

Stedman, H. H., H. L. Sweeney, et al. (1991). "The mdx mouse diaphragm reproduces the degenerative changes of Duchenne muscular dystrophy." Nature 352(6335): 536-539.

Tidball, J. G. and M. Wehling-Henricks (2004). "Evolving therapeutic strategies for Duchenne muscular dystrophy: targeting downstream events." Pediatr Res 56(6): 831-841.

Viollet, L., P. T. Thrush, et al. (2012). "Effects of angiotensin-converting enzyme inhibitors and/or beta blockers on the cardiomyopathy in Duchenne muscular dystrophy." Am J Cardiol 110(1): 98-102.

Welch, E. M., E. R. Barton, et al. (2007). "PTC124 targets genetic disorders caused by nonsense mutations." Nature 447(7140): 87-91.

III: Inherent elevated pAMPK in MRL skeletal muscle

 Increased AMP-activated protein kinase in skeletal muscles of Murphy Roth Large mice and its potential role in altered metabolism. Tirsit K. Berhanu , Jenan Holley-Cuthrell , Nathan W. Roberts , Aaron J. Mull , Ahlke Heydemann . Physiological Reports Published 20 March 2014 Vol. 2 no. e00252 DOI: 10.1002/phy2.252

A. **Abstract**

Wild-type Murphy Roth Large (MRL) mice have long been investigated for their superior healing ability when subjected to various wound and disease models. Despite this long history, the mechanisms causing their extraordinary healing ability remain undefined. As we have recently demonstrated that MRL mice with muscular dystrophy are resistant to the associated fibrosis and the Heber-Katz group has demonstrated MRL mitochondrial mutations, we decided to investigate the skeletal muscle metabolic characteristics of the MRL mouse strain compared to the commonly utilized C57BL/6J control mouse strain. We now have evidence demonstrating an altered metabolism in the MRL quadriceps, triceps brachii, and diaphragm of 8-week-old animals compared to tissues from control animals. The MRL skeletal muscles have increased activated phosphorylated AMP-activated protein kinase (pAMPK). The increased pAMPK signaling coincides with increased skeletal muscle mitochondrial content. These metabolic changes may compensate for insufficient oxidative phosphorylation which is demonstrated by altered quantities of proteins involved in oxidative phosphorylation and *ex vivo* metabolic investigations. We also demonstrate that the MRL muscle cells have increased metabolic physiologic reserve. These data further the investigations into this important and unique mouse strain. Why the MRL mice have increased pAMPK and how increased pAMPK and the resultant metabolic alterations affect the healing

ability in the MRL mouse strain is discussed. Understanding the molecular mechanisms surrounding the super healing characteristics of these mice will lead to relevant clinical intervention points. In conclusion, we present novel data of increased mitochondrial content, pAMPK, and glycolytic indicators in MRL skeletal muscles.

B. **Introduction**

The unique Murphy Roth Large (MRL)/MpJ scar-less wound healing abilities were first noted when ear punches used for identification closed and fully, scarlessly, healed within 4 weeks (Clark et al. 1998). Many, but not all, subsequent MRL wound models also display this unique healing ability (reviewed in (Heydemann 2012)). The MRL/MpJ-*Fas*^{Lpr}/J mouse strain has a homozygous null mutation in the *fas* gene which causes decreased apoptosis in lymphocytes (Juvet et al. 2013). The mouse strain used in the current work is the MRL/MpJ strain (MRL), which has an intact *fas* antigen gene (Adachi et al. 1993). Both the MRL/MpJ and MRL/MpJ-*Fas*^{Lpr}/J mouse strains have increased ear punch hole healing and both are prone to specific autoimmune diseases, although the MRL/MpJ mice succumb to autoimmune disease later in life (Theofilopoulos and Dixon 1985); well passed the 8-week-old mice used in this study. Therefore, we can surmise that the *fas* mutation is not necessary for the autoimmune phenotype, and additional genes in the MRL mouse strains contribute to the autoimmune phenotype.

The molecular and cellular mechanisms behind the MRL healing ability have not been fully elucidated. There are multiple well-supported hypotheses (reviewed in (Heydemann 2012)). Among the possible, and in no way mutually exclusive, ideas are; enhanced stem cell abilities (Baker et al. 2006; Naviaux et al. 2009), altered cell cycle regulation (Arthur et al. 2010; Bedelbaeva et al. 2010), immune differences (Donnelly et al. 1990; Alleva et al. 1997; Kench et al. 1999; Ueno et al. 2005), alterations in the extra-cellular matrix (Heber-Katz et al. 2004) and, metabolic differences (Naviaux et al. 2009).

We hypothesize, and have preliminary evidence which supports metabolic differences as an explanation for a significant portion of the MRL healing phenotype. MRL mitochondria have been shown to contain two significant heteroplasmies (multiple mitochondrial genomes present in a single cell, (Sachadyn et al. 2008)). Mitochondria contain multiple plasmid-like genomes which replicate and segregate randomly during fission. In the MRL strain some of these mitochondrial genomes contain mutations. The percentage of mutant mitochondrial genomes is different between animals and a threshold of mutant genomes is required for phenotypic penetrance confounding research into this discipline. The two MRL mitochondrial heteroplasmies contain mutant nucleotide sequences in mitochondrial tRNAs and are expected to cause variable and multiple translational errors. In a previous example, Ghezzi et al. identified that alteration in a mitochondrial tRNA modifying enzyme causes hypertrophic cardiomyopathy and lactic acidosis (Ghezzi et al. 2012). Similarly, mitochondrial tRNA mutations can cause hypertension in humans (Qiu et al. 2012). Although these example mutations are in different mitochondrial tRNA genes we can deduce that the MRL mitochondrial tRNA mutations also cause translational errors. These mitochondrial translational errors will lead to the metabolic alterations identified in MRL fibroblasts, MRL blastema-derived fibroblasts, and MRL heart tissue (Naviaux et al. 2009) and to the currently identified metabolic alterations in the MRL skeletal muscles.

A central regulator of many aspects of cellular metabolism is AMP-dependent protein kinase (AMPK, reviewed in (Hardie 2011)). AMPK is activated by kinases when cells become energetically stressed; the activation is rendered allosterically possible by an increase in the AMP/ATP ratio, which also renders phosphatases inactive (Davies et al. 1995; Ponticos et al. 1998). In general, AMPK activation induces increases in catabolism and decreases in anabolism, both intended to restore energy homeostasis. Although alternative AMPK activators exist, our data indicate that insufficient ATP levels due to inadequate mitochondrial function are the activators in the MRL skeletal muscle tissue.

In light of the cardiac metabolic differences (including increased glycolysis and reduced fatty acid oxidation) identified by Naviaux et al. (2009) and to further investigate the MRL regeneration abilities, we now show that multiple skeletal muscle types (quadriceps, triceps brachii, and diaphragm) of wild-type MRL mice have increased activated, phosphorylated, AMPK (pAMPK), and altered levels of mRNA and proteins involved in mitochondrial biogenesis and oxidative phosphorylation when compared to the commonly utilized C57BL/6J (B6) control mice. From previously published work and these new, novel data we present a model of MRL metabolic differences followed by a discussion of how these metabolic differences increase the regenerative abilities of the MRL mice.

C. Materials and Methods

Mice

Murphy Roth Large (MRL)/MpJ (MRL, 000486) and C57BL/6J (B6, 000664) male mice were purchased from the Jackson Laboratories (Bar Harbor, ME). The mice were housed 5 to a cage in the same room of a barrier facility, with unrestrained access to standard mouse chow and neutral water, and 12-h light/dark cycles. All protocols were conducted adhering to the rules of the National Institutes of Health Guide for the Care and Use of Laboratory Animals and by the University of Illinois at Chicago Institutional Animal Care and Use Committee.

Immunoblots

Tissues intended for immunoblots were harvested and snap frozen in liquid nitrogen. Proteins were prepared in 500 μL of lysis buffer (20 mmol/L HEPES [pH 7.4], 50 mmol/L β-glycerol phosphate, 2 mmol/L EGTA, 1 mmol/L DTT, 10 mmol/L sodium fluoride, 1 mmol/L sodium orthovanadate, 1% TritonX-100, 10% glycerol and protease inhibitors [ThermoScientific, 1862209, Waltham, MA]) with homogenization TissueRuptor (Qiagen) on ice, at full speed for 1 min. After centrifugation at 4500 *g* for 10 min the protein concentrations of the supernatants were quantified with the Bradford assay

(ThermoScientific). Acrylamide gels (BioRad, Hercules, California) were used to separate 30–60 μg of protein, and then transferred to PVDF membrane (iBlot, Invitrogen, Carlsbad, CA). Immunodetection was performed at room temperature; the membrane was blocked for 20 min in 5% nonfat dry milk in t-TBS (Tris-Buffered Saline with 0.1% Tween 20), incubated for 2 h in primary antibody [voltage-dependent anion channel 1 (VDAC1; AbCam, Cambridge, MA), pAMPK and AMPK (both antibodies recognize both α1 and α2 subunits and both are from Cell Signaling Technology #2535 and #2793, respectively), GLUT4 (Millipore, Billerica, MA), and OXPHOS (AbCam ab110413) diluted 1:1000 in 5% nonfat dry milk in t-TBS, washed three times 15 min in t-TBS, incubated for 1 h in appropriate secondary horseradish linked antibody (Jackson Immunologicals, Carlsbad, CA)] diluted 1:2500 in 5% nonfat dry milk in t-TBS, washed three times 15 min in t-TBS, developed with ECL (GE Healthcare, Little Chalfont, Buckinghamshire, UK), and visualized with a ChemiDoc (Bio Rad, Hercules, CA). Gels were stripped at 55°C for 30 min in 2% SDS, 100 mmol/L mercaptoethanol, 62.5 mmol/L Tris-HCL pH 6.8, and reprobed with GAPDH (1:3000; Santa Cruz Biotechnology, Santa Cruz, CA) for a loading control. Immunoblot bands were quantified with ImageJ, and the results are reported as a ratio of the GAPDH lane. Multiple exposures were used to quantify gels with a wide range of protein levels. In all cases the B6 average from the gels was set to represent 100% and the other bands were compared as ratios to this normalization. The number of biological replicates quantified for each strain are indicated in the figure legends.

Quantitative PCR (qPCR)

Quantitative mitochondrial DNA and nuclear DNA contents were analyzed as described (Moreno-Loshuertos et al. 2006). Small portions (~20 mg) of tissue were prepared with the Puregene kit (Qiagen, Hilden, Germany) as per the product protocol except that the final resuspension occurred in 30 μL. The mitochondrial encoded Subunit II of Cytochrome C Oxidase was amplified with forward primer

5′-CTACAAGACGCCACAT and reverse primer 5′-GAGAGGGGAGAGCAAT. PCR product intensity was compared to the single nuclear gene encoding Succinate Dehydrogenase Subunit A intensity, amplified with forward primer 5′-TACTACAGCCCCAAGTCT and reverse primer 5′-TGGACCCATCTTCTATGC. The PCR conditions were as follows: 95°C 10 min; then [95°C, 15 sec and 60°C, 1 min] times 40 cycles in a Rotor-Gene Q (Qiagen). Melt curves were utilized to verify a single product produced in each reaction, and dilution curves were generated to identify the efficiency of each primer pair. The ratio of the two products was determined using $^{\Delta}C^{t}$ comparisons for each animal. There is no reverse transcription step: we are comparing mitochondrial to nuclear DNA contents directly. We set the B6 animal ratios to 100% and report the MRL ratios as a percentage of this.

Citrate synthase activity

The assay was performed according to manufacturer's instructions (Sigma, St. Louis, MO). Six quadriceps samples were processed from each strain. Results are expressed as citrate synthase umol/min/mg mitochondrial extract.

ATP assay

The colorimetric assay was performed according to manufacturer's instructions (BioVision, Milpitas, CA). Four quadriceps samples were processed from each strain.

QuantiGene

Small portions (10–30 mg) of tissues were flash frozen in liquid nitrogen. The samples were prepared according to manufacturer's instructions (QuantiGene Affymetrix, Santa Clara, CA) and delivered to the DNA Services Facility section of The University of Illinois at Chicago Research Resources Core Facility. The samples were run in duplicate on a custom designed assay plate. At least eight

biological replicates were performed. The control transcript, transferrin receptor protein 1 (TfR1) was chosen as the control gene from a set of six potential control genes because TfR1 had the lowest standard deviation within the two animal groups but had sufficient expression (at least 50% of the control RNA sample). Therefore, all of the mRNA species were normalized to the TfR1 (transferrin receptor protein 1) level from that same sample. The expression levels of all genes, including the controls are investigated in a single reaction. These assays were conducted upon quadriceps (n = 8) and diaphragm (n = 10) tissues from the MRL and B6 mouse strains. To graph the results the data were again normalized to the average B6 expression level of the specific gene, so that results can be illustrated on one graph as a percentage, and the trends between genes can be easily viewed.

Primary cell culture

Primary neonatal mouse myoblasts were isolated with a modification of previously described methods (Rando and Blau 1994) as follows. Briefly, limb muscles were removed from P0 to P2 pups, deskinned, and minced. The slurry was pelleted and resuspended in 1 mg/mL collagenase/dispase (Roche Diagnostics Corporation, Indianapolis, IN) in Ham's F10 at 37°C for 45 min, triturating every 15 min. Digests were passed through a 100-μm cell strainer, pelleted, and resuspended in primary myoblast medium (Ham's F10, 20% FBS, 1% PSA (all media Gibco, Grand Island, NY) and 2.5 ng/mL recombinant human bFGF (Promega, Madison, WI)). Myoblasts were preplated for 10 min on uncoated dishes and then nonadherent cells (enriched myoblasts) were plated on gelatin-coated dishes (2% gelatin type B [Sigma]) at 37°C, 5% CO_2. Proliferation abilities were assessed by plating an equal number of cells into wells of a six-well gelatin-coated plate. The cells were given fresh media every 24 h and harvested with trypsin at 72 h after plating. The cells were carefully counted and mitosis/24-h period was calculated for each culture. Cultures from six different animals of each strain were assessed. In addition, routine desmin antibody (1:100 dilution, primary antibody from Santa Cruz Biotechnology, Alexa Fluor goat anti-

mouse 488 secondary antibody, Life Technologies) staining was performed on cultures used for the metabolism analysis.

Seahorse metabolic flux analysis

To gain further insight into the metabolic characteristics of the MRL skeletal muscles, primary isolated myoblast progenitor cells were analyzed in the Seahorse apparatus (Seahorse Biosciences, North Billerica, MA). Preliminary data indicated that 30,000 primary myoblast cells per well of the Seahorse plate yielded the most reproducible results for both primary cell lines. For oxygen consumption rate (OCR)/extracellular acidification rate (ECAR) experiments, cells frozen once and thawed were plated on coated or uncoated XF-24 plates (Seahorse Bioscience, North Billerica, MA) at 30–40,000 cells overnight, fed 675 μL Seahorse unbuffered assay media (modified DMEM, no bicarbonate or pyruvate, 4.5 g/L glucose) and the assay was performed as described in manufacturer's instructions with concentrations listed. The cells were treated with 1 μmol/L voligomycin, 500 nmol/L carbonyl cyanide p-trifluoromethoxyphenylhydrazone (FCCP), and 1 μmol/L antimycin and both OCR and ECAR measured in a Seahorse Extracellular Flux Analyzer. Then three experiments were conducted using three separate primary cultures from each mouse strain. Each experiment contained at least six wells of myoblasts from each strain. Values for metabolic responses were calculated by areas under the curve.

Statistics

As we are comparing two populations, MRL versus B6, student's *t*-tests were performed, and significant differences were considered when $P < 0.05$ (Excel Software; Microsoft, Seattle, WA).

D. **Results**

MRL skeletal muscle tissues have increased mitochondrial content

Previously reported qPCR results demonstrated an approximately twofold increase of mitochondrial to nuclear DNA ratios of MRL liver and cardiac tissues compared to B6 tissues (Naviaux et al. 2009). Similarly, electron microscopy demonstrated increased mitochondrial content in the MRL muscle tissues versus the 129 control strain (Heydemann 2012). As the mitochondrial content in skeletal muscle is dependent upon individual fiber type, the previous electron microscopy results are now supported by immunoblots of the VDAC1, also known as the mitochondrial porin protein levels. MRL quadriceps muscles contained significantly more VDAC protein then the controls (representative blot shown in Fig. 18A and quantified in Fig. 8B [$n \geq 10$]). The diaphragms and triceps brachii of the MRL mice also had increased VDAC protein levels (Data not shown). The differences were all statistically significant between the MRL and B6 controls: quadriceps (MRL 340 ± 147 standard deviations, B6 100 ± 72, P = 0.0048), diaphragms (MRL 189 ± 69, B6 100 ± 52, n = 6, P = 0.0372), and triceps brachii (MRL 183 ± 126, B6 100 ± 83, n = 12 P = 0.037).

To further confirm the increased quantity of mitochondria in MRL muscles, we employed qPCR comparing mitochondrial DNA to nuclear DNA ratios. The MRL quadriceps muscle tissue demonstrated increased $^{\Delta}C^{t}$ ratios of mitochondrial to nuclear DNA compared to the control strain (Fig. 2A, MRL 139 ± 36, B6 100 ± 50, n = 12, P = 0.018). The same analysis was performed upon DNA extracted from diaphragm and again the MRL mice had significantly increased $^{\Delta}C^{t}$ ratios (Data not shown, MRL 195 ± 42, B6 100 ± 27, n = 12, P = 0.0004 MRL vs. the B6).

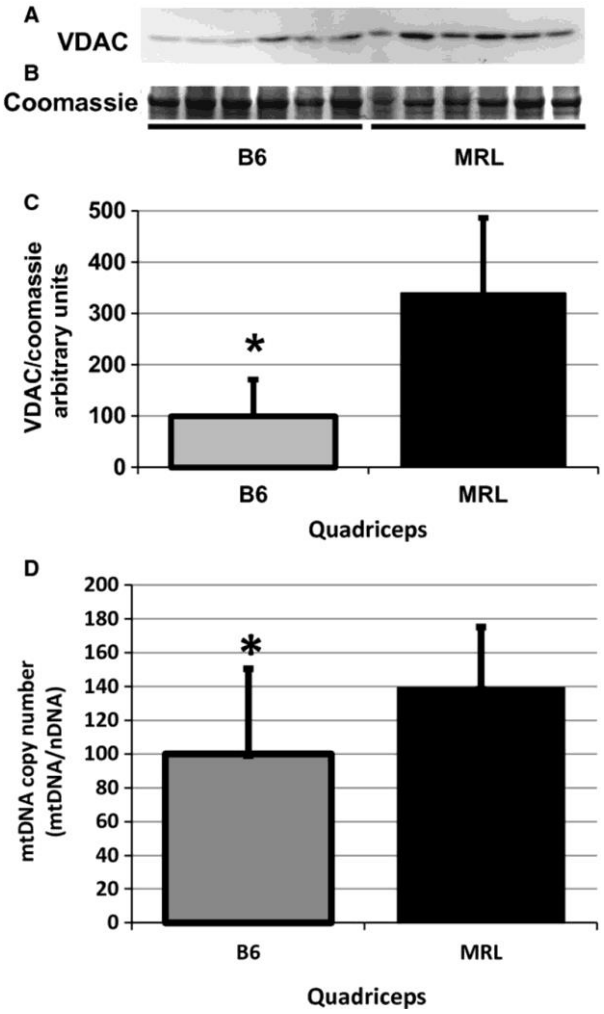

Figure 8-Increased mitochondrial markers in Murphy Roth Large (MRL) quadriceps muscle tissue. (A) VDAC1 (porin) specific antibody demonstrates significantly increased mitochondrial content in MRL quadriceps. (B) Coomassie stain of a duplicate gel demonstrating equal loading. (C) VDAC was quantified from six biological replicates and normalized to the coomassie stain. (D) Quantitative PCR demonstrates a significant increase in the mitochondrial to nuclear DNA ratio in the MRL quadriceps tissues. Twelve quadriceps from each strain were analyzed and compared, averages with standard deviations are shown. *represents $P < 0.05$ versus the MRL mice.

We also utilized the citrate synthase activity assay, a commonly utilized method for mitochondrial quantification. The B6 quadriceps had significantly higher levels of citrate synthase activity than the MRL quadriceps tissue (Fig. 9B), (MRL 0.848 ± 0.027, B6 0.792 ± 0.033, $P = 0.012$, $n = 6$). This apparent discrepancy will be clarified in the discussion.

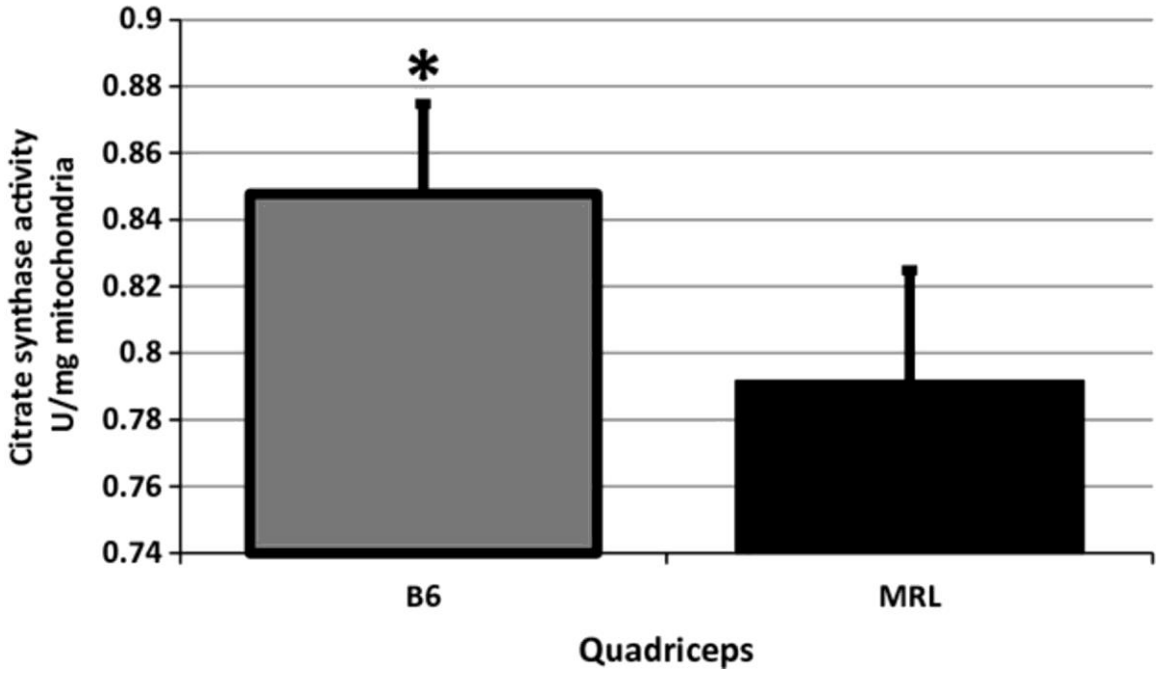

Figure 9-Citrate synthase activity is decreased in Murphy Roth Large (MRL) muscles. Six quadriceps from each strain were analyzed and compared, averages with standard deviations are shown. *represents $P < 0.05$ versus the MRL mice.

Increased transcripts of genes involved in mitochondrial biogenesis

Mitochondrial biogenesis requires the coordinated interactions of multiple transcription factors and their downstream targets. To investigate if these mitochondrial biogenesis regulating transcripts are significantly altered in the skeletal muscles of MRL mice QuantiGene assays were performed. Compared to B6 controls, quadriceps muscles of MRL mice had increased mRNA levels for all of the seven mitochondrial biogenesis factors interrogated (Fig. 10). Despite the large standard deviations provided by the MRL data, the differences were statistically significant for peroxisome proliferator-activated receptor gamma coactivator 1-alpha (PGC-1α), PGC-1β, nuclear respiratory factor (NRF1), and sirtuin3 (SIRT3); (P = 0.017, 0.021, 0.047, 0.039, respectively). In the QuantiGene analyzed MRL diaphragm tissues, only the mRNA for AMPKβ was significantly increased (P = 0.015), and the MRL diaphragms actually had decreased trends for the PGC-1α, PGC-1β, transcription factor A (TFAM), SIRT1 and SIRT3 expression levels compared to B6 controls (Data not shown).

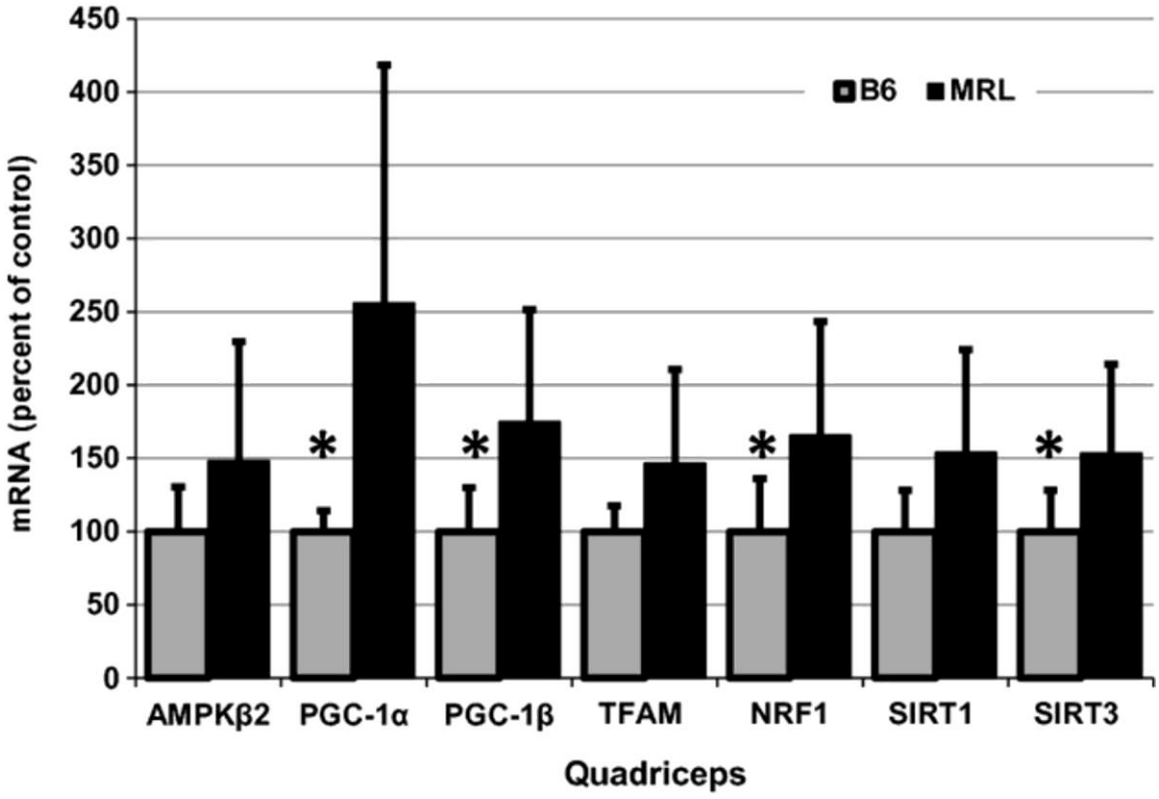

Figure 10-Transcripts for mitochondrial biogenesis are increased in Murphy Roth Large (MRL) quadriceps tissue. QuantiGene analysis indicates increases of key regulatory factors of mitochondrial biogenesis in MRL muscles. Nine muscles from each strain were compared and normalized to an internal control. The values were then normalized to the B6 values; averages with standard deviations are shown. AMPK*β*2, AMP-activated protein kinase beta 2 subunit; PGC-1*α* and 1*β*, peroxisome proliferator-activated receptor gamma coactivators 1-alpha; and 1-beta; transcription factor A, mitochondrial transcription factor A; NRF1, nuclear respiratory factor 1; SIRT1 and SIRT3, Sirtuin1 and 3. *represents $P < 0.05$ versus the MRL mice.

MRL skeletal muscles have increased activated AMPK protein levels

We next sought to investigate a molecular mechanism leading to increased mitochondrial content. Because of their mitochondrial heteroplasmies (Naviaux et al. 2009), we hypothesize that the MRL mice are being challenged with a chronic decrease of cellular energy, which would cause the cells to compensate by increasing mitochondrial quantity. Initially, the cell identifies decreased energy by an increase in the AMP to ATP ratio, which allows activation of AMPK through sustained phosphorylation at Thr-172. Phosphorylated AMPK (pAMPK) has multiple downstream effects including increased mitochondrial content (Zong et al. 2002). We now find that the MRL quadriceps tissues have significantly increased pAMPK (representative quadriceps immunoblot Fig. 11A, GAPDH loading control 11B, and quantified in 11C, $P = 0.0315$), and no change in AMPK levels (representative quadriceps immunoblot Fig. 11D and quantified in 11E, $P = 0.935$). Furthermore, the ratios of pAMPK over total AMPK are significantly increased in the MRL quadriceps tissue compared to the B6 muscles (Fig. 411F, $P = 0.0175$).

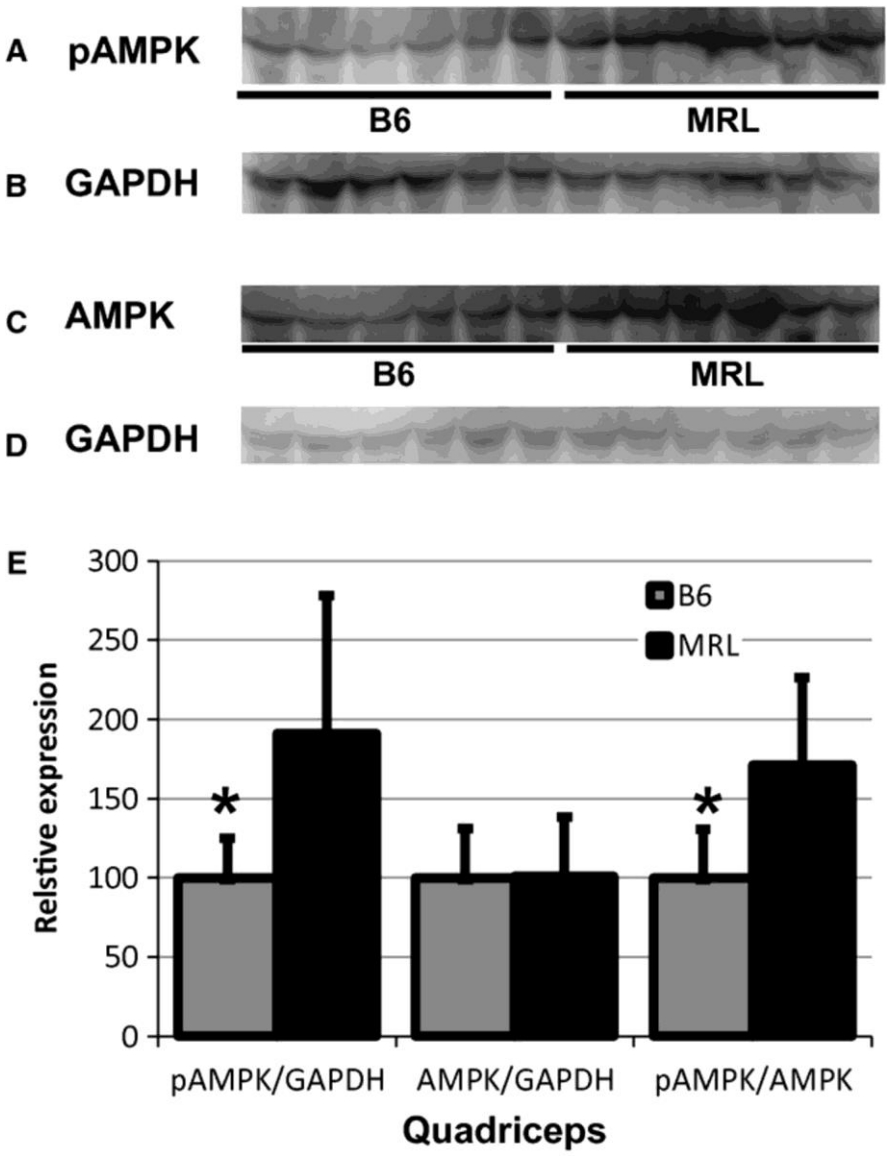

Figure 11-Increased phosphorylated AMP-activated protein kinase (pAMPK) and AMPK in Murphy Roth Large (MRL) quadriceps muscle. (A) A pAMPK-specific antibody demonstrates increases in MRL quadriceps. (B) GAPDH loading control of same gel. (C) AMPK-specific antibody analyzing quadriceps tissue. (D) GAPDH loading control of same gel. (E) Activated pAMPK over AMPK ratio, arbitrary units, normalized to B6 control levels, averages with standard deviations are depicted. n = 9, *represents P < 0.05 versus MRL tissue.

The increases of pAMPK and AMPK protein levels in MRL diaphragms and triceps brachii are also noteworthy. The MRL diaphragms demonstrated significantly increased pAMPK and AMPK levels (Data not shown, pAMPK $P = 0.005$, AMPK $P = 0.016$). The ratio of activated to unphosphorylated AMPK is slightly increased in the MRL diaphragm tissue ($P = 0.482$). The MRL triceps brachii have significantly increased AMPK and trending to an increased pAMPK (Data not shown; pAMPK $P = 0.089$, AMPK $P = 0.034$). In the triceps brachii tissue, the pAMPK/AMPK ratio is significantly increased in the MRL mouse tissue compared to the B6 control ($P = 0.028$).

We also assessed ATP levels in quadriceps tissue from the two mouse strains. No significant difference was detected between the two mouse strains (MRL 0.013 ± 0.0078 mmol/L ATP/mg protein, B6 0.009 ± 0.0029, $n = 4$, $P = 0.417$).

MRL skeletal muscles have increased metabolic transcripts and proteins

Increases in pAMPK initiate multiple downstream signaling cascades. In particular, we are interested in metabolic differences in the MRL mice and therefore have analyzed the levels of mRNAs and proteins involved in cellular glycolysis and mitochondrial oxidative phosphorylation. By QuantiGene analysis we identified a significant increase in four metabolic enzyme mRNA transcripts in MRL quadriceps in (Fig. 12). These significant increases were found for hexokinase 2 (HK2, $P = 0.016$), citrate synthase (CS, $P = 0.016$), carnitine palmitate 1b (CPT1b, $P = 0.042$), and fatty acid translocase (Fat/CD36, $P = 0.021$). When diaphragm tissues were compared (Data not shown) we found significant increases of glucose transporter 4 (GLUT4, $P = 0.021$) and CS ($P = 0.0421$) in MRL tissues.

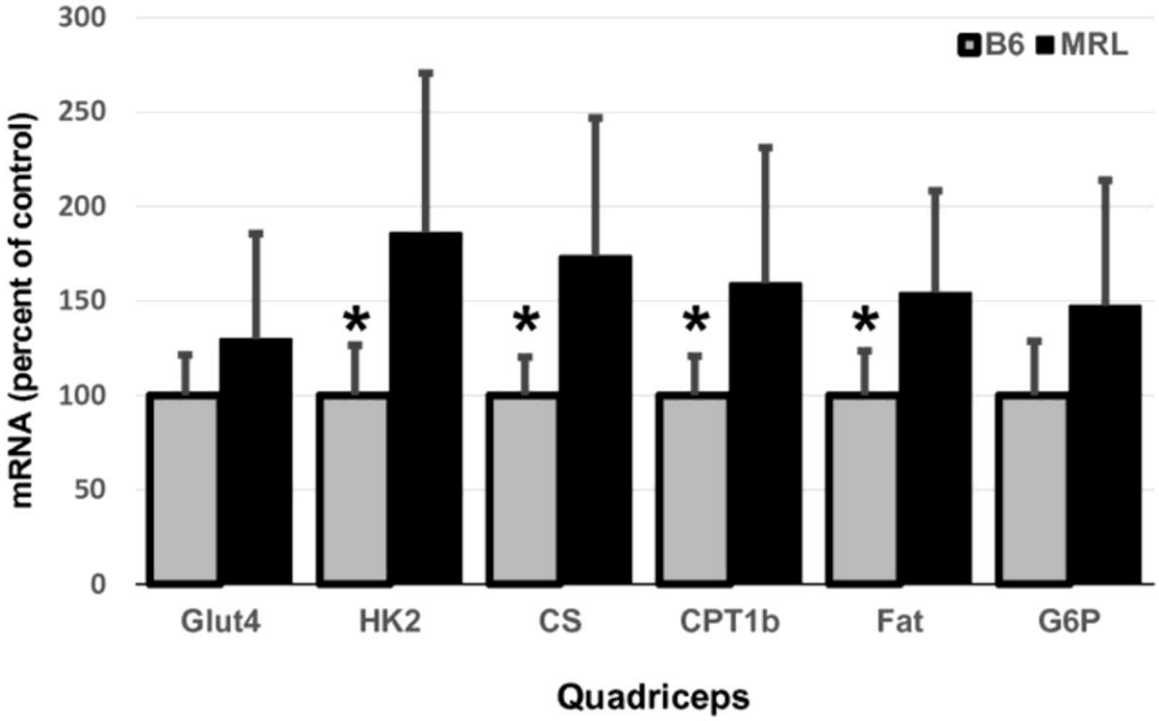

Figure 12-Increased metabolic transcripts in Murphy Roth Large (MRL) quadriceps. Nine muscles from each strain were compared via QuantiGene and normalized to an internal control. The values were then normalized to the B6 values; averages with standard deviations are shown. GLUT4, glucose transporter type 4; HK2, hexokinase 2; CS, citrate synthase; CPT1b, carnitine palmitoyltransferase 1; FAT, FAT/CD36; G6P, glucose 6-phosphate. *represents $P < 0.05$ versus the MRL mice.

By immunoblot of membrane fractions we also identified an increase in the protein product of GLUT4 in the membrane fraction of MRL quadriceps muscle (data not shown, values normalized to caveolin 3, MRL 155 ± 23, B6 100 ± 13, $n = 6$, $P = 0.0057$). This demonstrates an increase in a well-known pAMPK target.

Alterations in protein content of electron transport chain complex members

An oxidative phosphorylation (OXPHOS) antibody cocktail was used to quantitatively assess the changes in ETC proteins in the quadriceps muscle samples. The MRL mice were expected to have increased amounts of all complexes as they have more mitochondria. Interestingly, only the nuclear encoded Complex V protein, ATP5A was increased in MRL quadriceps (data not shown, normalized to GAPDH, MRL 189 ± 69, B6 100 ± 52, $n = 4$, $P = 0.0372$). The diaphragm OXPHOS immunoblots revealed no significant differences between the MRL and B6 mouse strains (data not shown).

Increased glycolysis and oxidative phosphorylation identified in MRL primary muscle cells

Supporting the mRNA expression data and previously reported data for other MRL tissues (Naviaux et al. 2009), we now show that MRL primary muscle progenitor cells perform more glycolysis than B6 progenitor cells. Using the Seahorse Metabolic Flux Analyzer we identified that the MRL cells have significantly increased acidification of their media indicating increased lactic acid levels, a definitive end product of anaerobic glycolysis (Fig. 13A). The metabolic data also indicate that the MRL skeletal muscles perform more basal oxidative phosphorylation demonstrated by increased oxygen consumption (Fig. 13B). MRL muscle progenitor cells also demonstrate increased maximal oxygen consumption after FCCP treatment, which permeabilizes the inner mitochondrial membrane to protons, thus it represents the maximum oxygen that the mitochondria can utilize as final electron acceptor (Fig. 13C). The MRL muscle cells also have a not significantly decreased ratio of oxygen consumption to acidification rate

(Fig. 13D). This further indicates that the MRL muscle cells favor glycolysis over oxidative phosphorylation.

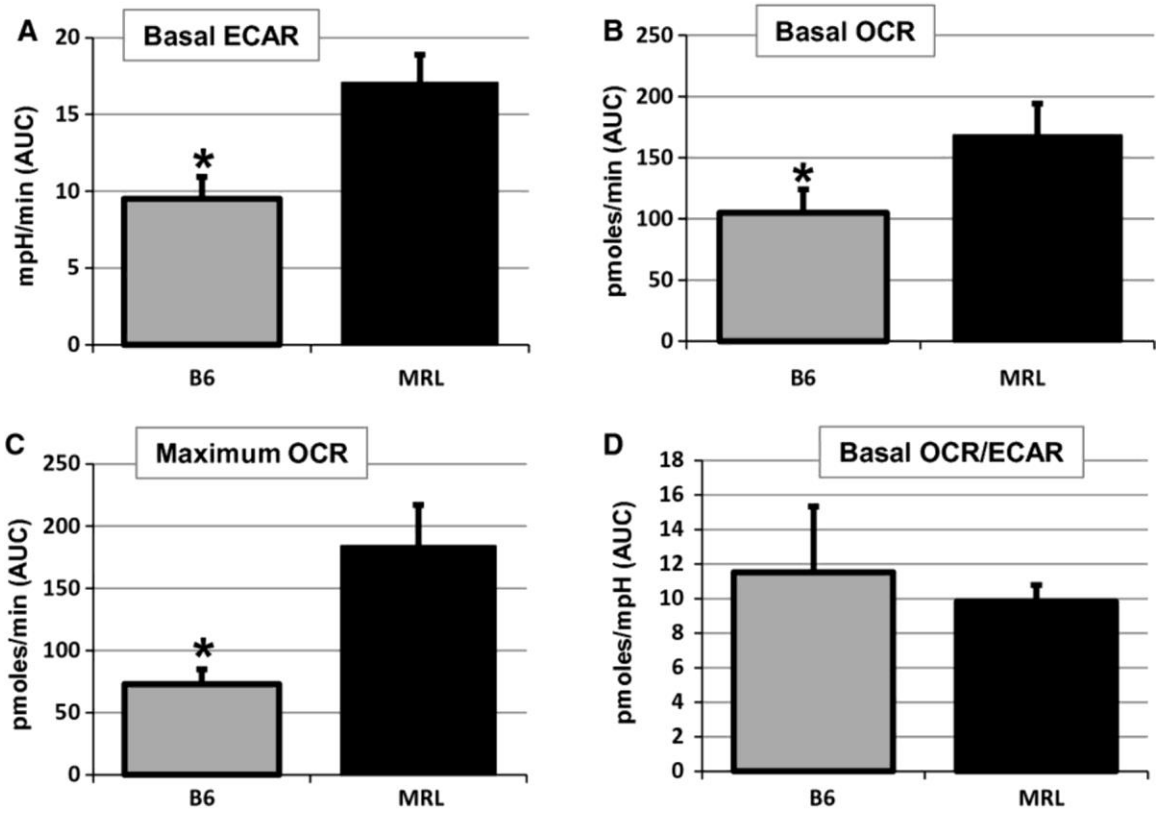

Figure 13-Metabolic differences in isolated primary muscle progenitor cells. Measurements of oxygen consumption rate (OCR) and extracellular acidification rate (ECAR) with a Seahorse XF24 Flux Analyzer reveal metabolic differences between Murphy Roth Large (MRL) and B6 cells. (A) Basal ECAR indicates increased glycolysis in MRL muscle progenitor cells. (B) Basal OCR is also significantly higher in MRL cells. (C) MRL cells have an increased physiologic reserve as demonstrated by the significantly increased maximal OCR after carbonyl cyanide p-trifluoromethoxyphenylhydrazone (FCCP) mediated uncoupling of the membrane potential. (D) Slightly decreased basal OCR/ECAR indicates MRL muscles do indeed favor glycolysis. * represents $P < 0.05$ versus the MRL cells.

To substantiate these metabolic quantifications, we confirmed that the primary muscle cultures were similar. There was no difference between the MRL and B6 cultures in regards to proliferation rates. Furthermore, all cultures were similarly positive (approximately 90% positive) for desmin staining indicating similar muscle precursor status.

E. Discussion

Integrative MRL metabolism model

We have generated a working model of metabolism differences in the MRL mice, integrating previously published and current data (Fig. 14). The MRL mice are known to have two nonsynonomous mitochondrial heteroplasmies (cells containing both normal and mutant mitochondrial DNA copies, (Sachadyn et al. 2008)). Because the heteroplasmies occur in mitochondrial tRNAs, we expect the mitochondrial encoded proteins of oxidative phosphorylation will be made at reduced levels (Irwin et al. 2012; Szczepanowska et al. 2012) and, therefore, in nonstochiometric amounts compared to the nuclear encoded mitochondrial destined proteins. This leads to decreased efficiency of oxidative phosphorylation, resulting in decreased ATP levels. The cell compensates with increased activated AMPK, and the resulting increased mitochondrial quantity and noted altered metabolism. How the change in activated AMPK-mediated metabolism may increase the regenerative capacity of these mice is yet to be determined. An increase in pAMPK through pharmaceuticals has been demonstrated a number of times to benefit animals with chronic muscular dystrophy associated necrosis and fibrosis (Ljubicic et al. 2011; Jahnke et al. 2012; Pauly et al. 2012). The working model schematic indicates some important intervention points that can be manipulated in future experiments to identify if the metabolic differences are causative for increasing regeneration.

Figure 14-

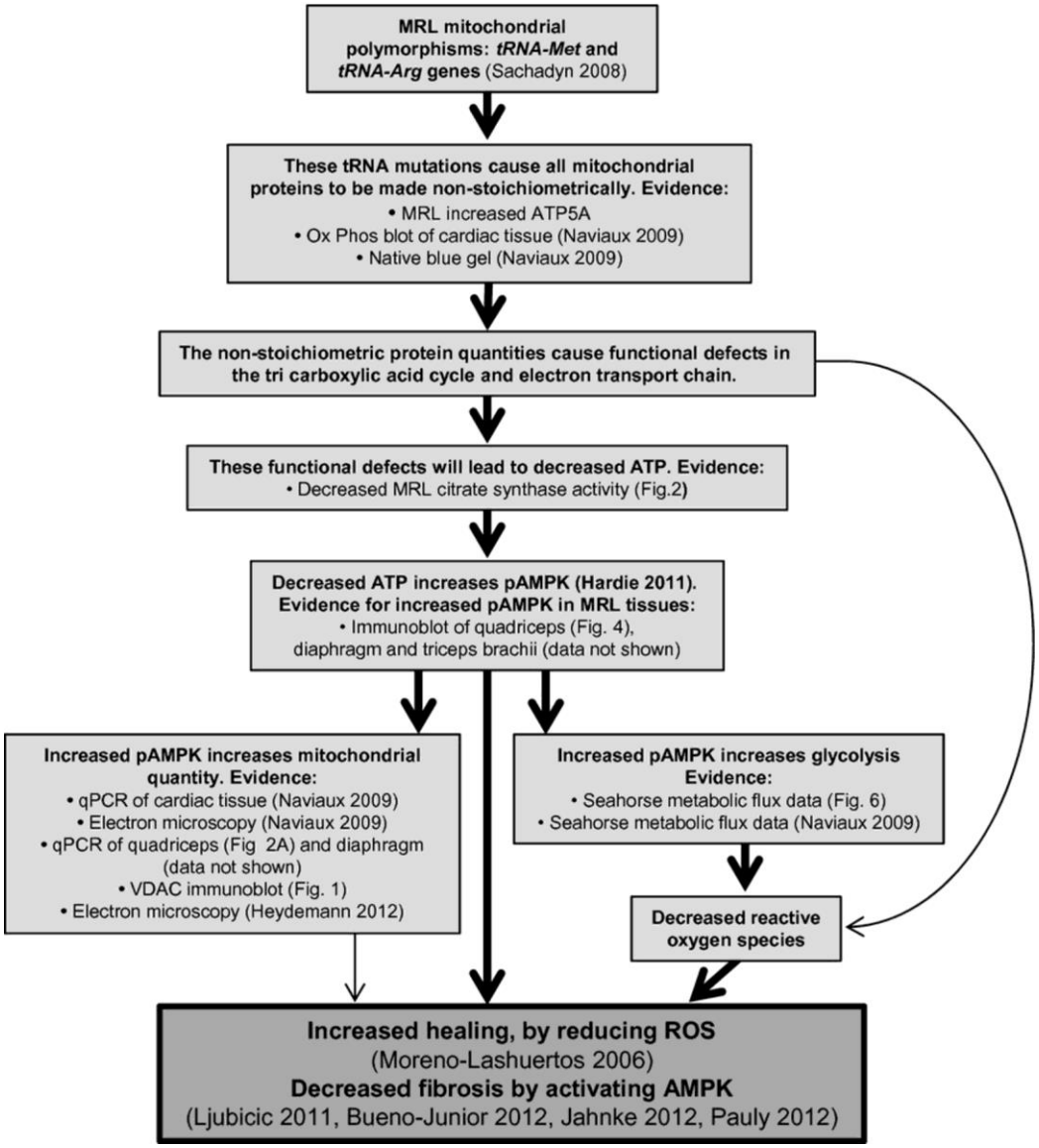

Schematic model of Murphy Roth Large (MRL) unique metabolic characteristics. Combining data from previously published results and current findings we propose this schematic model to aid in future investigations.

One of the downstream results of this altered metabolism is the observed decreased reactive oxide species (ROS, (Naviaux et al. 2009)). Usually mitochondrial dysfunction elicits increases in ROS (Gilliam et al. 2013). Again, the MRL mice behave unexpectedly, and again the mechanism(s) of MRL decreased ROS remain unknown. High ROS levels are well known to inhibit various cellular processes and are pathogenically associated with many diseases. However, low ROS levels are often utilized for cellular signaling (reviewed in (Droge 2002)). Therefore, the reduction of ROS may be beneficial to the MRL tissues, and may be a contributor to the super healing phenotype in the MRL mice.

AMP-dependent protein kinase activation is known to benefit a muscular dystrophy mouse model (Pauly et al. 2012). These changes are similar to the increases of pAMPK we are currently uncovering in the MRL mouse strain. We have previously shown that the MRL mouse strain is resistant to muscular dystrophy (Heydemann et al. 2012). Combining these data, it is a logical hypothesis to consider the increased pAMPK as central to the super healing of the MRL strain.

Increased mitochondrial content in MRL skeletal muscle

By three methods, we have demonstrated increased mitochondrial content in the skeletal muscles of the MRL mice. To corroborate the previously published electron microscopy images (Heydemann 2012), immunoblots with VDAC were performed upon quadriceps, triceps brachii, and diaphragm protein extracts. VDAC is located on the outer mitochondrial membrane. Although variably expressed between tissue types (Garcia-Cazarin et al. 2011), it appears to be uniformly expressed within skeletal muscles (Taub et al. 2012), and is therefore a valid surrogate marker for mitochondrial density (Jahnke et al. 2012).

As a further indicator of mitochondrial content, qPCR was performed upon triceps brachii and diaphragm muscles. We identified significant (1.5 to twofold) differences in mitochondrial DNA (mtDNA) quantities between MRL and B6 tissues. Naviaux et al. demonstrated twofold and threefold mtDNA increases in liver and heart tissue, respectively (Naviaux et al. 2009). The differences between the Heber-Katz and Heydemann laboratories may arise from gender differences (previously assayed females vs. our males), or age differences (10-week vs. our 8-week-old mice), a difference in tissue type, or, most likely, a combination of the listed factors with the last being preeminent.

As a final indicator of increased mitochondria in the MRL muscles a citrate synthase activity assay was conducted upon quadriceps muscle. This activity assay is commonly used to quantify intact mitochondria. The MRL quadriceps muscles have a reduction in the activity of this enzyme despite having increased mitochondria by three other quantitative measures. We believe that this data are not inconsistent but rather indicates the hypothesized inefficiency of the MRL mitochondria. If, as hypothesized, the MRL citric acid cycle is not performing correctly a bottle neck would ensue and the activity of the usually rate-limiting citrate synthase enzyme would decrease. We hypothesize that the nonstoichiometric amounts of the mitochondrial encoded proteins of the cycle would cause the cycle to be inefficient. The actual steps which are under performing will be investigated in the future.

Since we demonstrate increased mitochondria in the MRL muscle we expect an increase in mRNA species that are responsible for mitochondrial biogenesis. In general, this is what is revealed by QuantiGene analysis. Peroxisome proliferator-activated receptor gamma coactivator 1-alpha (PGC-1α) is a well-known control point for increasing mitochondrial content (Godin et al. 2012). The MRL skeletal muscles have significantly increased amounts of mRNA for this protein. For full activation PGC-1α phosphorylation by AMPK and deacetylation by SIRT are required (Lagouge et al. 2006). By immunoblot

we demonstrate an increase of pAMPK and by QuantiGene we demonstrate an increase of SIRT1 and SIRT3. SIRT3 also has ROS reducing abilities (Kong et al. 2010), low ROS is yet another characteristic found in the MRL mice (Naviaux et al. 2009). A slight increase of TFAM was also noted. This transcription factor is central to the expression of multiple mitochondrial genes including those required for replication (Kanki et al. 2004). Likewise, nuclear respiratory factor (NRF1) is an essential mitochondrial transcription factor (Virbasius and Scarpulla 1994) which is significantly increased in the MRL skeletal muscles. We have yet to investigate mitophagy in the MRL skeletal muscle. Decreased mitophagy would also contribute to the increased mitochondrial content in these muscles.

Of note, the QuantiGene differences are slight because we are investigating a mouse strain not a genetically manipulated mouse. The MRL mice are generally healthy, so large perturbations are unexpected. But these slight differences in mitochondria and metabolism could impact the mechanism of healing and push the MRL mice to their super-healing phenotype without establishing unwanted side effects.

AMPK is chronically activated in the MRL skeletal muscles

Activation of AMPK occurs in cells with reduced energy, often identified as an increase in the AMP/ATP ratio (Hardie 2003). Cellular energy can be reduced by ischemia (Kudo et al. 1995), exercise (Winder and Hardie 1996), calorie restriction (Salt et al. 1998), mitochondrial dysfunction (Trifunovic et al. 2005; Hiona et al. 2010), or through pharmaceuticals, such as metformin (Foretz et al. 2010) or AICAR (Corton et al. 1995). Molecularly AMPK can be phosphorylated and thus activated by LKB-1; the activation is maintained by allosteric hindrances to phosphatases provided by a high AMP/ATP ratio. As the large differences in AMPK activation occur between sedentary MRL and B6 mice, we reason that basal metabolic stress is the primary and chronic AMPK activator. The MRL cells attempt to compensate

for decreased ATP by increasing their mitochondrial content; this appears to be somewhat successful as ATP levels are not different from the B6 controls. However, some stress signals persist, such as phosphorylated AMPK. A tight feed-back loop is envisioned where the slightest decrease in ATP activates the AMPK to increase mitochondria and ATP output. This chronic condition is clearly different than acute pAMPK stimulation. Although we failed to detect decreased ATP in the MRL skeletal muscle tissues by the colorimetric assay; this assay may not be sensitive enough as we expect the actual difference to be slight. More sensitive HPLC detection assays are planned.

Altered MRL metabolism

The current work corroborates and extends previous work of altered metabolism in MRL fibroblasts and liver tissue (Naviaux et al. 2009). Now, by identifying increased pAMPK in the skeletal muscle tissue of the MRL animals, we have added an important mechanistic point in the MRL scheme of metabolic differences and phenotype (Fig. 14). The increased pAMPK can explain many metabolic alterations identified by Navieux et al. in fibroblasts; increased glycolysis, increased mitochondrial number, altered OxPhos protein levels, and lower membrane potential (Naviaux et al. 2009). We now corroborate and extend the results to skeletal muscles.

We also analyzed mRNA expression levels of multiple enzymes involved in metabolism. The MRL quadriceps muscles had significantly increased levels of four of the six enzymes analyzed. Hexokinase 2 is the predominant hexokinase isoform in skeletal muscle, phosphorylates glucose for the glycolytic and oxidative phosphorylation pathways and is upregulated by insulin (Irimia et al. 2012). Citrate synthase is also upregulated in MRL muscles; it is the first and rate-limiting step of the citric acid cycle. The fact that transcripts of carnitine palmitoyltransferase 1b (CPT1b) and CD36 fatty acid translocase (CD36/FAT) are also increased in MRL muscle tissue suggests that free fatty acid metabolism is also increased. CPT1b is

found on the outer mitochondrial membrane and transports long-chain fatty acids into the mitochondria. CD36/FAT is involved in long-chain fatty acid uptake by the cell (Lombardi et al. 2012). These data provide new insights into MRL metabolism; the citric acid cycle and fatty acid metabolism may also be increased in addition to the already known increase of glycolysis.

Metabolic flux analysis performed upon the primary skeletal muscle cells isolated from the MRL and B6 mice corroborates the increased glycolysis previously demonstrated in fibroblast cells (Naviaux et al. 2009). Glycolysis is increased as is demonstrated by the increase in ECAR, and oxidative phosphorylation may also be increased as is demonstrated by the increase in the oxygen consumption rate (OCR). Furthermore, the MRL muscle cells appear to have increased oxidative reserve capacity as is demonstrated by the maximum OCR after the addition of the mitochondrial membrane uncoupler FCCP. As we are using cell number for normalization, the apparent increases in oxidative phosphorylation and maximal oxygen consumption may reflect the demonstrated increase of mitochondria in MRL muscle cells. However, the data remain pertinent as it demonstrates that the MRL cells have increased oxidative phosphorylation and an increase in physiologic reserve. As glycolysis – indicated by acidification – occurs in the cytoplasm this increase likely reflects a true cellular rate change. Similarly, the MRL muscles have slightly decreased ratios of oxygen consumption to acidification rate. This further indicates that the MRL muscle cells have a higher ratio of glycolysis to oxidative phosphorylation than the B6 control muscle cells do.

F. **Conclusion**

We undertook these experiments to identify molecular metabolic differences between the fibrosis-resistant, super healing MRL mice, and the standard control B6 mice. We have found that the MRL mice have increased mitochondria and increased pAMPK to AMPK ratio. The data presented here

allow us to put forth a model of altered metabolism in the skeletal muscle of the MRL mouse. We hypothesize that these mice are inefficient at producing ATP by the normal methods – substrate level phosphorylation of the Kreb's cycle and oxidative phosphorylation by the electron transport chain – and, therefore, must compensate. We argue that the compensation has multiple avenues. The MRL mice perform more glycolysis (Naviaux et al. 2009), which is usually associated with short-term compensation as is required in acute exercise. The mice also have increased mitochondrial content and increased pAMPK which may be viewed as chronic adaptations to low energy levels. Although as pAMPK remains elevated the mice never fully compensate for their energy insufficiency. The mice also retain some embryonic markers and have decreased ROS (Naviaux et al. 2009). These many unique characteristics possibly increase the healing capabilities of these mice, although separating the salient differences from the bystander differences continues to prove challenging.

An abundance of studies with increased pAMPK either through exercise, transgenics or pharmacueticals have recently been published. With this novel MRL mouse strain data, the scientific community now also has a mouse strain with endogenously and chronically increased activated AMPK. AMPK activation is increasingly becoming discussed as an attractive therapeutic target to halt muscle wasting diseases. Roles for AMPK have been identified in mouse muscle cell autophagy and maintenance (reviewed in (Sanchez et al. 2012)), increasing utrophin expression for treatment of dystrophin mutant muscular dystrophy (Ljubicic et al. 2011), and halting muscular dystrophy pathology (Ljubicic et al. 2011; Bueno Junior et al. 2012; Jahnke et al. 2012; Pauly et al. 2012). Furthermore, increased mitochondrial content – as shown in the MRL muscles – may be of additional benefit in Muscular Dystrophy due to their ability to buffer the inappropriate calcium signaling occurring in MD muscles (Selsby et al. 2012). It is also becoming increasingly obvious that therapeutics utilized to combat type 2 diabetes require pAMPK for function (Viollet et al. 2012). As type 2 diabetes is ultimately a

disease of skeletal muscle this syndrome can also be considered in our list of muscle wasting diseases that respond favorably to AMPK activators.

The naturally increased pAMPK in MRL skeletal muscle tissue is of particular interest for the muscular dystrophy field. We have recently demonstrated that F2 MRL by DBA2/J intercross mice with a muscular dystrophy causing *γ*–sarcoglycan null mutation (Sgcg−/−) have a very mild disease with significantly reduced fibrosis in skeletal, diaphragm, and cardiac muscle compared to DBA2/J Sgcg−/− parental strain (Heydemann et al. 2012). Furthermore, the F2 Sgcg−/− mice, with only 50% of MRL contributed nuclear genome, have significantly better cardiac function. Now, in this current manuscript, we have identified a candidate molecular mechanism behind the MRL's mild muscular dystrophy disease. That increasing pAMPK will aid muscular dystrophy mouse models are becoming accepted. However, how increased pAMPK benefits the mice is still under scrutiny. We will continue to investigate the unique MRL mice and their unique metabolism to further the understanding of how increasing pAMPK is beneficial. Identifying the specific pAMPK targets which diminish muscular dystrophy is important for the identification of more specific therapies. In addition, therapies for other muscle diseases may become revealed with these mechanistic investigations.

G. Acknowledgments

We gratefully thank J. Rehman for the use of the Seahorse Glycolytic Flux Analyzer and D. Glick for her invaluable technical assistance with the Seahorse Glycolytic Flux Analyzer. We are also grateful to V. Liakaite and S. Green from the University of Illinois at Chicago, Research Resources Core, DNA Services Facility for guidance with the qPCR and performance of the Quantigene techniques.

H. Conflict of Interest

The authors have no conflicts, financial or otherwise to declare.

I. **Footnotes**

Funding Information

This research was funded by a grant from the National Institutes of Health RO1: RHL102322A. The funder had no role in study design, data collection and analysis, decision to publish, or preparation of the manuscript.

Both authors contributed equally to the experiments.

Manuscript Received: November 4, 2013.

Manuscript Revised: January 21, 2014.

Manuscript Accepted: January 26, 2014.

J. **References**

Adachi, M., R. Watanabe-Fukunaga, et al. (1993). "Aberrant transcription caused by the insertion of an early transposable element in an intron of the Fas antigen gene of lpr mice." Proceedings of the National Academy of Sciences of the United States of America 90(5): 1756-1760.

Alleva, D. G., S. B. Kaser, et al. (1997). "Aberrant cytokine expression and autocrine regulation characterize macrophages from young MRL+/+ and NZB/W F1 lupus-prone mice." Journal of immunology 159(11): 5610-5619.

Arthur, L. M., R. M. Demarest, et al. (2010). "Epimorphic regeneration in mice is p53-independent." Cell cycle 9(18): 3667-3673.

Baker, K. L., S. B. Daniels, et al. (2006). "Neuroblast protuberances in the subventricular zone of the regenerative MRL/MpJ mouse." The Journal of comparative neurology 498(6): 747-761.

Bedelbaeva, K., A. Snyder, et al. (2010). "Lack of p21 expression links cell cycle control and appendage regeneration in mice." Proceedings of the National Academy of Sciences of the United States of America 107(13): 5845-5850.

Clark, L. D., R. K. Clark, et al. (1998). "A new murine model for mammalian wound repair and regeneration." Clinical immunology and immunopathology 88(1): 35-45.

Corton, J. M., J. G. Gillespie, et al. (1995). "5-aminoimidazole-4-carboxamide ribonucleoside. A specific method for activating AMP-activated protein kinase in intact cells?" Eur J Biochem 229(2): 558-565.

Davies, S. P., N. R. Helps, et al. (1995). "5'-AMP inhibits dephosphorylation, as well as promoting phosphorylation, of the AMP-activated protein kinase. Studies using bacterially expressed human protein phosphatase-2C alpha and native bovine protein phosphatase-2AC." FEBS Lett 377(3): 421-425.

Donnelly, R. P., J. Levine, et al. (1990). "Aberrant regulation of IL-1 expression in macrophages from young autoimmune-prone mice." Journal of immunology 145(10): 3231-3239.

Foretz, M., S. Hebrard, et al. (2010). "Metformin inhibits hepatic gluconeogenesis in mice independently of the LKB1/AMPK pathway via a decrease in hepatic energy state." J Clin Invest 120(7): 2355-2369.

Garcia-Cazarin, M. L., J. L. Gamboa, et al. (2011). "Rat diaphragm mitochondria have lower intrinsic respiratory rates than mitochondria in limb muscles." Am J Physiol Regul Integr Comp Physiol 300(6): R1311-1315.

Ghezzi, D., E. Baruffini, et al. (2012). "Mutations of the mitochondrial-tRNA modifier MTO1 cause hypertrophic cardiomyopathy and lactic acidosis." Am J Hum Genet 90(6): 1079-1087.

Godin, R., F. Daussin, et al. (2012). "Peroxisome proliferator-activated receptor gamma coactivator1-gene alpha transfer restores mitochondrial biomass and improves mitochondrial calcium handling in post-necrotic mdx mouse skeletal muscle." J Physiol 590(Pt 21): 5487-5502.

Hardie, D. G. (2003). "Minireview: the AMP-activated protein kinase cascade: the key sensor of cellular energy status." Endocrinology 144(12): 5179-5183.

Hardie, D. G. (2011). "Sensing of energy and nutrients by AMP-activated protein kinase." Am J Clin Nutr 93(4): 891S-896.

Heber-Katz, E., J. Leferovich, et al. (2004). "The scarless heart and the MRL mouse." Philosophical transactions of the Royal Society of London. Series B, Biological sciences 359(1445): 785-793.

Heydemann, A. (2012). "The super super-healing MRL mouse strain " Front. Biol. 7(6): 522-538.

Heydemann, A., K. A. Swaggart, et al. (2012). "The superhealing MRL background improves muscular dystrophy." Skelet Muscle 2(1): 26.

Hiona, A., A. Sanz, et al. (2010). "Mitochondrial DNA mutations induce mitochondrial dysfunction, apoptosis and sarcopenia in skeletal muscle of mitochondrial DNA mutator mice." PLoS One 5(7): e11468.

Irimia, J. M., J. Rovira, et al. (2012). "Hexokinase 2, glycogen synthase and phosphorylase play a key role in muscle glycogen supercompensation." PLoS One 7(7): e42453.

Irwin, M. H., K. Parameshwaran, et al. (2012). "Mouse models of mitochondrial complex I dysfunction." Int J Biochem Cell Biol.

Jahnke, V. E., J. H. Van Der Meulen, et al. (2012). "Metabolic remodeling agents show beneficial effects in the dystrophin-deficient mdx mouse model." Skelet Muscle 2(1): 16.

Kanki, T., K. Ohgaki, et al. (2004). "Architectural role of mitochondrial transcription factor A in maintenance of human mitochondrial DNA." Mol Cell Biol 24(22): 9823-9834.

Kench, J. A., D. M. Russell, et al. (1999). "Aberrant wound healing and TGF-beta production in the autoimmune-prone MRL/+ mouse." Clinical immunology 92(3): 300-310.

Kong, X., R. Wang, et al. (2010). "Sirtuin 3, a new target of PGC-1alpha, plays an important role in the suppression of ROS and mitochondrial biogenesis." PLoS One 5(7): e11707.

Kudo, N., A. J. Barr, et al. (1995). "High rates of fatty acid oxidation during reperfusion of ischemic hearts are associated with a decrease in malonyl-CoA levels due to an increase in 5'-AMP-activated protein kinase inhibition of acetyl-CoA carboxylase." J Biol Chem 270(29): 17513-17520.

Lagouge, M., C. Argmann, et al. (2006). "Resveratrol improves mitochondrial function and protects against metabolic disease by activating SIRT1 and PGC-1alpha." Cell 127(6): 1109-1122.

Ljubicic, V., P. Miura, et al. (2011). "Chronic AMPK activation evokes the slow, oxidative myogenic program and triggers beneficial adaptations in mdx mouse skeletal muscle." Hum Mol Genet 20(17): 3478-3493.

Lombardi, A., R. De Matteis, et al. (2012). "Responses of skeletal muscle lipid metabolism in rat gastrocnemius to hypothyroidism and iodothyronine administration: a putative role for FAT/CD36." Am J Physiol Endocrinol Metab 303(10): E1222-1233.

Moreno-Loshuertos, R., R. Acin-Perez, et al. (2006). "Differences in reactive oxygen species production explain the phenotypes associated with common mouse mitochondrial DNA variants." Nat Genet 38(11): 1261-1268.

Naviaux, R. K., T. P. Le, et al. (2009). "Retained features of embryonic metabolism in the adult MRL mouse." Molecular genetics and metabolism 96(3): 133-144.

Pauly, M., F. Daussin, et al. (2012). "AMPK Activation Stimulates Autophagy and Ameliorates Muscular Dystrophy in the mdx Mouse Diaphragm." Am J Pathol 181(2): 583-592.

Ponticos, M., Q. L. Lu, et al. (1998). "Dual regulation of the AMP-activated protein kinase provides a novel mechanism for the control of creatine kinase in skeletal muscle." EMBO J 17(6): 1688-1699.

Qiu, Q., R. Li, et al. (2012). "Mitochondrial tRNA mutations are associated with maternally inherited hypertension in two Han Chinese pedigrees." Hum Mutat 33(8): 1285-1293.

Rando, T. A. and H. M. Blau (1994). "Primary mouse myoblast purification, characterization, and transplantation for cell-mediated gene therapy." J Cell Biol 125(6): 1275-1287.

Sachadyn, P., X. M. Zhang, et al. (2008). "Naturally occurring mitochondrial DNA heteroplasmy in the MRL mouse." Mitochondrion 8(5-6): 358-366.

Salt, I. P., G. Johnson, et al. (1998). "AMP-activated protein kinase is activated by low glucose in cell lines derived from pancreatic beta cells, and may regulate insulin release." Biochem J 335 (Pt 3): 533-539.

Sanchez, A. M., A. Csibi, et al. (2012). "AMPK promotes skeletal muscle autophagy through activation of forkhead FoxO3a and interaction with Ulk1." J Cell Biochem 113(2): 695-710.

Selsby, J. T., K. J. Morine, et al. (2012). "Rescue of dystrophic skeletal muscle by PGC-1alpha involves a fast to slow fiber type shift in the mdx mouse." PLoS One 7(1): e30063.

Szczepanowska, J., D. Malinska, et al. (2012). "Effect of mtDNA point mutations on cellular bioenergetics." Biochim Biophys Acta 1817(10): 1740-1746.

Taub, P. R., I. Ramirez-Sanchez, et al. (2012). "Alterations in skeletal muscle indicators of mitochondrial structure and biogenesis in patients with type 2 diabetes and heart failure: effects of epicatechin rich cocoa." Clin Transl Sci 5(1): 43-47.

Theofilopoulos, A. N. and F. J. Dixon (1985). "Murine models of systemic lupus erythematosus." Adv Immunol 37: 269-390.

Trifunovic, A., A. Hansson, et al. (2005). "Somatic mtDNA mutations cause aging phenotypes without affecting reactive oxygen species production." Proc Natl Acad Sci U S A 102(50): 17993-17998.

Ueno, M., B. L. Lyons, et al. (2005). "Accelerated wound healing of alkali-burned corneas in MRL mice is associated with a reduced inflammatory signature." Investigative ophthalmology & visual science 46(11): 4097-4106.

Viollet, B., B. Guigas, et al. (2012). "Cellular and molecular mechanisms of metformin: an overview." Clin Sci (Lond) 122(6): 253-270.

Virbasius, J. V. and R. C. Scarpulla (1994). "Activation of the human mitochondrial transcription factor A gene by nuclear respiratory factors: a potential regulatory link between nuclear and mitochondrial gene expression in organelle biogenesis." Proc Natl Acad Sci U S A 91(4): 1309-1313.

Winder, W. W. and D. G. Hardie (1996). "Inactivation of acetyl-CoA carboxylase and activation of AMP-activated protein kinase in muscle during exercise." Am J Physiol 270(2 Pt 1): E299-304.

Yuan, R., S. W. Tsaih, et al. (2009). "Aging in inbred strains of mice: study design and interim report on median lifespans and circulating IGF1 levels." Aging Cell 8(3): 277-287.

Zong, H., J. M. Ren, et al. (2002). "AMP kinase is required for mitochondrial biogenesis in skeletal muscle in response to chronic energy deprivation." Proc Natl Acad Sci U S A 99(25): 15983-15987.

IV: The MRL heart resists high fat diet and obesity induced dysfunction

A. Introduction

Type 2 Diabetes (T2D) accounts for 95% of Diabetes Mellitus (DM) cases in the United States (cdc.gov). According to the CDC as of 2014, 29.1 million people in the United States have DM (cdc.gov). This is a grave concern as the population of the United States in mid-July 2014 was roughly 319 million (census.gov). To add further concern and emphasis, the CDC also notes that roughly 1 in 3 adults have prediabetes (elevated blood glucose during the fasting state) and that 9 of every 10 who are prediabetic are unaware of their condition. Altogether DM gives the impression of another condition that will continue to impact society as a whole. In 1981 there were roughly 5.5 million citizens of the US with DM, just a bit over three decades to 2014 and there were 29 million people afflicted.

Metformin and other drugs that lower and help regulate blood glucose are prescribed to T2D patients along with behavioral modifications. Lowered blood glucose is achieved by metformin through the phosphorylation of AMP Kinase, (pAMPK, AMPK) (Viollet, Guigas et al. 2012). pAMPK stimulates cells to take in more nutrients and greatly slows down energy consuming events. Increased pAMPK causes the liver to greatly reduce glucose production and export into the blood (Viollet, Guigas et al. 2012). Increased pAMPK in skeletal muscle triggers the relocation of Glut4 (a glucose transporter) to the sarcolemma (muscle cell membrane) (Viollet, Guigas et al. 2012). Glut4 at the sarcolemma transports glucose from the blood stream into the muscle cell.

While metformin does reduce blood glucose to relatively normal levels, it does not treat the overall problem in T2D. Systemic glucose resistance still results in metabolic shifts within the tissues of the body. The heart is susceptible like every other organ. In particular T2D induces an increase in fat (lipid) uptake in the heart but does not increase fat usage. Over time fat accumulates in the heart and

disrupts cardiac metabolism. This in turn leads to cardiomyocytes (heart muscle cells) dying and being replaced with scar tissue (fibrosis). Due to the nature of electrical conductivity in the heart, buildup of scar tissue will disrupt proper heart contraction.

Sadly more than half of all diabetes related deaths involve the heart failing. Even with treatments such as metformin, the heart still develops abnormalities in its function. This necessitates research into the diabetic heart. Work from the lab has shown that the MRL mouse has elevated pAMPK in their skeletal muscle (Berhanu, Holley-Cuthrell et al. 2014). This was discovered as the lab was previously looking into the MRL mouse response to muscular dystrophy. AMPK is a major regulator of cellular metabolism and its phosphorylation has been shown to be beneficial to resisting the pathology of muscular dystrophy (Ljubicic, Miura et al. 2011).

This elevated pAMPK in the MRL skeletal muscle appears to mimic the effects of metformin. In turn the question was asked, will the MRL mice resist developing diabetes if given a high fat diet? The question was investigated in the 2014 Mull et al paper (Mull, Berhanu et al. 2014). High fat diet feeding does induce weight gain in the MRL mouse but the strain does not develop hyperglycemia. Elevated pAMPK was found in the skeletal muscle of the MRL mice fed the high fat diet and the chow diet. So the systemic assessment of the MRL mouse on a high fat diet demonstrated that the strain resists some of the pathology associated with diabetes. The question then turns to, is the heart protected? My aim was to assess the heart of the MRL and C57/Bl6 mice given either a high fat diet or the standard chow diet. Compare the differences between diets in each strain and determine if either strain develops diabetic cardiomyopathy after 12 or 20 weeks of the high fat diet.

B. **Background**

Despite 95% of DM cases being T2D, Type 1 Diabetic mouse models are largely preferred as research models. This is most likely due to T1D being more straightforward in development and cause. As T1D develops as the body stops producing insulin, it is very easy to replicate in mouse models. Streptozotocin (STZ) is the drug of choice for targeting and ablating the beta pancreas cells that produce insulin. Given to mice or rats STZ induces T1D after only a few weeks of treatment. It has been used alongside a high fat diet to induce what the authors of that paper refer to as T2D (Calligaris, Lecanda et al. 2013). Personally I found this suspect as T1D and T2D arise from vastly different sources. T1D occurs when the body stops producing insulin, either from outside insult or from autoimmunity. T2D occurs as the body becomes increasingly resistant to insulin. However Zhang, Z et al 2014 demonstrated that treating high fat diet fed mice with 1 injection of STZ develop far more fibrosis and lipid accumulation in the heart than high fat diet mice that did not receive the injection (Zhang, Wang et al. 2014). Thus showing that STZ can be useful to accelerate the progression of T2D in high fat diet fed mice in place of waiting for over a year for symptoms to develop significantly. Zhang et al did demonstrate that an AMPK activator reduced fibrosis, lipid accumulation, and gene expressions that were induced by the high fat diet and STZ.

AMPK, AMP protein dependent kinase, is a heterotrimeric protein complex that primarily regulates the metabolic "switch" between anabolic (constructive) and catabolic (destructive) pathways in cells. There are two AMPK alpha subunits, two beta, and three gamma. The subunits do display elevated expression in specific tissues and different combinations of alpha, beta, and gamma have been shown to possess different kinetics (Salt, Celler et al. 1998; Wu, Puppala et al. 2013). AMPK is activated by phosphorylation (via LKB), a process by which a phosphate is attached to threonine 172 on the alpha subunit. This in turn increases the activity of AMPK by over 1000x (Suter, Riek et al. 2006). pAMPK

interacts with other signaling components and regulates expression of proteins involved in nutrient uptake, nutrient usage, and cell growth (discussed in (Viollet, Athea et al. 2009)). Energy stress is one key event that facilitates the phosphorylation of AMPK. Increase of the AMP:ATP ratio increases the likelihood of AMP binding in the gamma subunit of the AMPK heterotrimer. Binding of AMP to the gamma subunit induces a conformational shift which is transferred through the beta subunit into the alpha subunit. This shift exposes the threonine targeted by LKB and greatly increases the probability of phosphorylation occurring.

AMPK's activity has been known for decades at this point. As it is heavily involved in metabolism and metabolic control; various research groups have genetically modified organisms to assess the impact of loss of an ampk subunit. A recent 2009 review by Benoit, Viollet et al titled "AMPK: Lessons from transgenic and knockout animals" extensively covers the research to date of publication (Viollet, Athea et al. 2009). I recommend that review to anyone interested in working with AMPK transgenic mice. A brief summary of key points from the review will follow.

Each subunit of the AMPK heterotrimer is encoded by a separate gene. Knocking out of both subunits of AMPK alpha resulted in a lethal phenotype seen around e10.5 (10.5 days post fertilization); this is not unexpected as AMPK alpha are responsible for the complexes activity. While knocking out one of the two alpha subunits is not lethal, Benoit et al do cite research from their group which has shown that knockout of the alpha2 subunit leads to impaired glucose tolerance and insulin resistance (Jorgenson, SB et al 2004; Viollet, B et al 2003). Meanwhile knockout of the alpha1 subunit showed no systemic metabolic changes.

In addition to AMPK alpha2 knockout leading to global insulin resistance, it has also been shown to reduce lipid oxidation and glucose metabolism within the heart. Benoit et al describe discoveries of how mutations in AMPK alpha 2 lead to cardiomyopathies. Of note, one study (Sakamoto, Zarrinpashneh et al. 2006) noted that LKB1 knockout hearts showed near identical phenotypic changes to AMPK alpha2 knockout hearts.

Activators of AMPK activity have been shown to help the heart resist ischemia/reperfusion damage following temporary occlusion of major arteries in the mouse heart (Horman, Beauloye et al. 2012). They have also been tested in diabetes mouse models. One such study, Zhang Z et al, used sulfrophane an AMPK activator to treat C57BL/6 mice with induced type 2 diabetes (Zhang, Wang et al. 2014). The authors fed groups of C57/Bl6 mice a chow diet or high fat diet (60%) for three months. At which time some of the mice were injected with a single dose of streptozotocin to partially ablate insulin producing cells in the pancreas. Five days later, injected mice were assessed for basal hyperglycemia, those with the condition were deemed the diabetes mellitus group. For the final four months half of the DM mice were treated with sulfrophane. All mice were maintained on their respective diets across the experiments.

Only the high fat diet animals without sulfrophane or the streptozotocin developed larger hearts, measured by heart weight over tibia length. Sulfrophane also reduced the development of fibrosis and lipid accumulation in the DM mice to near the HFD levels but not down to the chow diet controls. Markers of cardiac oxidative stress were normalized to near chow diet levels in the DM sulfrophane treated mice.

High fat diet has been given to the C57Bl/6 mice over a prolonged time course as well. Two studies, Petro, Cotter et al. 2004 and Calligaris, Lecanda et al. 2013, detail the effects of the high fat diet (Petro, Cotter et al. 2004; Calligaris, Lecanda et al. 2013). Petro et al demonstrated that within four weeks of a 58% fat, high fat diet, the high fat diet fed males had significantly greater blood glucose and significantly greater blood insulin than their chow diet counterparts. These results remained consistent across the full 11 weeks of high fat diet. Calligaris et al went for a long term study observing C57Bl/6 male mice at eight, twelve, and sixteen months. High fat diet, seemingly the same as in Petro et al manuscript, fed mice were found to be heavier, have higher blood glucose, insulin, and cholesterol at all three time points compared to their chow diet counterparts. Cardiac hypertrophy was observed at all three time points in the high fat diet group as well, measured by heart weight/tibia length, write out left ventricle posterior wall during diastole (LVPWd) and interventricular septum during diastole (IVSd).

These three papers demonstrate that the C57Bl/6 mouse is a valid model of type 2 diabetes in mice. This is important as the C57Bl/6 strain has been used as the control mouse in studies investigating the MRL mouse strain. There is not a good control mouse strain for the MRL as the MRL strain is the result of four other strains being bred together for autoimmunity research. As such the C57Bl/6 mouse was used for the study that follows.

High fat diets are not the fastest of methods to induce type 2 diabetes in a mouse model nor the most consistent. Streptozytocin in repeated doses is used to completely ablate beta-islet pancreas cells in mice. This method leads to a characteristic Type 1 Diabetes model as it mimics the cause of human Type 1 Diabetes. Ob/Ob and Db/Db mutants, the first a leptin knock out and the latter a leptin-receptor knock out, either mutation induces obesity and diabetes within months of birth. These two mouse groups fall under Type 2 Diabetes as their conditions result from obesity and insulin resistance. The

aforementioned mouse models, as well as examples of high fat diets inducing diabetes in mice, have been reviewed in (Bugger and Abel 2009).

While diabetes is a systemic disease and affects the body, its effects are particularly felt on the heart. Roughly sixty percent of all diabetes related deaths are cardiovascular in nature (heart.org). In Type 2 Diabetes, the heart upregulates fat(lipid) uptake in response to insulin resistance. However it does not upregulate metabolism of the acquired fat. Fat in turn accumulates within heart cells. Lipotoxicity develops over time as lipid (fat) content continues to rise. Though there is some argument within the literature as to whether it is just accumulation of lipids that triggers lipotoxicity or if a decrease in turnover of the lipid pool is what allows the lipids to be converted into ceramides. Regardless of how, this lipid accumulation leads to disrupted metabolic and cell signaling in time leading to cell death. Combined with reduced glucose uptake and metabolism due to systemic insulin resistance, the heart's functional capacity is impaired in diabetes. The above is a brief summary of a far more extensive review by (Amaral and Okonko 2015), with the exception of the argument within the literature which was derived from personal correspondences.

C. **Methods and Materials**

Methods used in this study were identical to the corresponding methods used in (Roberts, Holley-Cuthrell et al. 2015) and (Mull, Berhanu et al. 2014). Electron microscopy samples were placed into the required solution by the UIC RRC electron microscopy group and handed over to them for sampling and processing. Student T.tests were performed to determine the p-value, all error bars are standard error of the mean.

Left Ventricle mass normalized to tibia length

Both tibias were collected from each mouse. Following minor cleaning each tibia was measured by caliper and the lengths averaged. Left ventricle mass from the echocardiography data was divided by the average tibia length for each mouse and the resulting ratios grouped by mouse group.

Quantigene

Direct quantification of mRNA transcripts was attained using the Quantigene machine and associated protocols. In brief, apex samples weighing ~5 mg were collected during harvest and lysised in the presence of a buffer. The resulting suspension was handed over to the UIC RRC for the Quantigene protocol itself.

Protein Quantification

Quantification of protein in the hearts was assessed by lysising the apex section of assigned hearts. This was achieved through a combination of a lysis buffer and a tissueruptor (Qiagen). Following spin downs to remove as much debris as possible the resulting supernatant was stored in clean tubes. Small aliquots of each sample were used to quantify the protein concentration of each sample. 50 ng of each sample was prepared with lamina sample buffer (Biorad) and run on polyacrylamide gels. These gels are then placed into Invitrogen iBlot for a semi-dry transfer. This transfer uses electrical current to move the now weight separated proteins onto a PVDF membrane (Biorad) blot paper. Each blot is incubated in 3-5% milk or bovine serum albumin in tris buffered saline containing 1% Tween 20 (tbst) to block any proteins or blot paper that would grab proteins indiscriminately. This is necessary as it greatly reduces background and allows for cleaner visualization of the target proteins.

After three brief five minute washes the primary antibody is mixed into ten ml of tbst to a concentration of 1:5,000. Primary antibodies for this protocol are antibodies that target the protein, or protein sequence, of interest. The blot is then incubated in this mix overnight on a rocker at four degrees Celsius. Three more brief five minute washes using tbst are performed the following day. The blot is then incubated in a secondary antibody diluted at 1:10,000 in tbst at room temperature on a shaker for 1 hour. Following three more five minute washes the blot, ECL Prime (GE Healthcare) is placed on the blot and the blot is imaged on a Chemidoc (Biorad).

Electron Transport Chain

An oxidative phosphorylation cocktail antibody set (Abcam) which binds to one protein from each of the complexes was used to quantify the ETC in the samples acquired in this experiment.

D. Results

Echocardiography

Numerous assessments have been performed to quantify the effects of the high fat diet on the C57Bl/6 and MRL mice. Data falls into two broad categories, morphology and function, and signaling. Echocardiography is the predominant source of morphology and functional data for this experiment. Echocardiography uses vibration to visualize the heart while it is beating within the mouse; the procedure is near identical to sonograms performed on pregnant mothers to assess the growing fetus. Dr. Robert Gaffin of the Center for Cardiovascular Research Core performed echocardiography on the mice involved in this experiment.

Morphological, that is the structure of the heart, parameters from the twelve week animals revealed surprising data (Table I). C57Bl/6 mice fed the high fat diet had thicker left ventricular anterior

and posterior walls during diastole (LVAWd, LVPWd) and thicker left ventricular anterior walls (LVAWs) during systole. Left ventricular posterior walls during systole, as well as the left ventricular inner dimension during both diastole and systole are unchanged in the high fat diet mice. Relative wall thickness (RTW) was not significantly different between the two C57Bl/6 groups. C57Bl/6 high fat diet fed mice were heavier than their chow diet counter parts (34g vs 25g) and have greater left ventricular mass (92mg vs 78mg). In contrast to the C57Bl/6 mice, the MRL mice fed the high fat diet for twelve weeks showed no morphological differences by echocardiography compared to their chow diet counterparts. Assessing hypertrophy (abnormal cell enlargement) in the heart by left ventricle mass over tibia length showed that the C57Bl/6 high fat diet fed mice to have hypertrophic left ventricles (Table I). The observed thickening of the left ventricle in C57Bl/6 mice at twelve weeks of the high fat diet is a novel event to the author's knowledge. Tibia length is used as a normalizing factor as it is not dependent upon mouse weight; additionally no significant difference was found between the tibia lengths of MRL tibias from chow or high fat diet animals.

Groups	N	LVAWd (mm)	LVAWs (mm)	LVPWd (mm)	LV mass (mg)	*Mouse Wt (g)*	*LV Mass / Tibia Length*
B6 CD 12 wks	**13**	0.744±0.027	1.026±0.048	0.717±0.026	78.281±2.258	25.631±0.58	4.314±0.177
B6 HFD 12 wks	**26**	0.822±0.016	1.165±0.029	0.798±0.018	92.296±3.092	34.219±0.991	5.244±0.223
MRL CD 12 wks	**12**	1.035±0.036	1.524±0.063	1.027±0.037	143.334±6.542	43.558±0.79	6.759±0.23
MRL HFD 12 wks	**23**	1.001±0.031	1.398±0.036	1.06±0.035	136.596±5.260	51.417±1.145	7.086±0.413

Table I-Morphological echocardiography data demonstrating hypertrophy in the high fat diet fed C57Bl/6 hearts. Grey boxes indicate a p value <0.05 comparing the chow diet to high fat diet animals within each strain.

After twelve weeks the high fat diet C57Bl/6 mice do not show any diastolic differences compared to their chow diet counterparts (Table II). MRL high fat diet mice at 12 weeks showed decreased E', a measure of tissue movement next to the mitral valve during passive loading, compared to their chow diet counterparts. Statistically lower E'/A' was also found in the MRL high fat diet mice at 12 weeks, however the observed value is comparable to the C57Bl/6 heart. At 20 weeks of diet however E' in the MRL high fat diet mice was double of the chow diet animals. E'/A' showed no significant difference though E/E', another ratio used to assess diastolic function, was significantly lower in the high fat diet MRL mice.

Systolic analysis revealed one statistical difference between the C57Bl/6 high fat diet and chow diet mice at 12 weeks of diet (Table III). Cardiac output on its own is unchanged between the two groups. However the MRL high fat diet mice had reduced stroke volume (SV) and reduced cardiac output compared to their chow diet counterparts. Cardiac output / mouse weight is also reduced however this is not surprising as CO is lower and mouse weight greater in the high fat diet MRLs than their chow diet counterparts. Additionally cardiac output is not necessarily a valid variable as it is the result of stroke volume times the heart rate. In echocardiography of mice, the heart rate is largely dependent upon the percentage of isoflurane in the air supply to the mouse to keep it unconscious. However the decreased stroke volume observed in the high fat diet MRL mice is relevant and curious as there is not a statistical change in the end systolic volume between the two groups.

Group	E' (mm/ sec)	A' (mm/ sec)	E'/A'	E/E'	EDV (uL)
B6 CD 12 wks	23.2±1.72	23.2±1.77	1±0.08	35.5±2.36	65.8±3.09
B6 HFD 12 wks	22.9±0.91	22.2±0.96	1.1±0.1	35.3±2.1	67.5±2.18
MRL CD 12 wks	32.3±2.13	23.8±1.33	1.3±0.07	27.8±1.87	77±2.88
MRL HFD 12 wks	26.5±1.67	24.3±1.24	1.1±0.05	33.4±1.93	72.5±3.06

Table II-Diastolic echocardiography data showed minor differences within the MRL strain. However the observed significant difference in E'/A' is within physiological parameters. Grey boxes indicate a p value <=0.05 comparing the chow diet to high fat diet animals within each strain.

Groups	EF (%)	FS (%)	ESV (uL)	SV (μL)
B6 CD 12 wks	54.66±1.26	27.96±0.8	30.08±1.95	35.72±1.45
B6 HFD 12 wks	56.73±1.68	29.64±1.25	29.66±1.74	37.79±1.07
MRL CD 12 wks	68.78±2.43	38.67±2.01	24.71±2.63	52.33±1.06
MRL HFD 12 wks	61.67±2.27	33.38±1.73	28.26±2.25	44.27±2.08

Table III-Systolic echocardiography data showed only a change in the stroke volume in the MRL high fat diet mice. However no significant change was seen in Ejection Fraction (EF), Fractional Shortening (FS), or End Systolic Volume (ESV). Grey boxes indicate a p value <=0.05 comparing the chow diet to high fat diet animals within each strain.

At 20 weeks of the high fat diet MRL mice display increased ejection fraction (EF) and increased fractional shortening (FS). Ejection fraction is the percent of blood expelled from the left ventricle during contraction of the full volume present at the end of diastole. End systolic volume (ESV), the volume of blood left in the left ventricle following contraction, trends lower in the high fat diet fed MRL mice. Stroke volume trended to be higher in the high fat diet fed MRL mice

Cardiac Hypertrophy

Thicker left ventricle walls are associated with cardiac hypertrophy. However, echocardiography is not sufficient to definitively state that the C57Bl/6 hearts are swelling as a result of the diet Analysis of this data has shown that the C57Bl/6 high fat diet fed mice have greater ratios of left ventricle mass/tibia length than their chow diet counterparts (Figure 15). The MRL mice fed the high fat diet for 12 weeks did not show a significant increase in the ratio.

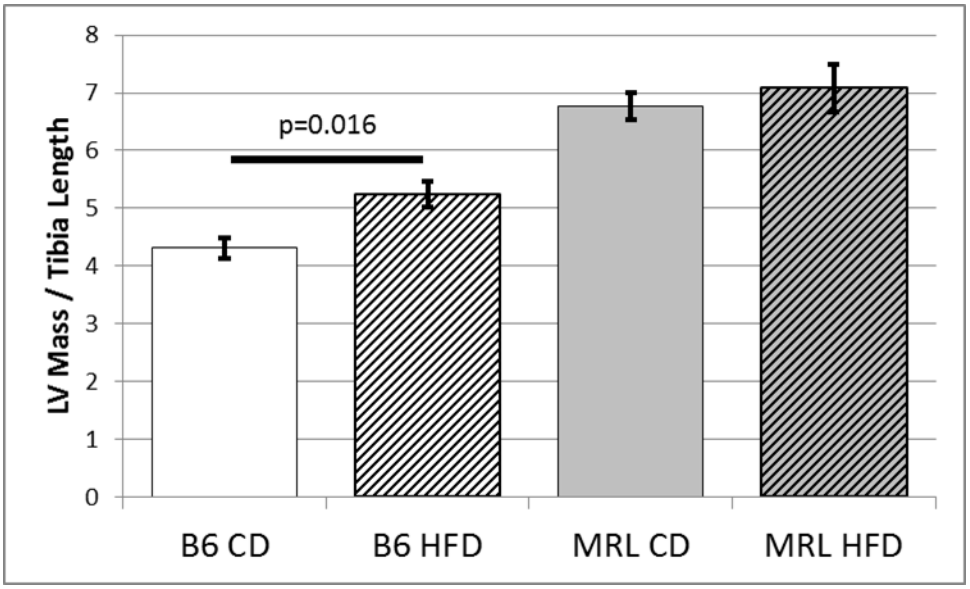

Figure 15-MRL mice fed the high fat diet do not develop larger left ventricles than their chow diet counterparts. No statistic difference was found between the MRL CD and MRL HFD left ventricle mass (echocardiography derived) over tibia length. Meanwhile the B6 HFD hearts have a larger ratio, indicating a greater left ventricle mass.

Electron Microscopy

The apex section of a heart from each group of twelve week mice was prepared for electron microscopy and handed off to the electron microscopy core at UIC. Analysis of prepared and imaged slices showed that the high fat diet fed C57Bl/6 male mouse had what appears to be lipid-like droplets within its cardiomyocytes (Figure 16). These appear both within the myofibers and the mitochondria. The high fat diet fed MRL mouse did not have these lipid-like droplets. Chow diet fed hearts showed no abnormalities.

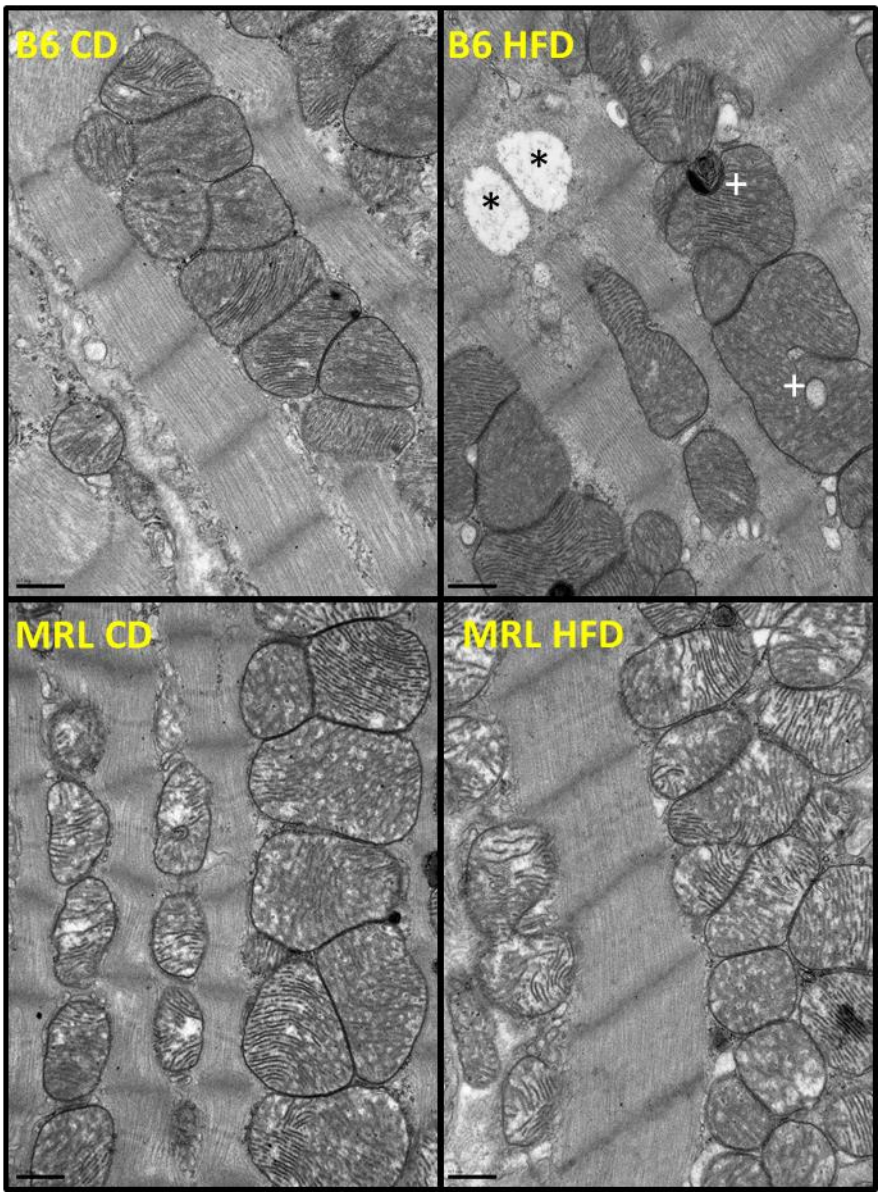

Figure 16- Electron microscopy revealed the accumulation of lipid like droplets within the C57Bl/6 high fat diet hearts. No such accumulation was found within the MRL HFD heart assessed.

* - cytoplasmic lipid-like droplets

\+ - mitochondrial lipid-like droplets

Quantigene

PGC1-Alpha, peroxisome proliferator-activated receptor gamma coactivator 1 alpha, a key component of metabolic gene regulation was found to be lower in the MRL high fat diet fed mice compared to their chow diet counterparts (Table IV). Chow diet MRL mice were found to have lower HKII, hexokinase II which phosphorylates glucose, than chow diet C57Bl/6 mice. Interestingly no significant differences were found in Glut4 mRNA within each strain or between the two strains. AMPK alpha 1, the alpha isoform typically found in endothelial cells within the heart (Viollet, Athea et al. 2009), was found to be lower in the MRL strain on both diets compared to the C57Bl/6 mice on the same diet. Conversely AMPK alpha 2 was found to be elevated in the chow diet fed MRL mice compared to the C57Bl/6 chow diet mice. The high fat diet MRL mouse does not have higher AMPK alpha 2 compared to the C57Bl/6 high fat diet mouse. High fat diet fed MRL mice trend to have lower AMPK alpha 2 ($p=.053$) than their chow diet counterparts. Interestingly AMPK beta 2 is lower in the MRL chow diet mice compared to the C57Bl/6 chow diet mice. However this difference is lost when both strains are placed on a high fat diet with the MRL expression of AMPK beta 2 increasing.

	PGC-1α	HKII	GLUT4	AMPKα1	AMPKα2	AMPKβ2
B6 CD	3.37±0.51	16.84±0.90	20.46±1.83	2.43±0.16	4.18±0.35	5.92±0.29
B6 HFD	3.46±0.60	14.43±1.07	16.92±1.92	2.35±0.15	4.30±0.45	5.73±0.30
MRL CD	3.99±0.32	12.91±0.74#	19.93±1.03	1.87±0.08#	5.47±0.19#	4.93±0.24#
MRL HFD	2.83±0.35*	13.52±1.20	17.15±1.30	1.88±0.09#	4.65±0.31	5.68±0.40

Table IV-Quantigene was used to assess mRNA levels of proteins of interest. PGC1-alpha was reduced in the MRL high fat diet samples compared to the chow diet MRL. HKII was found to be lower in the MRL chow diet compared to the C57Bl/6 chow diet. No statistical differences were found in Glut4 mRNA levels. AMPKα1 levels were lower in the MRL samples regardless of diet compared to the C57Bl/6 samples. AMPKα2 is higher in the MRL chow diet samples compared to the C57Bl/6 chow diet samples. AMPKβ2 mRNA was found to be lower in the MRL chow diet samples compared to the C57Bl/6 chow diet samples. n>10, * indicates p<=0.05 compared to the same strain, # indicates p<=0.05 compared to the other strain.

Protein Quantification

Phosphorylated AMPK and total AMPK were the key proteins of interest for this study. Data from (Berhanu, Holley-Cuthrell et al. 2014) and (Mull, Berhanu et al. 2014) both demonstrated that the MRL mouse has elevated pAMPK in its skeletal muscle. However analysis of pAMPK western blots from hearts has shown definitively that the MRL mouse has lower pAMPK in its heart on both the chow diet and high fat diet compared to the C57Bl/6 mice (Figure 17). This invalidates the hypothesis for this project. Unfortunately by the time a sufficient sample count (n=12) was reached western blots of other proteins were performed. Western blot analysis of AMPK (n=6) showed that the MRL chow diet fed hearts contain far greater quantities of AMPK than the C57Bl/6 chow diet mice (Figure 18). High fat diet feeding of the MRL mouse resulted in lower AMPK than the chow diet fed MRL hearts but greater than the high fat diet fed C57Bl/6 hearts. Reduced pAMPK is opposite of the MRL skeletal muscle and also calls into question how exactly the MRL heart handles the high fat diet.

Hexokinase II is one of many enzymes that phosphorylate glucose when the sugar enters the cell. This phosphorylation "locks" the glucose in the cell as the transports which import glucose cannot interact with and move glucose-6-phosphate. These enzymes are thus important for glucose metabolism and one of the major regulation steps of glycolysis. Here I can report that two western blots for HKII revealed that the MRL heart has longer HKII on both the chow and high fat diets than their C57Bl/6 counterparts (Figure 19). Contrary to the initial hypothesis Glut4 is lower in the MRL hearts in both diets compared to the C57Bl/6 mice (Figure 20). Again however this data agrees with the observed decreased pAMPK.

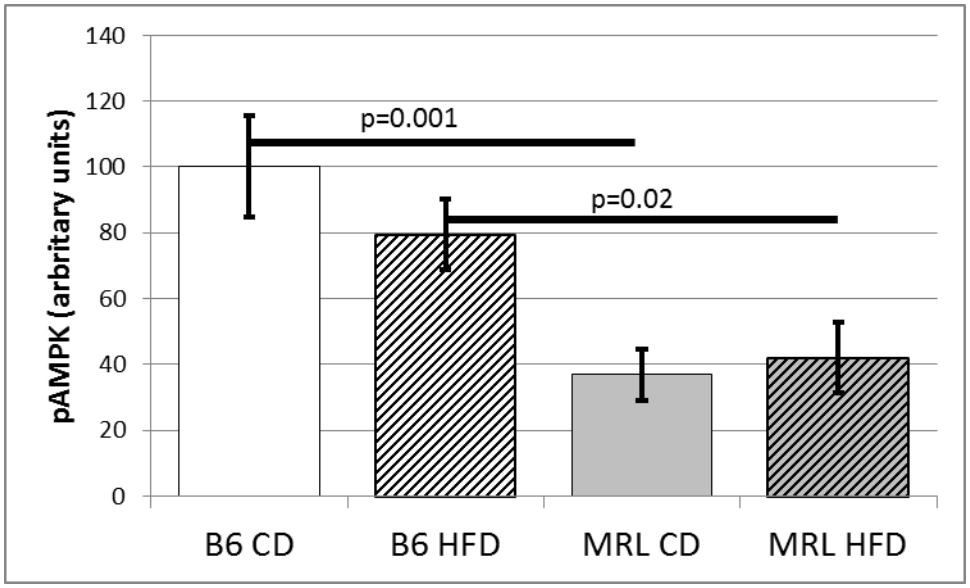

Figure 17-The MRL mouse has reduced levels of pAMPK compared to the C57Bl/6 mouse regardless of diet. Interestingly no difference was found within strain between the diet groups. n=12, normalized to B6 CD

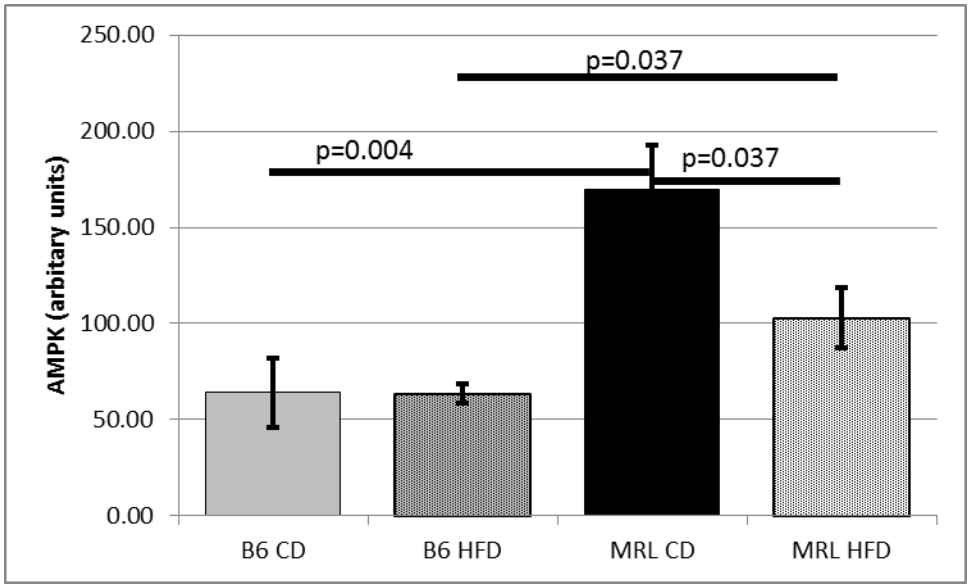

Figure 18-MRL hearts contain greater quantities of AMPK than the C57Bl/6 hears. AMPK levels were found to be elevated within both MRL hearts compared to their C57Bl/6 diet counterpart. However the high fat diet induced a decrease in AMPK within the MRL heart. n=6

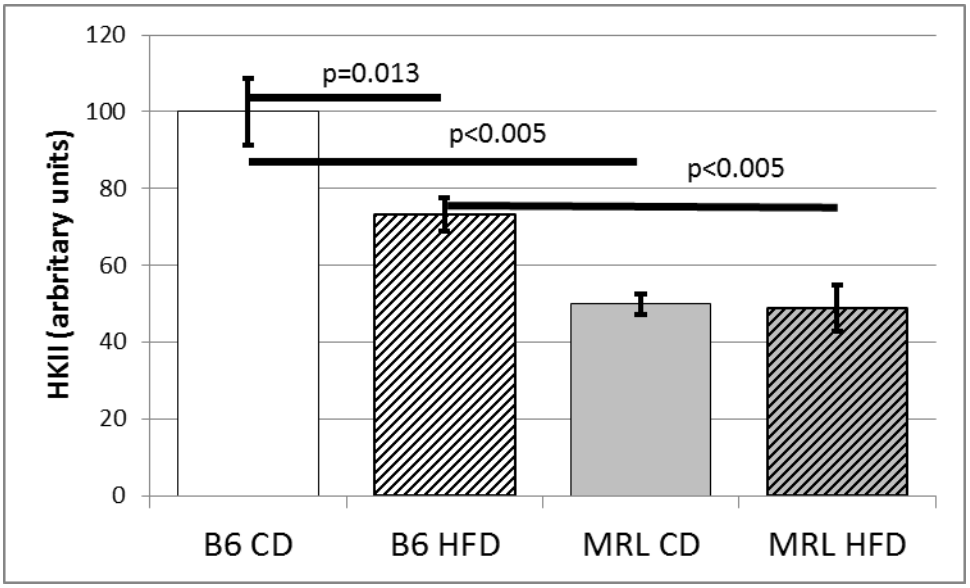

Figure 19-MRL hearts contain lower levels of HKII than C57Bl/6 hearts regardless of diet. Additionally the high fat diet results in less HKII within the C57Bl/6 hearts whereas there is no difference within the MRL hearts. n=9, Normalized to B6 CD

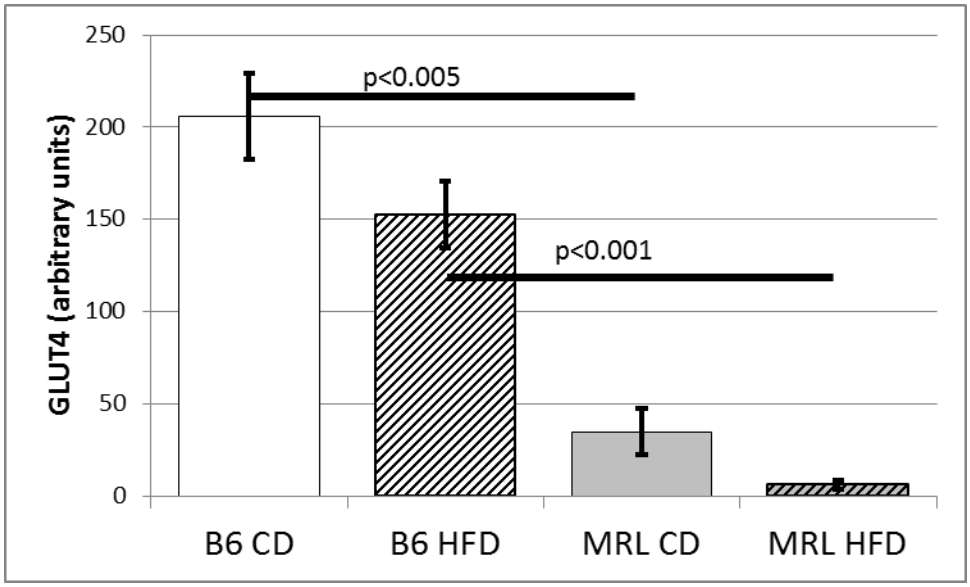

Figure 20-Glut4 is lower in the MRL mouse regardless of diet. Both high fat diet groups trend towards being lower than their chow diet counterparts. However neither achieve a p-value of <=0.05 (B6 CD vs B6 HFD p=0.14, MRL CD vs MRL HFD p=0.08) n=3

The MRL heart was found to contain greater quantities of Complex II through V on a chow diet compared to the C57Bl/6 heart (Figure 21). The high fat diet was only found to affect Complexes III and V in the MRL. Complex V is of note as it is the ATP generating complex within the chain. C57Bl/6 hearts on the high fat diet showed increased Complexes II through V compared to the C57Bl/6 chow diet hearts.

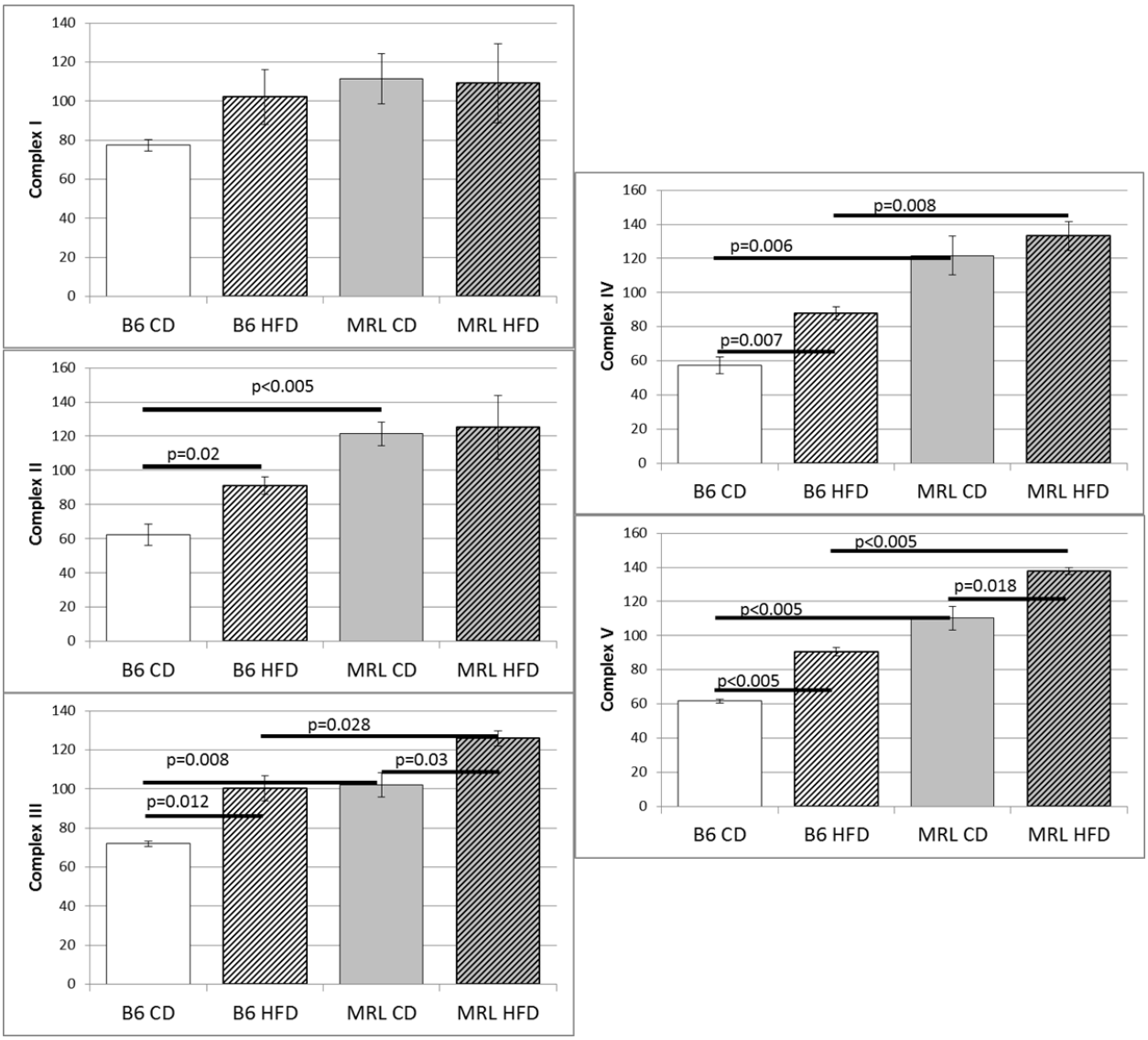

Figure 21-The MRL heart upregulates only two electron transport complexes while the C57Bl/6 heart upregulates four as a consequence of the high fat diet. Complexes II-V were found to be higher in the chow diet MRL hearts compared to the chow diet C57Bl/6 hearts. C57Bl/6 hearts from animals fed the high fat diet showed increases in Complexes II-V. MRL hearts from animals fed the high fat diet only showed increases in Complexes III and V. Complexes III, IV, and V were elevated in the MRL high fat diet hearts compared to the C57Bl/6 hearts. n=3

Quantification of PGC1-alpha in the acquired mouse samples revealed that the protein was lower in the high fat diet fed MRL hearts compared to chow diet MRL hearts and high fat diet C57Bl/6 hearts (Figure 22).

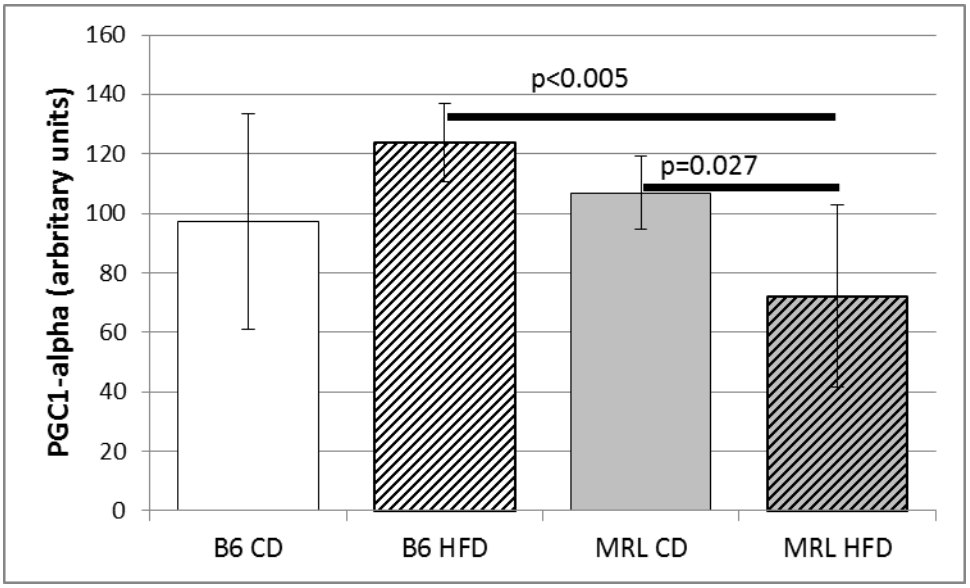

Figure 22-High fat diet MRL hearts displayed reduced PGC1-alpha protein content than their chow diet counterparts. No difference was found between the MRL and C57Bl/6 chow diet hearts, however high fat diet reduces PGC1-alpha content within the MRL heart significantly compared to the high fat diet C57/Bl6 hearts. n=6

Quantification of SERCA2A in the acquired samples revealed that the MRL chow diet hearts contain more SERCA2A than the C57Bl/6 chow diet hearts (Figure 23). No statistical difference was found between the two strains on the high fat diet. No statistical difference was found comparing each strain to itself.

PLN was found to be higher in the chow diet MRL hearts but no statistical difference was found between high fat diet groups or within strains (Figure 24) Phosphorylation state of PLN was not examined in these experiments.

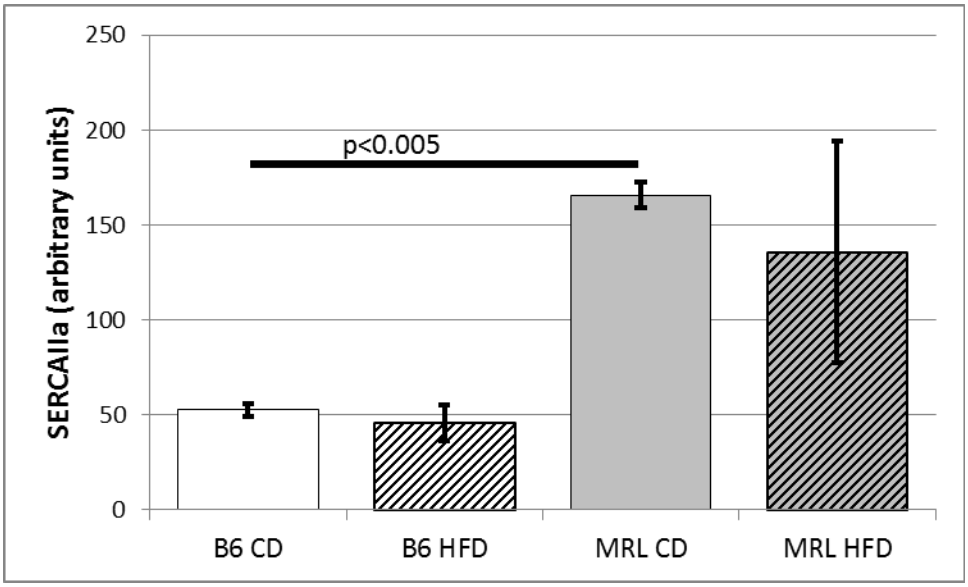

Figure 23-The baseline MRL heart contains greater quantities of SERCA2A than the C57Bl/6 heart. High fat diet feeding had no impact on SERCA2A levels within each strain. n=3

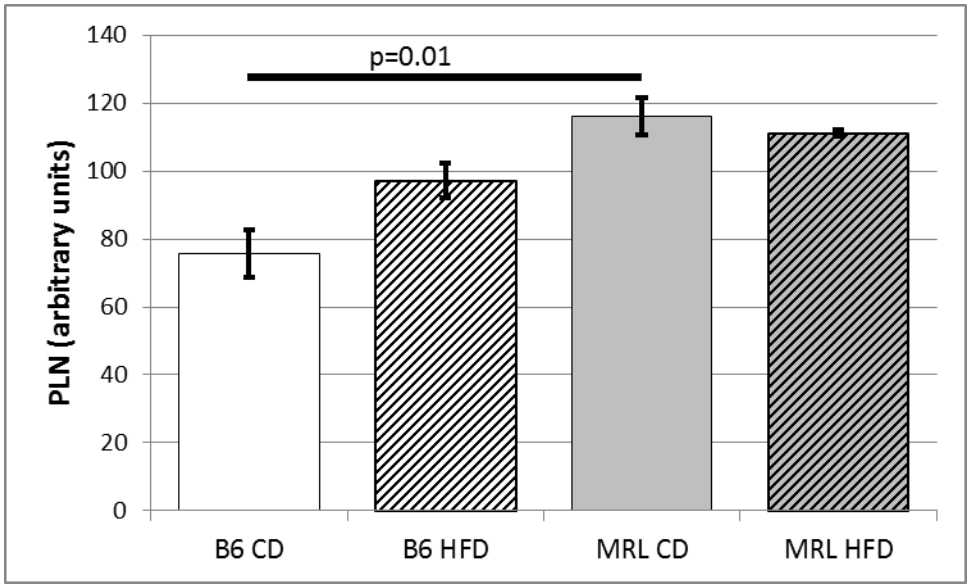

Figure 24-MRL chow diet hearts contain greater quantities of PLN than the C57Bl/6 chow diet hearts. The high fat diet C57Bl/6 heart trended towards greater PLN than the chow diet control animals (p=0.065). MRL high fat diet hearts trended to contain greater PLN than the C57Bl/6 hearts (p=0.056). n=3

FOXO1 was found to be elevated in the high fat diet fed MRL hearts (Figure 25) No changes were observed within the C57Bl/6 strain between the chow and high fat diets. No differences were found between the two strains.

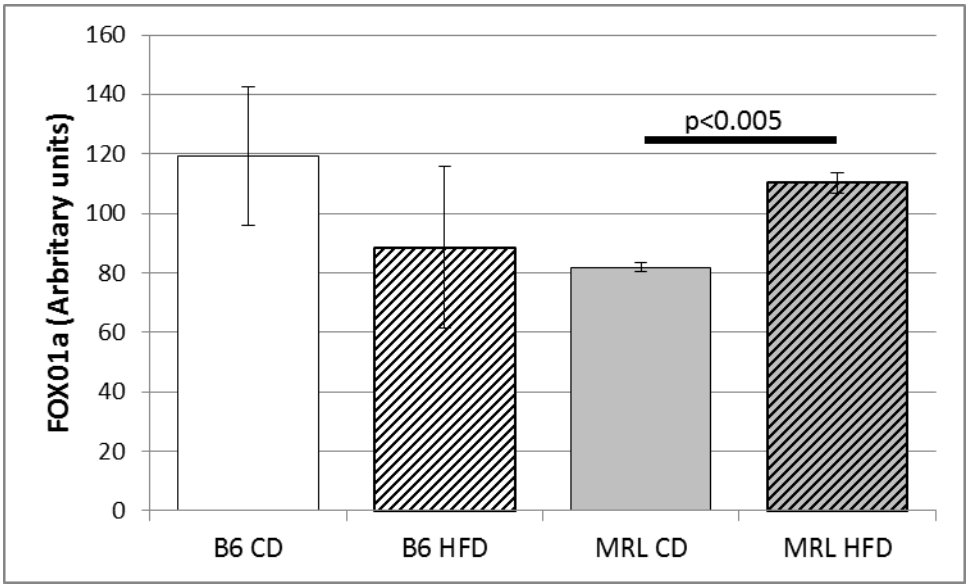

Figure 25-FOXO1a was found to be elevated in the MRL heart following the high fat diet. No other significant differences were found. n=3

E. Discussion and Conclusion

Presently the acquired data shows that the MRL heart does not hypertrophy after twelve weeks of a high fat diet while becoming obese. Conversely, this work is the first to show that the C57Bl/6 mouse develops cardiac hypertrophy at this time point. Previous high fat diet feeding studies examined eight months and longer feeding protocols. This is important as it verifies that our MRL mouse hearts do in fact resist the hypertrophic effects of obesity and a high fat diet. Mull et al showed that the MRL mouse resists hyperglycemia. As stated previously this raises the question as to whether or not the MRL heart is impacted by the obesity. In addition to hyperglycemia obesity also induces inflammation systemically (Gregor and Hotamisligil 2011). As the MRL mouse develops autoimmune conditions later in life the obesity induced inflammation could cause effects if the animals were kept on the diet longer. Preliminary data from the 20 week diet mice has shown no pathological parameters within the MRL mouse; interestingly ejection fraction and fractional shortening appear to be enhanced in the high fat diet fed MRL hearts (Roberts, unpublished data).

Morphology

The observed data is in line with our hypothesis. However when data from this project are assessed alongside the data from (Mull, Berhanu et al. 2014) a question arises: Is the MRL heart resisting the high fat diet or is the heart protected from the high fat diet due to systemic protection published in Mull et al? The MRL mouse is not hyperglycemic past the second to third week of the high fat diet. Cardiac assessment occurred following the twelfth week of the high fat diet. Thus is the MRL heart truly resisting the high fat diet or was the transitory hyperglycemia insufficient to induce pathology? High fat diet induced changes seen in this chapter clearly show that the MRL heart is affected. As the MRL mouse does not develop hyperglycemia, and the insulin tolerance tests show that the mice respond normally to insulin (Mull, Berhanu et al. 2014), I am unable to state that the MRL heart is being challenged

sufficiently. However, because we observe the hearts metabolically adapting to the HFD they are clearly being stressed to some degree.

Cardiac Function

Functional data acquired by echocardiography falls into two groups as defined by the two "modes" of heart function. Diastole is the stage when the heart relaxes after contraction and can be considered to be "at rest". Systole is the stage in which the heart contracts and blood is pushed into the body.

Electron Microscopy

The electron microscopy data shows what appear to be lipid-like droplets only within the C57Bl/6 high fat diet fed hearts. Lipid droplets accumulate within the hearts of obese and type 2 diabetic individuals as lipid uptake outpaces lipid oxidation (Boudina and Abel 2007). The sample size for each group is only one, so there is the distinct possibility that these samples happen to align with the anticipated results. As such we cannot rule out the accumulation of lipid like droplets within the high fat diet fed MRL hearts. However given that there was hypertrophy observed within the high fat diet fed C57Bl/6 hearts, I would assume that the MRL hearts do not have lipid droplets or have far fewer/smaller droplets.

Quantigene

AMPK alpha 2 is found in larger quantities in cardiomyocytes than the surrounding endothelial tissue in the heart (Viollet, Athea et al. 2009). Additionally localization of the alpha 1 and alpha 2 subunits is believed to relate to function of the AMPK heterotrimer formed with the subunit (discussed in Moffat, C et al 2010 Metabolic Functions of AMPK). Alpha 1 containing heterotrimers are believed to

function primarily in the cytoplasm whereas alpha 2 containing heterotrimers are believed to reside in the nucleus. Thus the differences in alpha subunit quantities in the MRL could indicate differences in signaling. Or it could merely be the result of the MRL mouse having fewer endothelial cells in their apex than the C57Bl/6 or be due to the small sample size. While it is tempting to say that this observed difference in mRNA can explain the MRL phenotype there is far from sufficient evidence to do so.

Quantigene found a few key differences in mRNA levels of AMPK isoforms. While these differences were found to be statistically significant the actual significance of the mRNA concentration is unknown. AMPK isoform specific antibodies were not used in western blotting; only total AMPK alpha was assessed. Additionally questions were raised by faculty members of the department about the observed changes in mRNA levels. In their opinions the observed changes in mRNA, while statistically significant, are not sufficient to actually induce a change; this from their own work involving alteration of mRNA expressions at 100+ times the initial expression. I have to side with their experience and knowledge at this time. To prove that the observed mRNA levels are responsible in some capacity for the MRL mouse's phenotype would require characterization of MRL progenitor cells in cell culture and experimentation with viral vectors or numerous genetically modified MRL strains. In either case these experiments are beyond the scope of the current project and this thesis.

Protein Quantification

Before the lower pAMPK was confirmed these results were puzzling. Initially I had anticipated that HKII would be upregulated in the MRL mouse heart as a result of the hypothesized elevated pAMPK. However the reduced HKII correlates with the reduced pAMPK. Determining that pAMPK was far lower in the heart was a surprise. Both the skeletal muscle (Berhanu, Holley-Cuthrell et al. 2014; Mull, Berhanu et al. 2014) show elevated pAMPK and unpublished data from the lab shows the liver has

elevated pAMPK as well (Gonzalez-Vega, unpublished). Thus the results I have shown invalidated my old schematic and left a large question mark.

Lower total Glut4 and HKII both agree with the lower pAMPK. Glut4 is one step above HKII in glycolysis. It is one of the two major glucose transporters present in cardiomyocytes. In the C57Bl/6 mouse heart Glut4 outnumbers Glut1 expression by ~10 fold (Aerni-Flessner, Abi-Jaoude et al. 2012). Glut1 is present at the sarcolemma basally while Glut4 is stored intracellularly until insulin interacts with the insulin receptor on the cell membrane. One result of this interaction is Glut4 is moved to the sarcolemma and begins importing glucose into the cell. This is also a major regulator of glucose metabolism.

In turn this data raises the possibility that there is reduced glucose uptake and utilization within the MRL heart at baseline. This would need to be proven by enzyme activity assays of key glycolysis components. To get a fuller picture of both glycolysis and beta-oxidation in the MRL heart nuclear magnetic resonance (NMR) imaging should be used to track metabolism in real time in isolated mouse hearts.

Questions have been raised as to whether or not the western blots represent cytosolic and/or membrane Glut4. To my current understanding the use of 1% Triton 100X in the cell lysis buffer during tissue preparation will fully extract membrane bound proteins. Thus the western blot data collected is for whole cell Glut4. In turn it appears that the MRL mouse has lower Glut4 over all compared to the C57Bl/6 mouse.

At the end of energy production five complexes of proteins exist in the inner membrane of mitochondria, the so called power plant of the cell. These complexes form the electron transport chain (ETC) which turns the generated electrons from glycolysis and beta-oxidation into ATP through a series of transporters. The ATP generated from the ETC outnumbers the ATP generated from glycolysis at 34 to 2. This makes the ETC the predominant energy production pathway for eukaryotic organisms. The MRL mouse heart has previously been shown to have greater quantities of mitochondria than the C57Bl/6 mouse (Naviaux, Le et al. 2009). They also showed that Complexes I and II have reduced activity normalized by citrate synthase compared to the C57Bl/6 mouse hearts.

Presently the impact of the observed changes, and lack thereof, of the ETC proteins within the high fat diet groups is unknown. Hypothetically elevated levels of complex V would lead to more ATP production if the electron gradient is maintained or increased as may be possible by elevated complexes I-IV. However no activity assays were conducted or electron gradient assessment performed. Both of these experiments would offer insight though the later may be challenging give the difficulties of sustaining cardiomyocytes ex vivo.

Changes in PGC1-alpha are interesting however PGC1-alpha does not work alone and as such further experiments are required to fully elucidate whether or not the observed change has an impact on the MRL heart. Possibly implying that the C57Bl/6 upregulate ETC complex proteins in response to the high fat diet. However, as no activity assays were performed I cannot say whether or not the elevated levels lead to elevated activity.

PGC1-alpha, peroxisome proliferator-activated receptor gamma coactivator 1 alpha, is down stream of AMPK activity and interacts with numerous co-factors to regulate many aspects of metabolism

and mitochondrial biogenesis. The protein represents another possible route by which the MRL mouse could have an altered metabolism and/or respond differently to a high fat diet. That, however, would entail assessing the interaction of PGC1-alpha with all of its co-factors, a task not conducted within this experiment.

Calcium regulation within the heart is essential for proper heart function and has been shown to be altered in disease. SERCA2A is the primary calcium transporter responsible for the uptake of calcium in the sarcoplasmic reticulum using ATP. It is important for the diastolic phase of cardiac function, removing calcium from the cytosol stops calcium-troponinC interaction in turn stopping myosin-actin cross bridge formation stopping contraction. As SERCA2A is elevated basally in the MRL heart, this could impact studies involving heart failure involving the MRL strain. However SERCA2A does not function alone, phospholamban (PLN) regulates the activity of SERCA2A by binding to and inhibiting its function.

However, the important point here is that SERCA2A and PLN interact with each other and can both be independently phosphorylated. This phosphorylation increases SERCA2A activity and induces PLN aggregation into tetramers, relieving their inhibition of SERCA2A activity. That phosphorylation is how the heart beats faster during times of stress. As phosphorylation states of SERCA2A and PLN were not assessed the overall impact of greater SERCA2A in the MRL heart can only be speculated.

FOXO1 has been shown to increase in C57Bl/6 male mice fed a high fat diet (60% fat) at both the mRNA and protein levels (Battiprolu, Hojayev et al. 2012). The authors followed by showing that a knockout of FOXO1 would not develop heart failure as a result of the high fat diet. Knock out of FOXO1 did not impact hyperglycemia, body weight, serum cholesterol, or serum insulin. Thus the mechanism of action clearly is within the heart itself. Unlike in Battiprolu et al, the C57Bl/6 mice fed the high fat diet in

this study did not have increased FOXO1 in their hearts. Thus despite whatever adaptive mechanisms are occurring that protect the MRL from the high fat diet, FOXO1 levels are not regulated as part of the response. It is important to note that FOXO1 activity is key to its effect and activity was not assessed in this experiment. Leaving the possibility that FOXO1 activity levels are reduced in the MRL despite the upregulation of protein.

While the observed changes within the electron transport chain proteins are intriguing, more information is required to assess activity and thus impact, if any, of the reduced protein quantification in the high fat diet MRL heart.

In all, this work has shown that the MRL mouse heart does not develop myocardial hypertrophy or cardiac dysfunction after twelve weeks of a 60% fat diet. I can report that the C57Bl/6 mouse was found to have cardiac disturbances at 12 weeks, earlier than previously reported for the strain. Contrary to the hypothesis driving the experiment pAMPK was found to be lower in the MRL heart with corresponding lower levels of two key glycolysis proteins. The MRL hearts do not develop lipid-like droplets.

V: Conclusions

A. Conclusions

Animal models have been and will be the best option for basic medical research. In this document I have summarize work conducted in the laboratory to that aim. Two mouse strains were of interest in these experiments the DBA2/J-sgcg muscular dystrophy mouse and the MRL super healing mouse. The DBA2/J mouse with a gamma sarcoglycan knockout mutation appears to be a better model of muscular dystrophy in mouse than the mdx mouse currently used by most researchers. This argued due to increased fibrosis and evans blue dye at 12 weeks of age. The MRL mouse has been shown to contain elevated pAMPK in its skeletal muscle (Berhanu, Holley-Cuthrell et al. 2014; Mull, Berhanu et al. 2014) with an increase in pAMPK linked gene expression. SeaHorse assessment of isolated myofiber progenitor cells indicates that the MRL skeletal muscle metabolism is significantly different than the control C57Bl/6 mouse skeletal muscle. Following a high fat diet protocol described in Mull et al, the MRL hearts were shown to have lower pAMPK, lower Glut4, lower HKII. Additionally other protein and mRNA levels were find to be changed in the MRL heart both between the chow and high fat diet animals and compared to the C57Bl/6 control mice. Importantly the MRL high fat diet fed hearts did not show any pathology after twelve weeks of the diet.

High fat diet was found to induce greater phosphorylation of AMPK within the MRL tricep (Mull, Berhanu et al. 2014). Oddly no increase was found basally between the MRL and CD triceps or quadriceps. This may be due to the intensity of the MRL HFD samples within the blots. Regardless, the high fat diet induced a change with some MRL skeletal muscle. Meanwhile within the heart the high fat diet did not affect phosphorylation of AMPK. It did reduce the total AMPK within the MRL heart but had

no impact on the C57Bl/6 heart. Likewise, the high fat diet had no impact on the C57Bl/6 skeletal muscle. Thus not only are the MRL skeletal muscles and cardiac behaving differently they are also responding different to the high fat diet. Again highlighting the altered MRL metabolism originally identified in (Naviaux et al. 2009)

These data have answered questions and in the time honored tradition of science raised many many more than they answered. The McNally laboratory is investigating observed genetic mutations found within the DBA2/J animal that correlate with disease severity in the muscular dystrophy animals. Combined with work from our laboratory the DBA2/J-sgcg mice could represent avenues for research into treatment for the disease itself alongside analysis of genetic co-factors which impact the severity of the disease. The MRL mouse now represents a looming question. It has been shown to heal ear punch injuries with no evidence of damage (Clark, Clark et al. 1998), numerous studies have examined its capacity to heal other insults (reviewed in (Heydemann 2012)), resist systemic hyperglycemia following a high fat diet (Mull, Berhanu et al. 2014), and here has been shown to resist cardiac complications associated with obesity and a high fat diet. Clearly the MRL mouse is worthy of being investigated for some time to come. This will be complicated by the fact that the events listed above arose in a mouse without any genetic manipulation. However determining how the MRL mouse heals and resist diabetes holds numerous prospects in the fields of regenerative medicine and preventing diabetes.

B. **Future Directions**

There was concern that the twelve week diet length was not sufficient to induce metabolic disturbances within the C57Bl/6 mouse. Additional mice were started in early 2015 for 20 weeks of diet following weaning at three weeks. Presently there are only sufficient MRL mice to look for statistical

differences. No differences have been found in left ventricle thickness between the MRL 20 week chow and high fat diet mice. Interestingly however there is no difference in body weight between those two groups. Mice from all four 20 week groups are continuing to age as of the time of this manuscript.

MRL metabolism has been a question with this research as well. A low carbohydrate diet would challenge the MRL's ability to conduct gluconeogenesis and a low fat diet would challenge the MRL heart which appears to favor fats even more than the C57Bl/6 heart. Additionally, radiolabeled substrates would allow for the tracking of sugars and fats as the MRL heart metabolizes them. This would allow for determiniation of the rates of glucose and fat usage.

VI: Citied Literature

Aerni-Flessner, L., M. Abi-Jaoude, et al. (2012). "GLUT4, GLUT1, and GLUT8 are the dominant GLUT transcripts expressed in the murine left ventricle." Cardiovascular diabetology 11: 63.

Amaral, N. and D. O. Okonko (2015). "Metabolic abnormalities of the heart in type II diabetes." Diabetes & vascular disease research 12(4): 239-248.

Battiprolu, P. K., B. Hojayev, et al. (2012). "Metabolic stress-induced activation of FoxO1 triggers diabetic cardiomyopathy in mice." The Journal of clinical investigation 122(3): 1109-1118.

Berhanu, T. K., J. Holley-Cuthrell, et al. (2014). "Increased AMP-activated protein kinase in skeletal muscles of Murphy Roth Large mice and its potential role in altered metabolism." Physiological reports 2(3): e00252.

Boudina, S. and E. D. Abel (2007). "Diabetic cardiomyopathy revisited." Circulation 115(25): 3213-3223.

Bugger, H. and E. D. Abel (2009). "Rodent models of diabetic cardiomyopathy." Disease models & mechanisms 2(9-10): 454-466.

Calligaris, S. D., M. Lecanda, et al. (2013). "Mice long-term high-fat diet feeding recapitulates human cardiovascular alterations: an animal model to study the early phases of diabetic cardiomyopathy." PloS one 8(4): e60931.

Clark, L. D., R. K. Clark, et al. (1998). "A new murine model for mammalian wound repair and regeneration." Clinical immunology and immunopathology 88(1): 35-45.

Gregor, M. F. and G. S. Hotamisligil (2011). "Inflammatory mechanisms in obesity." Annual review of immunology 29: 415-445.

Heydemann, A. (2012). "The super super-healing MRL mouse strain." Frontiers in biology 7(6): 522-538.

Horman, S., C. Beauloye, et al. (2012). "AMP-activated protein kinase in the control of cardiac metabolism and remodeling." Current heart failure reports 9(3): 164-173.

Ljubicic, V., P. Miura, et al. (2011). "Chronic AMPK activation evokes the slow, oxidative myogenic program and triggers beneficial adaptations in mdx mouse skeletal muscle." Human molecular genetics 20(17): 3478-3493.

Mull, A. J., T. K. Berhanu, et al. (2014). "The Murphy Roths Large (MRL) mouse strain is naturally resistant to high fat diet-induced hyperglycemia." Metabolism: clinical and experimental 63(12): 1577-1586.

Naviaux, R. K., T. P. Le, et al. (2009). "Retained features of embryonic metabolism in the adult MRL mouse." Molecular genetics and metabolism 96(3): 133-144.

Petro, A. E., J. Cotter, et al. (2004). "Fat, carbohydrate, and calories in the development of diabetes and obesity in the C57BL/6J mouse." Metabolism: clinical and experimental 53(4): 454-457.

Roberts, N. W., J. Holley-Cuthrell, et al. (2015). "Biochemical and Functional Comparisons of mdx and Sgcg (-/-) Muscular Dystrophy Mouse Models." BioMed research international 2015: 131436.

Sakamoto, K., E. Zarrinpashneh, et al. (2006). "Deficiency of LKB1 in heart prevents ischemia-mediated activation of AMPKalpha2 but not AMPKalpha1." American journal of physiology. Endocrinology and metabolism 290(5): E780-788.

Salt, I., J. W. Celler, et al. (1998). "AMP-activated protein kinase: greater AMP dependence, and preferential nuclear localization, of complexes containing the alpha2 isoform." The Biochemical journal 334 (Pt 1): 177-187.

Suter, M., U. Riek, et al. (2006). "Dissecting the role of 5'-AMP for allosteric stimulation, activation, and deactivation of AMP-activated protein kinase." The Journal of biological chemistry 281(43): 32207-32216.

Viollet, B., Y. Athea, et al. (2009). "AMPK: Lessons from transgenic and knockout animals." Frontiers in bioscience 14: 19-44.

Viollet, B., B. Guigas, et al. (2012). "Cellular and molecular mechanisms of metformin: an overview." Clinical science 122(6): 253-270.

Wu, J., D. Puppala, et al. (2013). "Chemoproteomic analysis of intertissue and interspecies isoform diversity of AMP-activated protein kinase (AMPK)." The Journal of biological chemistry 288(50): 35904-35912.

Zhang, Z., S. Wang, et al. (2014). "Sulforaphane prevents the development of cardiomyopathy in type 2 diabetic mice probably by reversing oxidative stress-induced inhibition of LKB1/AMPK pathway." Journal of molecular and cellular cardiology 77: 42-52.